

略 号

畜草研研報  
Bull NARO Inst Livest  
Grassl Sci

ISSN:1347-0825  
CODEN:CSKKCS



# Bulletin of NARO Institute of Livestock and Grassland Science



第12号〈No.12〉平成24年3月 -March2012-

**NARO Institute  
of Livestock and  
Grassland Science  
(NILGS)**

Ibaraki, Japan

独立行政法人 農業・食品産業技術総合研究機構

**畜産草地研究所**

---

畜産草地研究所編集委員会  
Editorial Board

所 長  
Director-General

松 本 光 人  
Mitsuto MATSUMOTO

草地研究監  
Director, Grassland Research

梨 木 守  
Mamoru NASHIKI

編集委員長  
Editor-in-Chief

竹 中 昭 雄  
Akio TAKENAKA

副編集委員長  
Deputy Editor

浦 川 修 司  
Shuji URAKAWA

編集委員  
Associate Editor

小 迫 孝 実  
Takami KOSAKO

間 野 吉 郎  
Yoshiro MANO

月 星 隆 雄  
Takao TSUKIBOSHI

山 本 嘉 人  
Yoshito YAMAMOTO

手 島 茂 樹  
Shigeki TEJIMA

平 子 誠  
Makoto HIRAKO

長谷川 三喜  
Sanki HASEGAWA

野 村 将  
Masaru NOMURA

---

# 畜産草地研究所研究報告

第12号 (平成24年3月)

## — 目 次 —

### — 原著論文 —

- ソルガム温度感応遺伝子に連鎖する DNA マーカーのマッピング (英文)  
..... 高溝 正・中津志野・長村吉晃・藤森雅博・樽本 勲..... 1

### — 技術論文 —

- 畜産草地研究所 (つくば地区) における分析型官能評価パネルの確立  
..... 佐々木啓介・本山三知代・成田卓美・大江美香・吉村 望・  
田島淳史・野村 将・千国幸一..... 9

### — 学位論文 —

- ラマン分光法によるトリアシルグリセロールの構造および相挙動解析 (英文)  
..... 本山三知代.....19

BULLETIN OF  
NARO INSTITUTE OF  
LIVESTOCK AND GRASSLAND SCIENCE

No.12 (2012.3)

CONTENTS

**Research Paper**

Tadashi TAKAMIZO, Shino NAKATSU, Yoshiaki NAGAMURA,  
Masahiro FUJIMORI and Isao TARUMOTO :

Mapping of DNA Markers Linked to a Thermosensitivity Gene in Sorghum ..... 1

**Technical Paper**

Keisuke SASAKI, Michiyo MOTOYAMA, Takumi NARITA, Mika OE, Nozomi YOSHIMURA,  
Atsushi TAJIMA, Masaru NOMURA and Koichi CHIKUNI :

Establishment of an Analytical Sensory Panel at the NARO Institute of Livestock and Grassland  
Science (Tsukuba) ..... 9

**Doctoral Dissertation**

Michiyo MOTOYAMA :

Structure and Phase Characterization of Triacylglycerols by Raman Spectroscopy ..... 19

## Mapping of DNA Markers Linked to a Thermosensitivity Gene in Sorghum

Tadashi TAKAMIZO, Shino NAKATSU<sup>1</sup>, Yoshiaki NAGAMURA<sup>2</sup>,  
Masahiro FUJIMORI<sup>3</sup> and Isao TARUMOTO<sup>1</sup>

Forage Crop Research Division,  
NARO Institute of Livestock and Grassland Science, Nasushiobara, 329-2793 Japan

<sup>1</sup> Osaka Prefecture University, Sakai, 599-8531 Japan

<sup>2</sup> National Institute of Agrobiological Sciences, Tsukuba, 305-8602 Japan

<sup>3</sup> NARO Tohoku Agricultural Research Center, Morioka, 020-0198 Japan

### Abstract

In sorghum (*Sorghum bicolor* Moench), flower initiation is reported to be controlled by the thermosensitivity locus *T*. Flower initiation by *T* (*TT* or *Tt*) genotypes is delayed by exposure to temperatures over 20°C under long-day conditions. DNA markers associated with this trait were isolated by bulk segregant analysis with amplified fragment length polymorphism (AFLP) markers. A total of 13 dominant and 1 co-dominant markers were identified from among the 1024 AFLP markers tested, and 7 of them could be assigned to a linkage map. Linkage analysis using 33 individuals from a BC<sub>1</sub>F<sub>2</sub> population, which were classified by phenotype as either *tt* or *T*, showed that the *T* locus for thermosensitivity was distal to the marker AFLP16. Quantitative trait locus (QTL) analysis also showed that the sorghum thermosensitivity trait is monogenic. Restriction fragment length polymorphism (RFLP) analysis was carried out to estimate a more precise location of AFLP16 by comparing it with 145 RFLP markers already mapped in the authentic sorghum genetic map. In the RFLP analysis, the *T* locus was mapped to sorghum chromosome 6, 4.0 cM from AFLP16.

**Key words:** AFLP, flower initiation, *Sorghum bicolor*, thermosensitivity gene

### Introduction

Flowering is the developmental turning point between the vegetative and reproductive phases in plants. The timing of flower initiation is critical for reproductive success, and the relationships between developmental stage and environmental factors such as photoperiod and temperature have been studied extensively. In sorghum (*Sorghum bicolor* Moench), which is a facultative short-day plant, the loci *Ma*<sub>1</sub> to *Ma*<sub>4</sub><sup>13)</sup>, *Ma*<sub>5</sub> and *Ma*<sub>6</sub><sup>14)</sup>, *T*<sup>17)</sup>, and *D*<sub>1</sub> and *D*<sub>2</sub><sup>18)</sup> control the relationships between flower initiation (FI) and environmental factors such as

photoperiod and temperature. Among these, the *T* locus controls the thermosensitivity of FI. The FI of *T* (*TT* and *Tt*) genotypes is accelerated by exposure to temperatures lower than 20°C under long-day conditions (over 12.5 h), whereas the opposite phenomenon occurs at temperatures over 20°C (i.e., FI of *T*-genotypes is delayed)<sup>17)</sup>. The characteristics controlled by the *T* locus are similar to those of genes controlling vernalization in winter-annual plants such as wheat, barley, and *Arabidopsis thaliana*, although exposure to temperatures below 20°C is not essential to induce FI in sorghum.

High-density restriction fragment length

polymorphism (RFLP) linkage maps have been constructed for gramineous species such as maize, wheat, and rice<sup>1,3,6</sup>. In sorghum, an RFLP linkage map was constructed using the mapped rice RFLP markers<sup>9</sup>. In addition, high-density genetic maps based on amplified fragment length polymorphism (AFLP), RFLP, and simple sequence repeat (SSR) markers have been constructed in sorghum<sup>8</sup>. To provide the information necessary to use the *T* gene to improve FI in crops, we conducted a detailed mapping study. We performed bulk segregant analysis to identify AFLP markers linked to the thermosensitivity gene (*T*) controlling FI in sorghum and mapped the chromosomal locations of these AFLP markers in greater detail by using RFLP analysis. We mapped the *T* locus in two ways: as a single gene and as a QTL. The mapping population was a BC<sub>1</sub>F<sub>1</sub> population constructed by making crosses of (*TT* × *tt*) × *tt*.

## Materials and Methods

### Plant material

Sorghum has at least nine loci for determining FI relative to photoperiod and temperature, including *Ma*<sub>1</sub> to *Ma*<sub>4</sub><sup>13</sup>, *Ma*<sub>5</sub> and *Ma*<sub>6</sub><sup>14</sup>, *T*<sup>17</sup>, and *D*<sub>1</sub> and *D*<sub>2</sub><sup>18</sup>. To construct a mapping population for *T* in a genetic background that was simplified with respect to the other FI loci, a BC<sub>1</sub>F<sub>2</sub> population was established by backcrossing Daikoukaku (*tt**d*<sub>1</sub>*D*<sub>2</sub>*D*<sub>2</sub>) to an F<sub>1</sub> hybrid (Natuibuki, *Tt**d*<sub>1</sub>*D*<sub>2</sub>*D*<sub>2</sub>) produced by crossing MS175 (*TT**d*<sub>1</sub>*D*<sub>2</sub>*D*<sub>2</sub>) and Daikoukaku<sup>17</sup>. The progeny of this backcross (BC<sub>1</sub>F<sub>1</sub>) were then selfed to generate the BC<sub>1</sub>F<sub>2</sub> population. The BC<sub>1</sub>F<sub>2</sub> plants were grown at 15-h daylength at 25°C in a natural-light greenhouse to express the effect of *T* on the delay of FI. The days-to-emergence of the flag leaf (DEFL) in the BC<sub>1</sub>F<sub>2</sub> population (90 plants) exhibited a segregation ratio that was not significantly different from 3 late: 1 early using chi-square, as would be expected for a single dominant gene controlling late flowering<sup>17</sup>.

### AFLP analysis

To identify AFLPs linked to the thermosensitivity trait, two bulk samples were prepared, each consisting of 12 individuals from the BC<sub>1</sub>F<sub>2</sub> population having either

late or early DEFL. To map the thermosensitivity gene as a Mendelian single gene, 15 individuals with *tt* and 18 with *T*- were used. DNA was isolated from 8 g of fresh leaf tissue per individuals by the CTAB method. AFLP analysis for the bulk DNA was performed following the procedure of Vos *et al.*<sup>19</sup> with some modifications. DNA digestion and ligation was performed using the fluorescent dye-based AFLP Plant Mapping Kit from Perkin Elmer Applied Biosystems (Foster City, CA, USA). Two pre-selective amplification steps were performed. First, amplification with an *Eco*RI (E) primer with the sequence 5'-GACTGCGTACCAATTC-3' (E-000) and an *Mse*I (M) primer with sequence 5'-GATGAGTCCTGAGTAA-3' (M-000) was performed to reduce nonspecific background on the polyacrylamide gels. This was followed by amplification with a second set of *Eco*RI (E-000 + A) and *Mse*I (M-000 + C) primers, each containing one selective nucleotide. Selective amplification was then conducted using the pre-amplified products and selective *Eco*RI and *Mse*I primers, each of which had three selective nucleotides. All of the *Eco*RI selective primers were 5'-end-labeled with the fluorescent dye FAM (Amersham Pharmacia Biotech, Tokyo, Japan). A total of 32 primer combinations of 4 E-primers with the 3' ends AAC (e02), AAG (e03), ACA (e05), ACC (e06), and 8 M-primers with the 3' ends CAA (m17), CAC (m18), CAG (m19), CAT (m20), CTA (m29), CTC (m30), CTG (m31) and CTT (m32) were used to construct the linkage map. Each AFLP marker was given a suffix according to its position from the top of the gel (i.e., e02m17-1 was above e02m17-2 on the gel). To obtain good separation of the amplified DNA fragments, buffer gradient electrophoresis was conducted with 1 × TBE (100 mM Tris, 100 mM boric acid, 2 mM EDTA, pH 8.0) as the cathode buffer (–) and 1 × TBE plus 0.5 M sodium acetate as the anode (+) buffer<sup>12</sup>. The amplification products were run on a 40-cm, 5% denaturing polyacrylamide gel at 1100 V for 2 h 45 min. After electrophoresis, the gels were scanned in a Molecular Imager (Bio Rad, Hercules, CA, USA).

### RFLP analysis

To more accurately map the AFLP markers and the *T* locus, the same BC<sub>1</sub>F<sub>2</sub> population and Daikoukaku parent as in the AFLP analysis were used for RFLP analysis.

DNA was isolated from 8 g of fresh leaf tissue by the CTAB method, and bulk DNA samples were made from pools of 10 individuals predicted to carry either *tt* or *T*- based on the position of the AFLP16 marker band. (The AFLP16 marker was found to be the closest to the locus controlling days-to-heading and thermosensitivity; see Results).

Restriction enzyme treatment, electrophoresis, and Southern hybridization analysis were carried out according to the method of Kurata *et al.* <sup>6)</sup>. DNA probes created by the Rice Genome Program (RGP) of MAFF were used as hybridization probes (<http://rgp.dna.affrc.go.jp/publicdata/geneticmap2000/index.html>). Linkage analysis was performed by using the F<sub>2</sub> model in MAPMAKER/EXP 3.0 <sup>7)</sup> and MAPMAKER/QTL ver. 1.1 <sup>10)</sup>

## Results and Discussion

The BC<sub>1</sub>F<sub>2</sub> population, which was raised at 15-h daylength and constant 25°C, segregated for early and late flowering, as assessed based on DEFL (Fig. 1). The values of the BC<sub>1</sub>F<sub>2</sub> individuals flanked 60 days, which was the mean of the parental DEFLs.

### AFLP analysis

AFLP markers associated with the thermosensitivity gene were identified by screening 4 bulk DNA samples (E-1, E-2, L-1, and L-2) each made from 6 individuals predicted to carry *tt* (E) or *T*-(L) based on DEFL. From

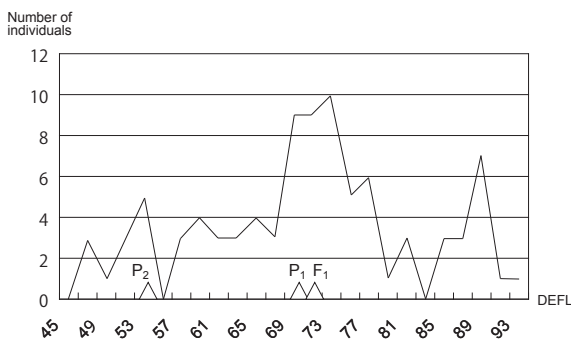


Fig.1. Segregation of days-to-emergence of flag leaf (DEFL) in a BC<sub>1</sub>F<sub>2</sub> population derived from backcrossing of Daikoukaku (*tt**d*<sub>1</sub>*D*<sub>2</sub>*D*<sub>2</sub>) to Natuibuki (*Tt**d*<sub>1</sub>*d*<sub>2</sub>*D*<sub>2</sub>*D*<sub>2</sub>), an F<sub>1</sub> between MS175 (*TT**d*<sub>1</sub>*d*<sub>2</sub>*D*<sub>2</sub>*D*<sub>2</sub>) and Daikoukaku. P<sub>1</sub>=MS175, P<sub>2</sub>=Daikoukaku, F<sub>1</sub>=Natuibuki.

1024 primer combinations, we identified 9 markers in a coupling phase with *T* (i.e., not observed in bulks E-1 and E-2 but present in bulks L-1 and L-2; Fig. 2A), 4 markers in repulsion phase with *T* (i.e., not observed in L-1 and L-2 but present in E-1 and E-2; Fig. 2B), and 1 co-dominant marker showing size polymorphism between the L and E groups (Fig. 2C). Using these 14 markers, AFLP analysis was performed on 90 individuals of the BC<sub>1</sub>F<sub>2</sub> population, and a genetic linkage map was constructed with 7 of the markers.

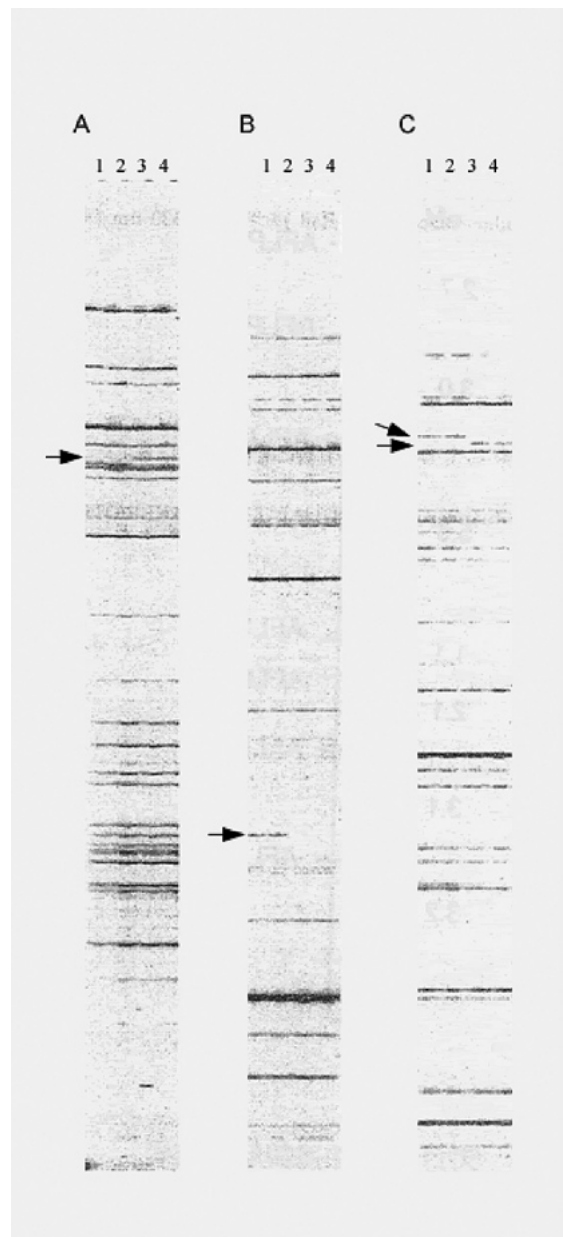


Fig.2. Examples of band types observed in AFLP analysis. A=coupling-phase marker (arrowhead=AFLP), B=repulsion-phase marker (arrowhead=AFLP11), C=co-dominant marker (arrowhead=AFLP16) Lane 1=bulk E-1 (*tt*), Lane 2=bulk E-2 (*tt*), Lane 3=bulk L-3 (*T*-), Lane 4=bulk L-4 (*T*-).

To map the thermosensitivity locus as a Mendelian single gene, a genetic linkage map was constructed using 15 individuals with *tt* and 18 with *T*, after omitting 57 ambiguous individuals. The result showed that the thermosensitivity locus was located 3.2 cM from the AFLP16 marker (Fig. 3A). The very low frequency of polymorphic AFLP markers (15 out of 1024=1.5%) seemed to be due to the lack of polymorphism in the BC<sub>1</sub>F<sub>2</sub> population.

Since traits associated with heading are generally considered to be quantitative<sup>20)</sup>, we used QTL interval mapping to investigate the precise position of the thermosensitivity locus by treating it as a quantitative trait. A QTL with LOD=14.2 was found at the location of AFLP16, providing further evidence that the thermosensitivity gene controls DEFL under long day length at temperatures over 20°C behaves as a single gene and is located distal to AFLP16 (Fig. 3B). Although AFLP16 was located at the end of the linkage group and the thermosensitivity gene was not flanked on both sides by AFLP markers, the result of the QTL analysis confirmed the location of this gene.

### RFLP analysis

RFLP markers were screened for their ability to detect polymorphism in MS175, Daikoukaku, and the four bulk DNA samples (E-1, E-2, L-1, and L-2) after digestion by eight common restriction enzymes. A set of 145 DNA markers out of approximately 607 RFLP markers in a recently constructed sorghum genetic map<sup>9)</sup> were tested, and 79 of them were polymorphic (54.5%). Then, we compared the RFLP alleles in the parental varieties with those in the bulk populations to estimate the map location of the thermosensitivity gene. The markers were classified into three categories. The first category contained markers for which the Daikoukaku allele was found within the early-flowering bulk samples and the MS175 allele was found in the late-flowering bulk samples. The second category had both parental alleles in both bulk samples, and the third category contained markers for which the allele in both bulk samples was the same as that in Daikoukaku, showing that each of these regions was fixed for the genetic segment from Daikoukaku. Since markers of the first type were located on the chromosome 6<sup>9)</sup>, the thermosensitivity gene was tentatively placed on the chromosome 6.

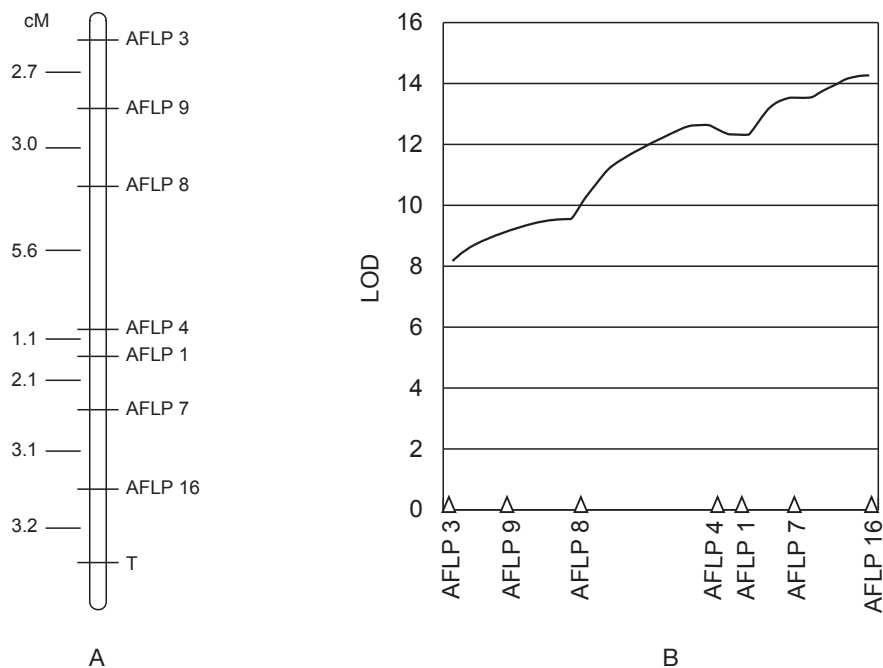


Fig.3. AFLP linkage map (A) and LOD scores from QTL analysis (B) of a sorghum BC<sub>1</sub>F<sub>2</sub> generated from a backcross of Daikoukaku (*ttd<sub>1</sub>d<sub>1</sub>D<sub>2</sub>D<sub>2</sub>*) to (Natuibuki, *Ttd<sub>1</sub>d<sub>1</sub>D<sub>2</sub>D<sub>2</sub>*), an F<sub>1</sub> between MS175 (*TTd<sub>1</sub>d<sub>1</sub>D<sub>2</sub>D<sub>2</sub>*) and Daikoukaku<sup>18)</sup>.

A genetic linkage map consisting of the 8 RFLP markers in the first category and AFLP16 was constructed by using DNAs from 15 individuals with *tt* and 18 individuals with *T*<sup>-</sup>, which were the same individuals as in the AFLP analysis. The result showed that the thermosensitivity locus *T* was located 4.0 cM from AFLP16 (Fig. 4A). Interval mapping of the locus was also carried out using DNA of all 90 individuals to investigate the position of the thermosensitivity by treating it as a quantitative trait. A QTL showing LOD of 15.7 was found at AFLP16, providing further evidence that the thermosensitivity trait is monogenic (Fig. 4B).

The integrated relationship between the QTL for DEFL, the linkage map of the thermosensitivity gene, and a previously constructed sorghum RFLP linkage map<sup>9)</sup> are shown in Fig. 4C. As shown in Fig. 4C, neither the thermosensitivity locus nor the QTL of DEFL could capture the locus, because it was beyond the last marker on either map. In this study, both bulk samples in BC<sub>1</sub>F<sub>2</sub> showed the Daikoukaku pattern in the region from S10644 to the end of chromosome, indicating that it was fixed for the genomic region from Daikoukaku. Since the mapping population segregated for thermosensitivity, the *T* locus could not reside in this fixed region (Fig. 4C),

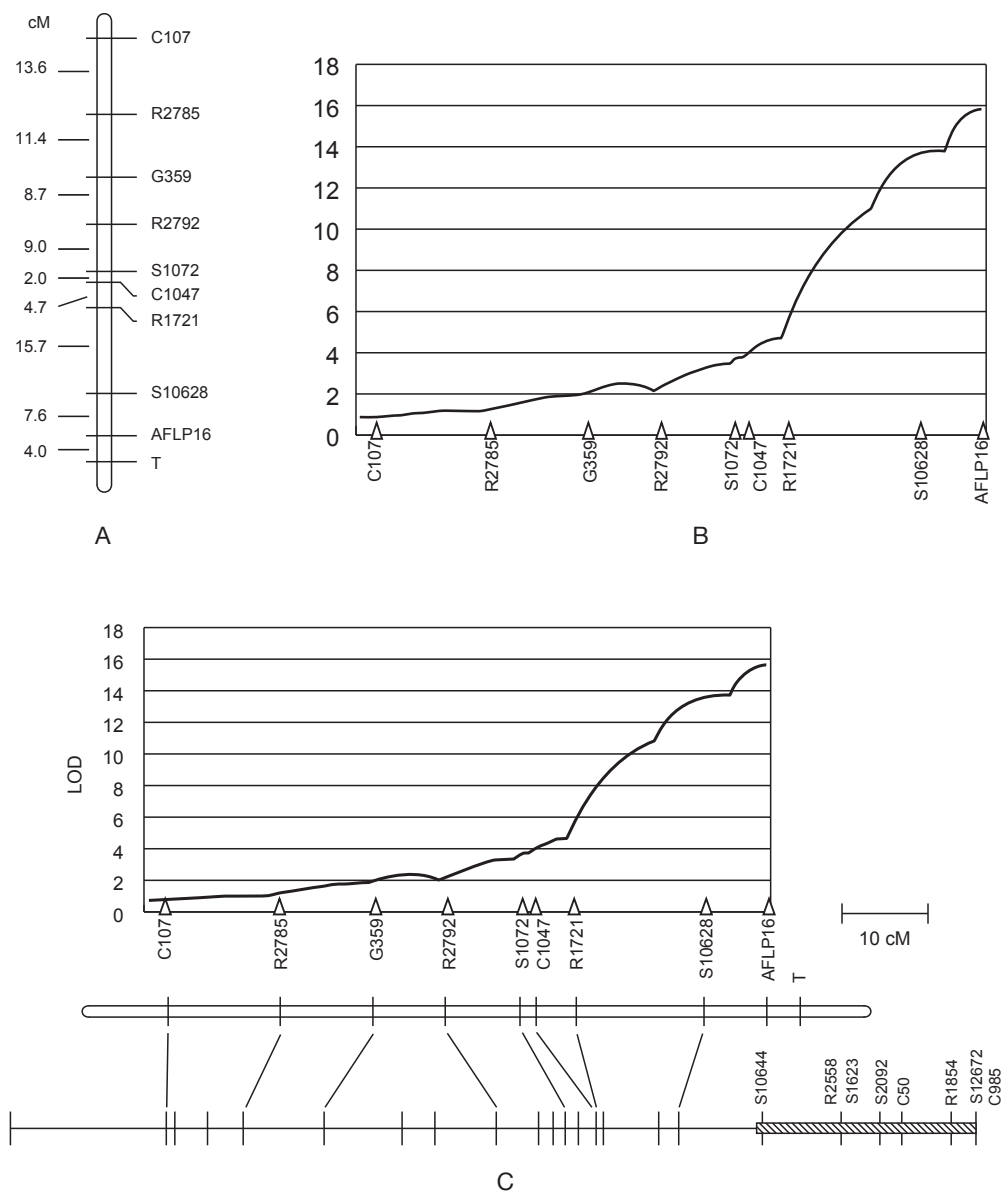


Fig.4. RFLP linkage map (A), LOD scores from QTL analysis (B), and their relationships to a published RFLP linkage map<sup>9)</sup> (C) based on mapping in a sorghum BC<sub>1</sub>F<sub>2</sub> population generated from backcrossing Daikoukaku (*tt*<sub>1</sub>*d*<sub>1</sub>*D*<sub>2</sub>*D*<sub>2</sub>) to (Natuibuki, *Ttd*<sub>1</sub>*d*<sub>1</sub>*D*<sub>2</sub>*D*<sub>2</sub>), an F<sub>1</sub> between MS175 (*TTd*<sub>1</sub>*d*<sub>1</sub>*D*<sub>2</sub>*D*<sub>2</sub>) and Daikoukaku<sup>18)</sup>.

and because the region did not segregate for any of the markers we tested, we could not construct a complete genetic linkage map. However, in a previously reported sorghum linkage map<sup>9)</sup>, 6 RFLP markers were distal to marker S10628, which we mapped in this study and is the closest RFLP marker to the thermosensitivity locus; based on this information, the *T* locus appears to be located between RFLP markers S10644 and R2558.

RFLP marker is too laborious to use in conventional breeding and other more convenient DNA markers should be created after further narrowing down the flanking region. Then the thermosensitivity gene itself would be isolated and its introduction into flowering crops by genetic transformation would be very meaningful in various aspects. Because of its unique function, flower initiation of transgenic plant carrying the thermosensitivity gene is delayed by exposure to over 20°C under long-day condition. Recently, Japanese rice culture is endangered by the occurrence of white-back kernel induced by high temperature damage in summer. Retardation of heading in high temperature sensitive rice excellent cultivars by the thermosensitivity gene would be one of possibilities to circumvent the damage. In many horticultural plants, the control of flowering time is very essential and the thermosensitivity gene could be also used practically.

By the way, Sorghum is considered to be a good candidate for biomass production, and transgenic approaches to improvement of this trait are expected. However, gene dispersal by pollen into Johnsongrass<sup>11,15,16)</sup>, which is a notorious perennial rhizomatous weed closely related to sorghum, is likely to raise concerns about the environmental safety of transgenic sorghum. If the thermosensitivity gene (*T*) is cloned and modified to enable control of flowering of sorghum, this might be a method to prevent hybridization with unwanted species. A high-density genetic recombination map of sequence-tagged sites for sorghum is available<sup>2)</sup> so it seems feasible to determine the position of this thermosensitivity gene in the near future with the aid of BAC-based fluorescent *in situ* hybridization<sup>4,5)</sup>.

### Acknowledgments

We thank Prof. Dr. Shigemitsu Kasuga in Shinshu

University for giving us the plant materials and Dr. Yoshiro Mano in NARO Institute of Livestock and Grassland Science for helpful discussion in this study.

### References

- 1) Anderson, J.A., Ogihara, Y., Sorrells, M.E. and Tanksley, S.D. (1992). Development of a chromosomal arm map for wheat based on RFLP markers, *Theor. Appl. Genet.*, 83, 1035-1043.
- 2) Bowers, J.E., Abbey, C., Anderson, S., Chang, C., Draye, X., Hoppe, A.H., Jessup, R., Lemke, C., Lenington, J., Li, Z.K., Lin, Y.R., Liu, S.C., Luo, L.J., Marler, B.S., Ming, R.G., Mitchell, S.E., Qiang, D., Reischmann, K., Schulze, S.R., Skinner, D.N., Wang, Y.W., Kresovich, S., Schertz, K.F. and Paterson, A.H. (2005). A high-density genetic recombination map of sequence-tagged sites for sorghum, as a framework for comparative structural and evolutionary genomics of tropical grains and grasses, *Genetics*, 165, 367-386.
- 3) Burr, B., Burr, F.A., Thompson, K.H., Albertson, M.C. and Stuber, C.W. (1988). Gene-mapping with recombinant inbreds in maize, *Genetics*, 118, 519-526.
- 4) Islam-Faridi, M.N., Childs, K.L., Klein, P.E., Hodnett, G., Menz, M.A., Klein, R.R., Rooney, W.L., Mullet, J.E., Stelly, D.M. and Price, H.J. (2002). A molecular cytogenetic map of sorghum chromosome 1, Fluorescence *in situ* hybridization analysis with mapped bacterial artificial chromosomes, *Genetics*, 161, 345-353.
- 5) Kim, J.S., Klein, P.E., Klein, R.R., Price, H.J., Mullet, J.E. and Stelly, D.M. (2005). Molecular cytogenetic maps of sorghum linkage groups 2 and 8, *Genetics*, 169, 955-965.
- 6) Kurata, N., Nagamura, Y., Yamamoto, K., Harushima, Y., Sue, N., Wu, J., Antonio, B.A., Shomura, A., Shimizu, T., Lin, S.Y., Inoue, T., Fukuda, A., Shimano, T., Kuboki, Y., Toyama, T., Miyamoto, Y., Kiri-hara, T., Hayasaka, K., Miyao, A., Monna, L., Zhong, H.S., Tamura, Y., Wang, Z.X., Momma, T., Umehara, Y., Yano, M., Sasaki, T. and Minobe, Y. (1994). A 300 kilobase interval genetic map of rice including 883 expressed sequences, *Nature Genetics*, 8, 365-372.

- 7) Lander, E., Abrahamson, J., Barlow, A., Daly, M., Lincoln, S., Newburg, L. and Green, P. (1987). Mapmaker, a computer package for constructing genetic-linkage maps, *Cytogenetics and Cell Genetics*, 46, 42-642.
- 8) Menz, M.A., Klein, R.R., Mullet, J.E., Obert, J.A., Unruh, N.C. and Klein, P.E. (2002). A high-density genetic map of *Sorghum bicolor* (L.) Moench based on 2926 AFLP (R), RFLP and SSR markers, *Plant Mol. Biol.*, 48, 483-499.
- 9) Nagamura, Y., Tanaka, T., Nozawa, H., Kaidai, H., Kasuga, S. and Sasaki, T. (1998). Syntenic regions between rice and sorghum genomes, *Proc. Intern. Workshop Utilization of Transgenic plant and genome analysis in forage crops*, NGRI Working Report, 1998-9, 97-103.
- 10) Paterson, A.H., Lander, E.S., Hewitt, J.D., Peterson, S., Lincoln, S.E. and Tanksley, S.D. (1988). Resolution of quantitative traits into Mendelian factors by using a complete linkage map of restriction fragment length polymorphisms, *Nature*, 335, 721-726.
- 11) Paterson, A., Schertz, K.F., Lin, Y.R., Liu, S.C. and Chang, Y.L. (1995). The weediness of wild plants, Molecular analysis of genes influencing dispersal and persistence of Johnsongrass, *Sorghum halepense* (L.), *Proc. Natl. Acad. Sci. USA*, 92, 6127-6131.
- 12) Qi, X. and Lindhout, P. (1997). Development of AFLP markers in barley, *Mol. Gen. Genet.*, 254, 330-336.
- 13) Quinby, J.R. (1967). The maturity genes of sorghum, In *Advances in Agronomy*, 19 (Ed. Norman, A.G.), 267-305, Academic Press Inc, New York.
- 14) Rooney, W.L. and Aydin, S. (1999). Genetic control of a photoperiod-sensitive response in *Sorghum bicolor* (L.) Moench, *Crop Sci.*, 39, 397-400.
- 15) Takai, T., Kasuga, S., Goto, K. and Kaidai, H. (2005). Evaluation of reproduction system in perennial Sorghum and dispersal of modified gene by hybridization, In *Research Report*, 428, Assurance of safe use of genetically modified organisms (Ed. Agriculture, Forestry and Fisheries Research Council, MAFF), Tokyo, 52-56. (in Japanese).
- 16) Tang, H. and Liang, G.H. (1988). The genomic relationship between cultivated sorghum [*Sorghum bicolor* (L.) Moench] and Johnsongrass [*S. halepense* (L.) Pers.], a re-evaluation, *Theor. Appl. Genet.*, 76, 277-284.
- 17) Tarumoto, I., Yanase, M., Iwahara, Y., Kuzumi, Y., Morikawa, T. and Kasuga, S. (2003). Inheritance of a thermo-sensitivity gene controlling flower initiation in sorghum, *Breed. Sci.*, 53, 353-357.
- 18) Tarumoto, I., Yanase, M., Kadowaki, H., Yamada, T. and Kasuga, S. (2005). Inheritance of photoperiod-sensitivity genes controlling flower initiation in sorghum, *Sorghum bicolor* Moench, *Grassl. Sci.*, 51, 55-61.
- 19) Vos, P., Hogers, R., Bleeker, M., Reijans, M., Vandele, T., Hornes, M., Frijters, A., Pot, J., Peleman, J., Kuiper, M. and Zabeau, M. (1995). AFLP: a new technique for DNA fingerprinting, *Nucleic Acids Res.*, 23, 4407-4414.
- 20) Yano, M., Katayose, Y., Ashikari, M., Yamanouchi, U., Monna, L., Fuse, T., Baba, T., Yamamoto, K., Umehara, Y., Nagamura, Y. and Sasaki, T. (2000). *Hd1*, a major photoperiod sensitivity quantitative trait locus in rice, is closely related to the Arabidopsis flowering time gene *CONSTANS*, *Plant Cell*, 12, 2473-2483.

## ソルガム温度感応遺伝子に連鎖する DNA マーカーのマッピング

高溝 正・中津志野<sup>1</sup>・長村吉晃<sup>2</sup>・藤森雅博<sup>3</sup>・樽本 勲<sup>1</sup>

農研機構畜産草地研究所 飼料作物研究領域, 那須塩原市, 329-2793

<sup>1</sup>大阪府立大学, 堺市, 599-8531

<sup>2</sup>農業生物資源研究所, つくば市, 305-8602

<sup>3</sup>農研機構東北農業研究センター, 盛岡市, 020-0198

### 摘 要

ソルガムの花芽分化は、長日条件下で 20 度以上の温度により遅延する温度感応遺伝子により制御されていると言われる。AFLP を用いたバルク解析法によりソルガム温度感応遺伝子の DNA マーカーを単離した。1024 個の AFLP マーカーから 13 個の優性マーカーと 1 個の共優性マーカーが得られ、それらのうち 7 個が連鎖地図に割り当てられた。*#* または *T* の表現型を示す 33 個体の BC<sub>1</sub>F<sub>2</sub> 集団による連鎖解析の結果、温度感応を司る *T* 座位は第 16AFLP マーカーの末端にあった。QTL 解析の結果もまた、温度感応性遺伝子が単一遺伝子であることを示した。第 16AFLP マーカーのより詳細な位置を特定するため、すでにマッピングされている 145 個の RFLP マーカーとの比較を行った結果、温度感応遺伝子の座位は第 6 染色体上にあり、第 16AFLP マーカーからの距離は 4.0cM と推定された。

キーワード：AFLP, 花芽分化, ソルガム, 温度感応遺伝子

## 畜産草地研究所（つくば地区）における分析型官能評価パネルの確立

佐々木啓介・本山三知代・成田卓美・大江美香・吉村 望<sup>1a</sup>・田島淳史<sup>1</sup>・野村 将・千国幸一<sup>2</sup>

農研機構畜産草地研究所 畜産物研究領域, つくば市, 305-0901

<sup>1</sup>筑波大学, つくば市, 305-8577

<sup>2</sup>農研機構畜産草地研究所 畜産研究支援センター, つくば市, 305-0901

### 要 約

畜産草地研究所（つくば地区）の職員を対象とした分析型官能評価パネリストの選抜を行った。候補者 116 名を、第一次選抜として 5 味選択試験、第二次選抜として味の濃度差識別試験、第三次選抜として食品の違い識別試験ならびに香りの識別試験を用いて選抜した。候補者は、第一次選抜で 69 名、次いで第二次選抜で 40 名に絞り、第三次選抜を経て最終的に 21 名のパネリスト候補者を選抜した。うち 17 名に官能評価の方法および用語に関する訓練を施し、訓練された分析型官能評価パネルを確立した。また、選抜試験の実施時刻は第一次選抜における苦味溶液の選択に、候補者の年齢は第二次選抜における酸味の濃度差識別に、候補者の性別は第三次選抜における香りの識別に、それぞれ統計的に有意な影響をおよぼした。

キーワード：官能評価, 分析型パネル, 選抜, 畜産物, おいしさ

### 緒 言

近年、畜産物の高付加価値化の方向として、「おいしさ」が改めて注目されている。農林水産省が平成 22 年 7 月に公表した家畜改良増殖目標においては、肉用牛について将来的に消費者の視点に立った「おいしさ」指標の必要性が、豚についても消費者ニーズを踏まえた肉質改良の必要性が、それぞれ指摘されている<sup>16)</sup>。また、酪農及び肉用牛生産の近代化を図る基本方針<sup>17)</sup>においても、牛乳・乳製品や牛肉において「消費者・実需者ニーズに対応した生産への質的転換」が謳われている。さらに、牛肉や豚肉においては、やわらかさやジューシーさをもたらすとされる筋肉の脂肪交雑を目指した育種や飼養技術の改良が進められているが、実際には全ての消費者が脂肪交雑を求めているということはなく、牛肉<sup>20,22)</sup> および豚肉<sup>24)</sup> のいずれにおいても、脂肪交雑の少ないものを求める消費者群が一定規模で存在することが示されている。これらの現状を踏まえた場合、これま

での格付や評価手法では評価が困難な特徴ある「おいしさ」を有する畜産物の開発に役立つ新たな品質評価技術がよりいっそう求められていると言える。

「おいしさ」を評価するためには、味や香り、食感に関係する成分や物性を機器分析で測定する手法も有力な手段の一つであり、味や香りについてはセンサー技術を活用した評価も試みられている<sup>2,21)</sup>。しかし、最終的に「消費者が食べたときにどのような味や香り、食感と感じるか」「どのような消費者が、どの程度好む（好まない）か」について調べるためには、ヒトが直接食べて判定する官能評価が現状では不可欠である。

著者らはこれまでに、官能評価を用いた畜産物の品質評価ならびに評価法の開発に取り組んできた。具体的には、研究所内の一般パネルを用いて「エコフィード」利用型豚肉の官能特性と嗜好性の関係を調べ、豚肉における脂肪の溶けやすさに対するパネリストの好みは 2 つの類型に分類できることを示す<sup>23)</sup> とともに、「飼料米」利用型豚肉を原料としたハムについて慣行品との識別はで

きず、嗜好性も遜色ないことを示した<sup>20)</sup>。さらに、著者らは当所内において、食感に関する訓練を施された食感の専門型官能評価パネルを確立し、牛肉の食感を評価する用語を選択するとともに<sup>26)</sup>、牛肉の脂肪交雑はISO5492:1992<sup>5)</sup>において定義される「かみ切りやすさ」「変形しやすさ」の両方を改善することを示した<sup>27)</sup>。これら既報において用いられたパネルは、消費者のモデルである研究所内一般パネルか、もしくは食感専門型パネルである。しかし、今後、多様な飼料資源や家畜品種を活用した、より多様な品質の畜産物についてその特徴を評価するためには、食感だけではなく、味や香りも含めた官能特性について一定水準以上の識別ならびに評価能力を有し、さらに評価手法や多様な評価用語に関する訓練を施した分析型パネルを用いた官能評価が必要である。

そこで著者らは、今後の多様な畜産物の特徴的な「おいしさ」評価に活用するため、畜産草地研究所（つくば地区）の職員を候補者として分析型官能評価パネリストの選抜を実施するとともに、これら選抜されたパネリストに対して訓練を施すことで、畜産物の官能特性評価に適したパネルの確立を目指した。

## 材料と方法

### 選抜試験方法

一般的に、分析型官能評価パネリストの選抜は、甘味、塩味、酸味、苦味、およびうま味の5基本味の感知

能力を調べる5味選択試験、苦味を除く4基本味について濃度差の識別能力を調べる味の濃度差識別試験、および実際の食品の識別試験を組み合わせる。現在一般的な指針とされている「食肉の官能評価ガイドライン」<sup>3)</sup>においても、分析型パネルの選抜方法として古川<sup>4)</sup>の5味識別試験ならびに味の濃度差識別試験が推奨されている。今回の一連の選抜においては、これにさらに、実際の畜産物の味、香り、および食感による総合的な識別能力を判定する食品の差識別試験、ならびに市販のカード型嗅覚検査キットを用いた簡易試験<sup>12,14)</sup>を加え、味、香り、および食感について一定水準以上の感知および識別能力を有するパネリストの選抜を行うこととした。

### パネリスト候補者

パネリスト候補者は、畜産草地研究所（つくば地区）に在籍する一般職員、技術専門職員、研究職員、契約職員、ならびに技術講習生から募集し、121名の応募を得た。応募者のうち、第一次選抜を受験した116名のプロフィールを表1に示す。

### 第一次選抜・5味選択試験

第一次選抜試験は、古川<sup>4)</sup>の5味選択試験によった。具体的には、甘味サンプルとして4.0g/L ショ糖（グラニュー糖、ジェフダ JSN、東京）水溶液、塩味サンプルとして1.5g/L 食塩（精製塩、財団法人塩事業センター、東京）水溶液、酸味サンプルとして0.05g/L 酒石酸（日

表1. 第一次選抜受験者および第三次選抜合格者のプロフィール

性別	一次選抜受験者		三次選抜合格者	
	人数	割合(%)	人数	割合(%)
女性	45	38.8	13	61.9
男性	71	61.2	8	38.1
年齢層				
20代以下	11	9.5	4	19.1
30代	35	30.2	6	28.6
40代	38	32.8	8	38.1
50代以上	32	27.6	3	14.3
平均年齢(平均±標準偏差)	42.5±10.7		38.5±9.8	
喫煙履歴				
喫煙経験なし	78	67.2	17	81.0
過去に喫煙経験あり	18	15.5	2	9.5
喫煙中	20	17.2	2	9.5

本薬局方「酒石酸」、日興製薬、岐阜市）水溶液、苦味サンプルとして0.2g/L無水カフェイン（日本薬局方「無水カフェイン」、エビス製薬、大阪）水溶液、うま味サンプルとして0.5g/L L-グルタミン酸ナトリウム（食品添加物「L-グルタミン酸ナトリウム」、和光純薬、大阪）水溶液の5種類に、蒸留水3個を加えた合計8個のサンプルから、甘味、塩味、酸味、苦味、うま味の5基本味に該当するものを選ばせた。サンプルの提示順序はラテン方格を用いて各味溶液の提示順位が均等になるよう設計した。実施時刻は午前11時、午後1時15分、および午後3時の3通りとし、評価環境は22℃、蛍光灯による照明下とした。また、口すすぎ用に市販のペットボトル充填された純水（「森永やさしい赤ちゃんの水」、森永乳業、東京）を配布し、試験中には自由に使用させた。純水の配布と使用については第二次および第三次選抜においても同様とした。

合格基準は古川<sup>4)</sup>の方法に基づき、8種類の溶液から甘味、塩味、酸味、苦味、およびうま味として選択した5つの回答中の誤数が1個以下とした。

### 第二次選抜・味の濃度差識別試験

第二次選抜試験は、古川<sup>4)</sup>の味の濃度差選択試験によった。具体的には、甘味、塩味、酸味、およびうま味について、表2に示す組み合わせでわずかな濃度差の2個の水溶液を提示し、各味のより強い方を選ばせた。サンプルの提示順序はラテン方格を用いて、味の強い方の提示順序が均等になるよう設計した。実施時刻は第一次選抜と同様に午前11時、午後1時15分、および午後3時の3通りとし、評価環境は22℃、蛍光灯による照明下とした。

合格基準は古川<sup>4)</sup>の方法に基づき、表2に示す全8問中の誤数が2個以下とした。

### 第三次選抜・食品および香りの識別試験

第三次選抜試験では、食品の識別試験および香りの識別試験を行った。食品の識別試験においては、畜産物に関連する味、香り、および食感の識別能力による選抜を行うという目的に照らし、濃度の異なるコンソメスープの識別、牛乳と低脂肪乳の識別、および豚ロース肉と豚もも肉の識別について、それぞれ3点識別試験を行った。コンソメスープについては、市販のコンソメスープ粉末（「クノール ビーフコンソメ」、味の素、東京）を9.6g/Lまたは11.2g/Lの濃度で溶解させたものをサンプルとして用い、2点の9.6g/Lコンソメスープと1点の11.2g/Lコンソメスープの組み合わせから、1つだけ異なるものを選ばせた。また、牛乳についてはトモエ乳業（古河市）製の牛乳および低脂肪乳をサンプルとし、2点の牛乳と1点の低脂肪乳の組み合わせから、一つだけ異なるものを選ばせた。豚肉については、つくば市内の小売店で購入したカナダ産豚ロースブロックおよび豚大腿二頭筋ブロックを筋線維に垂直に5mm厚にスライスし5%食塩水にくぐらせたものを230℃のオープン（SSC-05SCNU、マルゼン、東京）で5分間調理し、その後直径3cmの円形に整形したものをサンプルとした。設問においては、2点のロースと1点の大腿二頭筋の組み合わせから、一つだけ異なるものを選ばせた。各種食品の3点識別試験について、それぞれ2回ずつ合計6問を出題し、合格基準は6問中の誤数が1個以下とした。

香りの識別試験においては、カード型嗅覚検査キット「オープンエッセンス」（和光純薬、大阪）<sup>12,14)</sup>を用いた。これは、12種類一組のカードからなる測定キットであり、カードを広げた際にカード内側に塗布されている匂いを嗅ぎ、選択肢からその匂いを表す用語を選択・解答させるものである。本キットは従来のスティック型嗅覚検査法を比較して簡便性に優れるとともに、本キットの検査結果は基準嗅力検査結果と有意な相関が認められ

表2. 味の濃度差識別試験用の提示サンプル濃度

味の種類	溶質	1回目			2回目		
		提示溶液1 (g/L)	提示溶液2 (g/L)	濃度比	提示溶液1 (g/L)	提示溶液2 (g/L)	濃度比
甘味	ショ糖	50.0	55.0	1.10	50.0	52.5	1.05
塩味	食塩	10.0	10.6	1.06	10.0	10.3	1.03
酸味	酒石酸	0.20	0.24	1.20	2.00	0.22	1.10
うま味	グルタミン酸ナトリウム	2.00	2.66	1.33	2.00	2.42	1.21

当性も高く<sup>14)</sup>、パネリストの選抜に用いる手法として適当であると考えられた。小早川<sup>11)</sup>によれば、本カードキットを用いた場合、全12問中10問以上正解した場合に、香りの識別能力が被験者全体の上位50%以内に入ることが示されている。本選抜試験では、香りの識別に関して平均的な被験者以上の能力を有する候補者を選抜するという目的を有することから、合格基準は12問中の正解数が10問以上とした。

実施時刻は午前11時、午後1時15分、および午後3時の3通りとし、評価環境は22℃、食品の識別試験については外観での判別がなされないよう、赤色灯による照明下で、香りの識別試験については蛍光灯下でそれぞれ実施した。

第三次選抜における最終合格基準は、食品の識別基準の合格基準および香りの識別試験の合格基準の双方を満たすこととした。

#### 候補者の訓練

最終的に選抜された候補者19名のうち17名について、味、香りおよび食感のより詳細な評価手法や評価用語に関する訓練を施した。具体的には、官能評価の手法および味覚、嗅覚、および食感の感知メカニズムに関する講義を行った。味の評価に関する訓練としては、5基本味溶液について、第一次選抜における5味選択試験で用いた濃度を用いた識別訓練を行うとともに、うま味におけるグルタミン酸と核酸系うま味物質のちがいについて、L-グルタミン酸ナトリウム水溶液および核酸系うま味調味料(リボヌクレオチドナトリウム「WP」、味の素株式会社、東京)水溶液を用いた識別訓練を実施した。さらに、味と口中香の区別について、5.0g/L ショ糖溶液および400 μL/L バニラエッセンス(「バニラエッセンス」、明治屋、東京)添加5.0g/L ショ糖溶液による2点比較法による訓練をそれぞれ実施した。嗅覚についてはパネル訓練用匂いキット(Training 80、第一薬品産業、東京)とともに、食肉で生じることがある香り表現用語について、それらに相当する香気物質をにおい紙法により実際にかがせながら説明し、訓練とした。具体的には、金属臭、糞臭、雄臭、発酵乳に特有なバター臭、および食肉と乳製品の双方で魚臭の原因となる各化合物として1-オクテン-3-オン<sup>7)</sup>(シグマ・アルドリッチ、ドイツ)、スカトール<sup>15)</sup>(パネル選定用基準臭、第一薬品産業、東京)、アンドロステノン<sup>18)</sup>(5a-Androst-16-en-3-one、シグマ・アルドリッチ、ドイツ)、ジアセチル<sup>9)</sup>(2,3-ブタンジオン、和光純薬、大阪)、トリメチルアミ

ン<sup>19,28)</sup>(トリメチルアミン標準液、和光純薬、大阪)をそれぞれ用いるとともに、酸化臭については市販のサラダ油を金属製秤量缶に移し、インキュベーター内で120℃、72時間処理することで実際に酸化臭を呈するに至ったものを香気サンプルとして用いた。食感についてはISO5492:2008<sup>6)</sup> 収載食感表現用語について、参照となる食品<sup>6)</sup>を実際に食べさせながら用語説明を実施し、訓練とした。

#### 統計解析

候補者のプロフィール等が試験結果におよぼす影響を検討するために、第一次および第二次試験については各設問の正解・不正解を、第三次試験については、食品については設問ごとの正解数を、香りについては全体の正解数を目的変数とした一般化線形モデル分析を行った。分析には統計パッケージSAS(バージョン9.13、SASインスティテュートジャパン、東京)のgenmodプロシジャを用い、説明変数としては、性別、喫煙履歴(喫煙中、過去に喫煙経験あり、喫煙経験なし)、および試験の実施時刻をカテゴリカル変数として、年齢を連続型変数としてそれぞれ用いた。第一次および第二次選抜の結果については、目的変数の分布は二項分布、リンク関数としてロジット関数を指定した。また、第三次選抜の結果については、目的変数の分布はポアソン分布、リンク関数としては対数関数を指定した。

#### 結果および考察

##### 第一次選抜・5味選択試験

応募者121名中の受験者は116名であり、受験率は95.9%であった。各基本味の正答率を表3に、正答数ごとの人数分布を表4に示す。苦味の正解率が他の基本味と比較して低かった。また、全体の平均正答数は3.8問であり、設定した合格ラインに達したものは69名、合格率は59.5%であった。

表3. 第一次選抜試験における各基本味の正答率

	正答率(%)
甘味	85.3
塩味	73.3
酸味	86.2
苦味	53.4
うま味	77.6

一般化線形モデル分析の結果、甘味および酸味の選択に対して候補者のプロフィールや試験実施時刻は影響をおよぼさなかった。塩味の選択に対しては、候補者の年齢が増加した場合正答率が低下する傾向が認められた（ $P=0.067$ ）。うま味の選択に対しては、女性の方が正答率が高い傾向（ $P=0.097$ ）および実施時刻が午後1時15分の場合に正答率が低い傾向（ $P=0.080$ ）がそれぞれ認められた。さらに、苦味については、実施時刻が午後1時15分の場合において、正答率が有意に上昇するとともに（ $P=0.031$ ）、年齢の上昇により正答率が低下する傾向（ $P=0.051$ ）および現在喫煙中の場合に正答率が低下する傾向（ $P=0.053$ ）がそれぞれ認められた。

**第二次選抜・味の濃度差識別試験**

第一次選抜合格者69名のうち68名が第二次選抜を受験し、受験率は98.6%であった。設問ごとの正答率を表5に、正答数ごとの人数分布を表6にそれぞれ示す。全体の平均正答数は5.7問であり、設定した合格ラインに達した候補者は40名、合格率は58.8%であった。

表4. 第一次選抜試験の正答数ごとの人数分布

正答数	人数	割合(%)
5問	43	37.1
4問	26	22.4
3問	28	24.1
2問	15	12.9
1問	3	2.6
0問	1	0.9

表6. 第二次選抜試験における正答数ごとの人数分布

正答数	人数	割合(%)
8問	6	8.8
7問	12	17.6
6問	22	32.4
5問	13	19.1
4問	10	14.7
3問	5	7.4
2問	0	0
1問	0	0
0問	0	0

一般化線形モデル分析の結果、うま味に関する設問の1回目については、喫煙履歴と回答の傾向に偏りがあり、係数を推定できなかった。また、酸味に関する設問の2回目については、年齢の上昇により正答率が有意に低下した（ $P=0.030$ ）。性別および実施時刻は、どの設問においても正答率に影響をおよぼさなかった。

**第三次選抜・食品および香りの識別試験**

第二次選抜合格者40名のうち35名が第三次選抜を受験し、受験率は87.5%であった。食品の識別については設問ごとの平均正答数を、香りの識別については全体の平均正答数を表7に示す。食品の識別における全体の平均正答数は5.0問であり、設定した合格ラインに達した候補者は26名であった。また、香りの識別については、全体の平均正答数は9.9問であり、設定した合格ラインに達した候補者は24名であった。食品および香りの識別試験において両方とも合格ラインに達した候補者は21名であった。最終的に選抜された21名の候補者のプロフィールを表1に示す。

表5. 第二次選抜試験における各設問の正答率

	正答率(%)	
	1回目	2回目
甘味	76.5	63.2
塩味	63.2	64.7
酸味	77.9	69.1
うま味	83.8	66.2

表7. 第三次選抜における各設問の正答数

設問	識別の内容	出題数	正答数 (平均値±標準偏差)
コンソメスープ	濃度差	2	1.71 ± 0.52
牛乳	牛乳と低脂肪乳	2	1.91 ± 0.28
豚肉	ロースともも	2	1.37 ± 0.81
香り		12	9.89 ± 1.60

一般化線形モデル分析の結果、食品の識別試験においては、候補者のプロフィールや試験実施時刻は各設問および全体の正答数に影響をおよぼさなかった。香りの識別試験においては、性別が女性の場合、正答数を増加させる傾向が認められた ( $P=0.073$ )。

### 総合考察

分析型官能評価パネルが具備すべき条件として、幅広い感覚について感度が高いことが複数の方法によって保証されている<sup>4)</sup>とともに、一定以上の人数が必要である<sup>30)</sup>ことが示されている。

本研究においては、一般的に推奨される5味選択試験、味の濃度差識別試験、および食品の識別試験を通じ、味覚の基本的な感度や畜産物の味・香り・食感を識別する能力を対象とし、さらに香りの識別試験を併用し、香りの識別能力についても対象とした分析型パネルの選抜を実施した。特に、食品の識別試験において畜産物を供試サンプルとしたことで、畜産物の官能特性に対してより感度が高いパネルが選抜されたものと考えられた。また、本選抜では幅広いプロフィールの候補者から応募を得ることができ、年齢および性別について極端な偏りのない(表1)パネルが選抜されたものと考えられた。

これらのパネルリストに対し、味覚、嗅覚、および食感に関して感じ方や評価用語、および評価方法について訓練を施した。それぞれの訓練を通じ、パネルリストは官能評価方法について理解するとともに、各感覚の用い方や表現についても十分理解したものと思われ、今後の官能評価において的確かつ再現性の高い結果が得られるものと期待される。訓練終了後に実施した発酵乳に関する官能評価においても、3点識別法において高い正解率が確認されたことから(データ示さず)、官能評価手法を十分理解し、なおかつ高い識別能力を有する分析型パネルが確立されたものと考えられた。官能評価に関する規格を定めるJIS Z9080においては、望ましい評価者数として順位法、採点法、および格付け法では「選ばれた評価者」で5名以上、識別試験においては、2点試験法の例では「専門家」で7名以上とされている<sup>30)</sup>。さらに必要な訓練や経験を積み重ねることで、より信頼性の高いパネルとすることが必要である。

本選抜においては、候補者のプロフィールと選抜試験結果の関係についてもあわせて検討を行った。一般的に、年齢、性別、および喫煙履歴は味覚および嗅覚感受性に影響をおよぼすものと考えられている。箕原<sup>11)</sup>はうま

味を除く4基本味について、その識別能におよぼす年齢、性別、および喫煙の影響を調べ、女性より男性が4基本味の全てにおいて敏感に識別できること、加齢は味覚識別能を低下させること、そして喫煙は味覚識別能を鈍化させるが、その度合いがもっとも高いのは苦味であることを示している。また、年齢と味覚識別能については、年齢による識別能の低下が、特に塩味については閾値レベルで、酸味と苦味については閾値・知覚強度ともに感受性が低下するとまとめられている<sup>29)</sup>。本研究においては、第一次選抜において年齢の増加により塩味と苦味の正答率の低下傾向や、喫煙により苦味の正答率が低下する傾向、第二次選抜における酸味の濃度差識別の正答率の年齢上昇による低下がそれぞれ認められたが、これは上記で述べた既報の結果とよく符合しており、本研究において認められた年齢、性別および喫煙履歴と選抜試験における回答の関係についても妥当な結果であると考えられた。また、嗅覚感受性は年齢による減少<sup>10)</sup>、喫煙による減退<sup>8)</sup>、性別による違い<sup>1)</sup>がそれぞれ報告されているが、本研究においては性別による違いのみが認められた。本研究で実施した香りの識別試験は被験者が35名と少なく、またこの段階での喫煙者および喫煙経験者が2名および3名と極めて少ない人数であったことや、平均正答数が全12問中9.9問であり、かつ全員が6問以上正解するなど高水準の結果であったことが、年齢および喫煙による影響が認められなかった原因の一つであると考えられた。

以上のことより、本研究において実施された官能評価パネルリストの選抜結果は妥当なものであると結論づけられた。今後、多様な飼料資源や家畜品種を活用して生産された畜産物の特徴的な官能特性を評価するために本研究で確立されたパネルを活用し、その結果を消費者型官能評価の結果と組み合わせることで、多様な消費者ニーズに応えられる特徴的な「おいしさ」を有する畜産物の評価および表示技術、ならびに生産技術を開発していく必要がある。

### 謝 辞

本研究実施にあたり、パネルリスト候補者として選抜試験へのご協力をいただいた畜産草地研究所つくば地区在籍の一般職員、技術専門職員、研究職員、契約職員、および技術講習生各位に深く感謝いたします。また、技術的な支援をいただいた畜産物研究領域契約職員、遠藤弓美子氏ならびに清水明美氏に感謝いたします。なお、本

研究は、農林水産省委託プロジェクト「自給飼料を基盤とした国産畜産物の高付加価値化技術の開発（4系・自給飼料多給による高付加価値豚肉生産技術の開発）」において行われた。

## 引用文献

- 綾部早穂・斉藤幸子・内藤直美・三瀬美也子・後藤なおみ・市川寛子・出口雄一・小早川達（2005）. スティック型嗅覚同定能力検査法（OSIT）による嗅覚同定能力：年代と性別要因, *Aroma Research*, 6, 368-371.
- Chikuni, K., Oe, M., Sasaki, K., Shibata, M., Nakajima, I., Ojima, K. and Muroya, S. (2010). Effects of muscle type on beef taste-traits assessed by an electric sensing system, *Anim. Sci. J.*, 81, 600-605.
- 独立行政法人家畜改良センター（2005）. 食肉の官能評価ガイドライン, 日本食肉消費総合センター, 東京, 151p.
- 古川秀子（1994）. おいしさを測る, 幸書房, 東京, 140p.
- International Organization for Standardization (1992). ISO5492: 1992 Sensory analysis – Vocabulary, International Organization for Standardization, Geneva, 22p.
- International Organization for Standardization (2008). ISO5492: 2008 Sensory analysis – Vocabulary, International Organization for Standardization, Geneva, 107p.
- Im, S., Hayakawa, F., and Kurata, T. (2004). Identification and sensory evaluation of volatile compounds in oxidized porcine liver, *J. Agric. Food Chem.*, 52, 300-305.
- Ishimaru, T., and Fuji, M. (2007). Effects of smoking on odour identification in Japanese subjects, *Rhinology*, 45, 224-228.
- 伊藤敏敏（1998）. (4) 乳酸菌の作る代謝産物の特性, 動物資源利用学（伊藤敏敏・渡邊乾二・伊藤良編）, 文永堂出版, 東京, 142-146.
- Kaneda, H., Maeshima, K., Goto, N., Kobayakawa, T., Ayabe-Kanamura, S., and Saito S. (2000). Decline in taste and odor discrimination abilities with age, and relationship between gestation and olfaction, *Chem. Senses*, 25, 331-337.
- 小早川達（2008）. 新しい検査法 – Open Essence（嗅覚同定能力研究用カードキット）-, <http://riodb.ibase.aist.go.jp/db068/db2/new.html>
- 小林正佳（2010）. 嗅覚に関する検査 嗅覚同定検査, *JOHNS*, 26, 1117-1122.
- 箕原美奈恵・伊藤宜則・大谷元彦・佐々木隆一郎・青木國雄（1988）. 健常成人の味覚識別能に関する研究 – 喫煙との関連性について –, *日本衛生学雑誌*, 43, 604-615.
- 西田幸平・小林正佳・荻原仁美・竹尾哲・北野雅子・竹内万彦（2010）. カード型嗅覚同定検査「Open Essence」の有用性, *日本耳鼻咽喉科学会会報*, 113, 751-757.
- 西岡輝美・石塚譲・因野要一・入江正和（2011）. 豚脂肪中のスカトール含量と官能評価への影響, *日本畜産学会報*, 82, 147-153.
- 農林水産省（2010）. 家畜改良増殖目標（平成22年7月）, 農林水産省, 東京, 35p.
- 農林水産省（2010）. 酪農及び肉用牛生産の近代化を図るための基本方針（平成22年7月）, 農林水産省, 東京, 37p.
- Pearson, A.M., Gray, J.I. and Brennand, C.P. (1994). Species-specific flavors and odors, In *Quality Attributes and Their Measurement in Meat, Poultry, and Fish Products*, *Advances in Meat Research*, 9, 222-249, Blackie Academic & Professional, Glasgow, United Kingdom.
- Poste, L.M. (1990). A sensory perspective of effect of feeds on flavor in meats: poultry meats, *J. Anim. Sci.*, 68, 4414-4420.
- Sasaki, K. and Mitsumoto, M. (2004). Questionnaire-based study on consumer requirements for beef quality in Japan, *Anim. Sci. J.*, 75, 369-376.
- Sasaki, K., Tani, F., Sato, K., Ikezaki, H., Taniguchi, A., Emori, T., Iwaki, F., Chikuni, K. and Mitsumoto, M. (2005). Analysis of pork extracts by taste sensing system and the relationship between umami substances and sensor output, *Sens. Mater.*, 17, 349-356.
- 佐々木啓介・三津本 充・合崎英男（2006）. 牛肉購入時における消費者の着目点の分類, *日本畜産学会報*, 77, 67-76.
- Sasaki, K., Nishioka, T., Ishizuka, Y., Saeki, M., Kawashima, T., Irie, M. and Mitsumoto, M. (2007).

- Comparison of sensory traits and preferences between food co-product fermented liquid (FCFL)-fed and formula-fed pork loin, *Asian-Aust. J. Anim. Sci.*, 20, 1272-1277.
- 24) 佐々木啓介・本山三知代・中島郁世・大江美香・勝俣昌也 (2009). 豚肉の外観, 「飼料米給与」表示, ならびに価格が消費者の豚肉選択に及ぼす影響 - 研究所一般公開来場者を対象とした検討 -, 日本養豚学会誌, 46, 60-70.
- 25) 佐々木啓介・本山三知代・成田卓美・澤田一彦・吉野宗明・齊藤真二・石田藍子・京谷隆侍・中島一喜・橋内克弘・勝俣昌也 (2009). 飼料用玄米給与豚肉を原料としたハムの識別性および嗜好性, 日本養豚学会誌, 46, 200-203.
- 26) Sasaki, K., Motoyama, M., Yasuda, J., Yamamoto, T., Oe, M., Narita, T., Imanari, M., Fujimura, S. and Mitsumoto, M. (2010). Beef texture characterization using internationally established texture vocabularies in ISO5492: 1992: Differences among four different end-point temperatures in three muscles of Holstein steers, *Meat Sci.*, 86, 422-429.
- 27) Sasaki, K., Motoyama, M. and Narita, T. (2012). Increased intramuscular fat improves both 'chewiness' and 'hardness' as defined in ISO5492: 1992 of beef Longissimus muscle of Holstein × Japanese Black F1 steers, *Anim. Sci. J.*, in press.
- 28) Uebach, G. (1990). Effect of fees on flavor in dairy foods. *J. Dairy Sci.*, 73, 3639-3650.
- 29) 横向慶子 (1997). 高齢者の味覚と嗜好, 最新味覚の科学 (佐藤昌康・小川尚編), 朝倉書店, 東京, 58-82.
- 30) 財団法人日本規格協会 (2004). JIS Z9080: 2004 官能評価分析一方法, 財団法人日本規格協会, 東京, 58p.

## Establishment of an Analytical Sensory Panel at the NARO Institute of Livestock and Grassland Science (Tsukuba)

Keisuke SASAKI, Michiyo MOTOYAMA, Takumi NARITA, Mika OE, Nozomi YOSHIMURA<sup>1a</sup>,  
Atsushi TAJIMA<sup>1</sup>, Masaru NOMURA and Koichi CHIKUNI<sup>2</sup>

Animal Products Research Division,  
NARO Institute of Livestock and Grassland Science, Tsukuba, 305-0901 Japan

<sup>1</sup> University of Tsukuba, Tsukuba, 305-8577 Japan

<sup>2</sup> Livestock Research Support Center,  
NARO Institute of Livestock and Grassland Science, Tsukuba, 305-0901 Japan

### Summary

Screenings of an analytical sensory panel were conducted by staff at the NARO Institute of Livestock and Grassland Science (Tsukuba). A hundred and sixteen candidates were subjected to a first screening discrimination test of 5 basic tastes, a second screening discrimination test between the differences of seasoning concentration, and a third screening discrimination test of the differences of food and of the characteristics of odours. As a result, 69, 40, and 21 candidates were selected based on the first, second, and third screenings, respectively. Seventeen successful candidates of the third screening were trained in the methodology and terminology of the sensory test. The time of day and the age and gender of the candidate had statistical significant effects on the results of the screening tests, such as bitterness discrimination at the first screening, discrimination among the differences of sourness intensity at the second screening, and odour discrimination at the third screening. From these screening tests and the follow-up training, a trained analytical sensory panel was established in the institute.

Key words: sensory evaluation, analytical panel, screening, animal products, preference

---

<sup>a</sup> Technical student, Animal Products Research Division, NILGS, Tsukuba, 305-0901 Japan

# Structure and Phase Characterization of Triacylglycerols by Raman Spectroscopy

Michiyo MOTOYAMA

Animal Products Research Division,  
NARO Institute of Livestock and Grassland Science, Tsukuba, 305-0901 Japan

## Abstract

Triacylglycerols (TAGs) are one of the main forms of energy storage in living organisms. Natural fats, which are nothing but the multicomponent TAG systems, are widely used in industrial products such as food, medicine and cosmetics. Industrial demands promote the studies on thermophysical properties of the multicomponent TAG systems for a long time; however, the whole picture of their phase behavior is yet to be drawn. With a view to understand the complicated phase behavior of natural fats, I have investigated on the physical mixtures of TAGs by Raman spectroscopy.

Firstly, the background of this study is introduced (Chapter 1). Raman spectroscopy is the appropriate method to characterize TAGs, particularly when they exist in multicomponent systems. The structure and phase behavior of TAGs are then summarized with emphasis on the recent developments (Chapter 2). The interesting phase properties of TAGs, polymorphism and “molecular compound” formations, are introduced. The factors affecting these phase properties, such as crystallization conditions, are also mentioned. Next, the spectral features of TAGs are described in relation to their phase specific structures (Chapter 3). On the basis of the accumulated spectroscopic data, Raman spectroscopy has contributed to reveal the detailed structure of TAG polymorphs. Based on the knowledge described in these chapters, two TAG systems are studied. They include a TAG binary system that is known to form a molecular compound (Chapter 4) and several natural fats that are widely used in industrial products (Chapter 5).

The results of the present study indicate that a third component, a molecular compound, is formed in the TAG binary system and its structure seems to be influenced decisively by crystallizing procedures. The molecular compound may be the phase dynamically formed by crystallization, rather than existing stationary in the liquid phase as previously considered (Chapter 4). In addition, the present study implies that the molecular compound may exist not only in a model binary system but also in real multicomponent systems. It is also shown that one can differentiate the origin of natural fats by detecting the difference in their polymorphic phases by using Raman spectroscopy (Chapter 5).

Finally, future prospects of Raman spectroscopic studies on TAG systems for deepening the present understanding are presented (Chapter 6). Recent developments on the spectrometer offer bright future prospects for Raman spectroscopic studies on multicomponent TAG systems. Raman spectroscopy helps us to draw the whole picture of the phase behavior of natural fats.

**Key words:** polymorphism, triacylglycerol multicomponent system, porcine fat, bovine fat, discrimination technique

## Chapter 1

### Introduction

Triacylglycerols (TAGs) possess ideal properties for the energy storage in living organisms. They have high oxidation energy that is more than twice as high as those of sugars or proteins. Their hydrophobicity enables TAGs to self-assemble and exist without raising the osmotic pressure in a cell. They are one of the most important constituent of the life system. Despite these facts, TAGs have been put to the marginal area of biological studies, presumably because of their varying chemical structures and complex phase behaviors.

TAGs are familiar to anybody. They are used widely in many industrial products. Natural fats, which are nothing but the multicomponent TAG systems, are the major components of food as well as those of the matrices of cosmetics and medicine.<sup>23)</sup> They are made up of more than 30 TAG species<sup>32)</sup> with major constituent fatty acid generally being oleic acid.<sup>78)</sup> Oleic acid is a representative unsaturated fatty acid that has one *cis* C=C double bond. Industrial demands, especially those for better chocolate production, have promoted the studies on thermophysical properties of TAGs in the past 100 years.<sup>21,93)</sup> By the use of differential scanning calorimetry and pulse nuclear magnetic resonance, the crystallization and polymorphism of natural fats have been studied.<sup>115)</sup> It is widely known today that TAG crystal polymorphism has considerable influence on the texture, fluidity and appearance of the final fat products.<sup>28)</sup> However, the whole picture of polymorphic phase behavior of natural fats is yet to be drawn.

In order to study the polymorphic behavior of natural fats in more detail, TAG binary-systems as well as single-TAG systems are important as model systems. In fact, these systems have been investigated extensively by X-ray diffraction (XRD). XRD is powerful for TAG polymorph identification since each polymorph has its own wide angle and small angle XRD patterns derived from their particular subcell and layer structures. Furthermore, introduction of high flux X-ray beam by synchrotron radiation enables time resolved measurements ( $\sim 10$  s)<sup>118)</sup> of polymorphic transformations of TAGs. This makes it possible to detect and measure transient phases which

were often difficult to study because of their thermal instability.<sup>34)</sup> Thanks to these XRD studies, a number of interesting phenomena occurring in TAG model systems have been elucidated.

The formation of "molecular compounds" is one of these interesting phenomena.<sup>18,48)</sup> When two TAG species that have specific interactions with each other are mixed, they form a molecular compound at a fixed mixing ratio. A molecular compound behaves like a new, pure TAG species with unique phase behavior that differs from those of its component TAGs. All TAG species that have so far been reported to form molecular compounds have the oleic acyl moieties. The formation of molecular compounds is thought to be mediated by the incompatible interaction between oleic and saturated acyl moieties and the compatible interactions between the oleic acyl moieties of the component TAGs.<sup>33)</sup>

Another interesting phenomenon is the polymorphism. It has been suggested that the structure of the polymorph that appears first on crystallization determines the structure of the subsequently formed polymorphs and therefore the phase behavior.<sup>24)</sup> The TAG species having both unsaturated and saturated acyl moieties shows this first-appearing polymorph whose structure can be distinguished from those of the other TAGs.<sup>70)</sup> It is suggested that this may be one of the causes for the complicated polymorphic behavior of natural TAGs containing both saturated and unsaturated acyls.

Despite the above mentioned interesting indications, no precise structural data of the TAGs containing unsaturated acyls are available from single-crystal XRD analysis. The primary reason for this is the difficulty in obtaining the single crystals of TAGs. Crystals with adequate size for single-crystal XRD are difficult to be obtained. Even though they are obtained, the crystals are too soft to handle. Also, the crystal quality is often low especially for the TAGs which contain unsaturated acyls. Single-crystal XRD data have been reported so far only for three on TAGs and they are TAGs having saturated acyls only.<sup>22,30,51)</sup>

Vibrational spectroscopies, namely Raman spectroscopy and infrared absorption spectroscopy, have contributed to reveal the detailed TAG structures on the basis of the accumulated spectroscopic data

of basic molecules such as polyethylene,<sup>97-99,108,110-114)</sup> paraffins,<sup>43,95,96)</sup> *n*-alkanes<sup>42,101,103,105,130)</sup> and fatty acids.<sup>40,41,47,54)</sup> The oleoyl acyl conformation,<sup>16,106)</sup> the alkyl-chain-plane orientation<sup>45)</sup> and the length of *trans* C-C chain<sup>126)</sup> of TAG polymorphs have been studied in detail using these methods. The vibrational bands reflecting the alkyl-chain-plane orientation have been used to distinguish the TAG polymorphs.<sup>4,12,13,90,127)</sup> Though it has not been fully appreciated, vibrational spectroscopy has a distinct advantage when one tries to deal with multicomponent TAG systems. A vibrational spectrum as a whole is often called “molecular finger print”. By using this characteristic of vibrational spectra, one can extract information on the phases existing in complex TAG systems.

Within the context of “metabolic syndrome” in recent years, it can be said that Raman spectroscopy is a promised method to study TAGs. It has been used to study the status of TAGs in cells.<sup>107)</sup> Raman spectroscopy is most suitable to study TAGs in the aqueous systems because it is not too sensitive to the presence of water. Even when the system contains more than 90w/w% of water, well resolved spectral features of lipids are obtainable.<sup>54)</sup> The large polarizability of lipids gives strong Raman scattering; lipids are therefore tractable molecules for Raman spectroscopy. Their structural changes are reflected with high sensitivity in the spectra even though they are in aqueous systems. For example, Raman spectroscopy has been applied to monitor the breakdown of TAG complex in lipoprotein particles in an aqueous system.<sup>9)</sup>

I have used Raman spectroscopy to study several selected binary/multi- component TAG systems, with a view to clarify the complicated phase behavior of natural fats. In the present thesis, the structure and phase behavior of TAGs are summarized with emphasis placed on recent developments (Chapter 2). The spectral features of TAGs are then described in relation to their phase specific structures (Chapter 3). On the basis of these, two TAG systems are studied. They include a TAG binary system that is known to form a molecular compound (Chapter 4) and several natural fats that are widely used in industrial products (Chapter 5). Future prospects of Raman spectroscopic studies on TAG systems for

deepening the present understanding are also presented (Chapter 6).

## Chapter 2 Structure and Phase Behavior of Triacylglycerols

### Abstract

TAGs possess the basic structure of lipids: a glycerol backbone and acyl chains attached to it. They are the biological molecules, and oleoyls are the major constituent acyls of the TAGs observed in natural fats. TAGs form crystals with layer structure just like other long chain molecules, and exhibit a complex polymorphic phase behavior. Three polymorphs with different subcell structure,  $\alpha$ ,  $\beta'$  and  $\beta$ , are generally observed. Polymorphic transformation goes monotropically in this order in accord with thermal conditions. It is also known that TAGs form “molecular compound” in their binary systems. A molecular compound behaves like a new, pure TAG species with unique phase behavior that differs from those of its component TAGs. The formation of a molecular compound is thought to occur in terms of the specific intermolecular interactions between oleic acyl moieties of the component TAG molecules. In this chapter, the factors affecting TAG structures and phase behavior are summarized with emphasis on the recent developments.

### Structure of TAGs

TAGs possess the basic structure of lipids: a glycerol backbone and acyl chains attached to it (Fig. 1). This basic structure is also conserved in the other important lipids, such as the main classes of phospholipids and glycolipids (Fig. 2).

In order to designate the stereochemistry of TAGs, the “*sn*” notation which stands for ‘stereochemical numbering’ is used in a manner similar to that used for the other glycerol containing lipids. When the glycerol molecule is drawn in a Fisher projection with the secondary hydroxyl group to the left of the central prochiral carbon atom, the carbons are numbered 1, 2 and 3 from top to bottom. Molecules that are stereospecifically numbered in this fashion have the prefix “*sn*” immediately preceding the term “glycerol” in the name

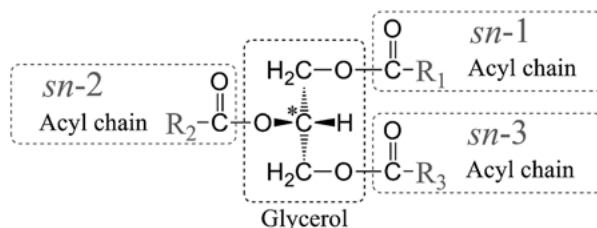


Fig. 1. Structure of a triacylglycerol (TAG). TAGs are esters of a glycerol (propane-1,2,3-triol) and three fatty acids.

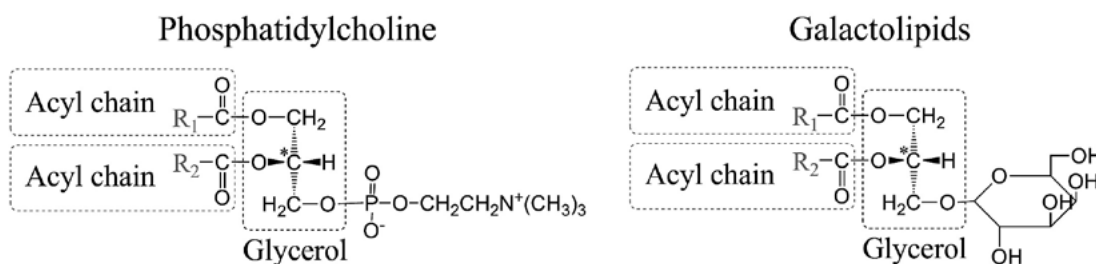


Fig. 2. A phospholipid and a glycolipid: The basic structure is widely observed in lipids

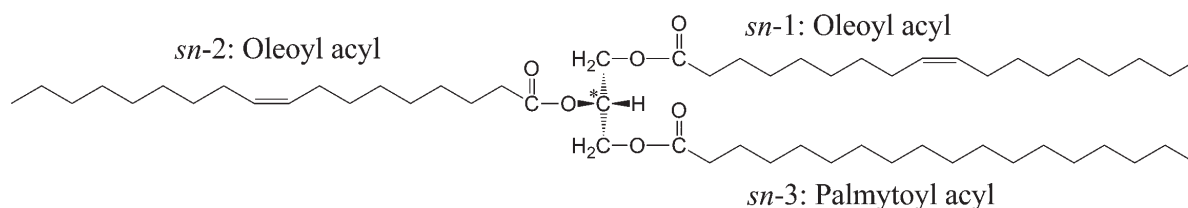


Fig. 3. 1,2-Dioleoyl-3-palmitoyl-*sn*-glycerol (OOP).

of the compound. The TAG molecule in Fig. 3 is therefore called “1, 2-dioleoyl-3-palmitoyl-*sn*-glycerol”. This TAG molecule is also called “OOP” for short: “O” being the abbreviation for “oleic acyl” and “P” being for “palmitic acyl” wherein they are arranged in *sn* order.

The shape of a TAG molecule in solid phase is often compared to a “tuning fork” or the alphabet “h” (Fig. 4). To achieve these shapes, dihedral angles different from  $180^\circ$  which is normally expected are introduced along the skeletal bonds of the glycerol and of the acyl chains approximated to the glycerol. Generally, *sn*-1 and -3 acyl chains are oriented in one direction and *sn*-2 in the opposite direction as shown in Figs. 1 and 3. When the chain placed in *sn*-1 and -3 position are very different in their structure (*e.g.* short or unsaturated), this configuration (*sn*-1 and -3 opposed to -2) is not possible. There is an X-ray diffraction study which indicates that, in

some crystal forms of PPO and SSO (S: stearic acyl), *sn*-1 and -2 chains point same direction.<sup>92)</sup> Such a conformation is common in glycerophospholipids and glyceroglycolipids (Fig. 2).

The major factors that influence the physical properties of TAGs are the chemical structure of each acyl

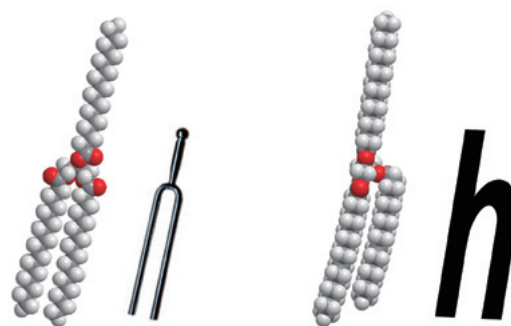


Fig. 4. Shapes of a triacylglycerol molecule

chain and its *sn* position. They are described in detail in the next section.

### Mechanism deciding TAG composition

TAGs are the biological molecules and the major constituents of natural fats and oils.<sup>87)</sup> All types of eukaryotes and a small group of prokaryotes accumulate TAGs as their energy source.<sup>74,131)</sup>

Table 1 shows the fatty acid composition of natural fats. Oleic acid (C18:1), palmitic acid (C16:0), stearic acid (C18:0) and linoleic acid (C18:2) are the main constituents of TAGs. The fatty acid chains occurring in nature generally have even numbers of carbon atoms. This is because of the units of fatty acid synthesis. The *de novo* synthesis of fatty acids begins with introducing two carbons from malonil coenzyme A, and the fatty acid chain elongation proceeds with adopting also two carbons from malonil coenzyme A and acyl coenzyme A (Fig. 5).

The melting points of saturated fatty acids are shown in Fig. 6. The longer acids show the higher melting points. They show the odd-even-chain length effects: even numbered fatty acids have higher melting points than odd numbered ones. This trend is consistent with common knowledge of the odd-even-chain length effects on melting point observed in *n*-alkanes.<sup>52)</sup>

Table 1. Fatty acid composition of a plant oil and an animal fat (w/w%)<sup>78)</sup>

Fatty acid <sup>a</sup>	Olive oil	Porcine fat
C10:0	0.0	0.1
C12:0	0.0	0.1
C14:0	0.0	1.5
C14:1	0.0	0.1
C15:0	0.0	0.1
C16:0	9.9	24.7
C16:1	0.7	3.3
C17:0	0.7	0.3
C17:1	0.0	0.4
C18:0	3.2	11.7
C18:1	75.0	44.7
C18:2, n-6	10.4	10.9
C18:3, n-3	0.8	0.6
C20:0	0.0	0.2
C20:1	0.0	0.7
C20:2, n-6	0.0	0.5
C20:3, n-6	0.0	0.0
C20:4, n-6	0.0	0.2
C20:5, n-3	0.0	0.0

<sup>a</sup> Number of carbon atoms: number of C = C double bonds, position of C = C bonds

Fig. 7 shows the viscosities of stearic acid (C18:0) and oleic acid (C18:1).<sup>91)</sup> Both fatty acids have the same number of carbons while oleic acid has one *cis* C = C bond. Oleic acid show lower viscosity than stearic acid due to the *cis* C = C which introduces a bent conformation to the molecule. This conformation prevents the fatty acids from packing tightly and alters the van der Waals force existing among the molecules.

The fatty acids are esterified to the glycerol *sn*-carbons in accord with enzyme substrate specificities.<sup>89)</sup> The difference in *sn*-specific fatty acid composition is thus genetic in origin and it leads to the differences in physical properties (Table 2). These sets of fatty acids in Table 2, *e. g.* POP and PPO, have the same fatty acid composition, two palmitic acids and one oleic acid; however, there is a difference in their melting points which is derived from the difference in *sn* positions.

By using above mentioned mechanisms, living organisms control TAG physical properties in order to accommodate environmental temperature change. When the temperature becomes lower, the composition of TAGs becomes the one with higher unsaturated fatty acids in order to maintain the TAG fluidity. If TAGs are completely crystallized due to the low temperature, the cells are probably not able to use TAGs as the energy source. Homeoviscous adaptation, the term which is often used for cell membrane, can be also applied for TAGs in living organisms.

Table 2. Comparison of melting points between the TAGs consisting of same fatty acids<sup>24)</sup>

TAG species <sup>a</sup>	Melting point(°C) <sup>b</sup>
POP	37
PPO	35
SOS	43
SSO	41
PSP	67
SPP	62
SPS	68
PSS	64

<sup>a</sup> P, palmitic acyl; O, oleic acyl; S, stearic acyl

<sup>b</sup> Average values of the experimental data shown in the reference

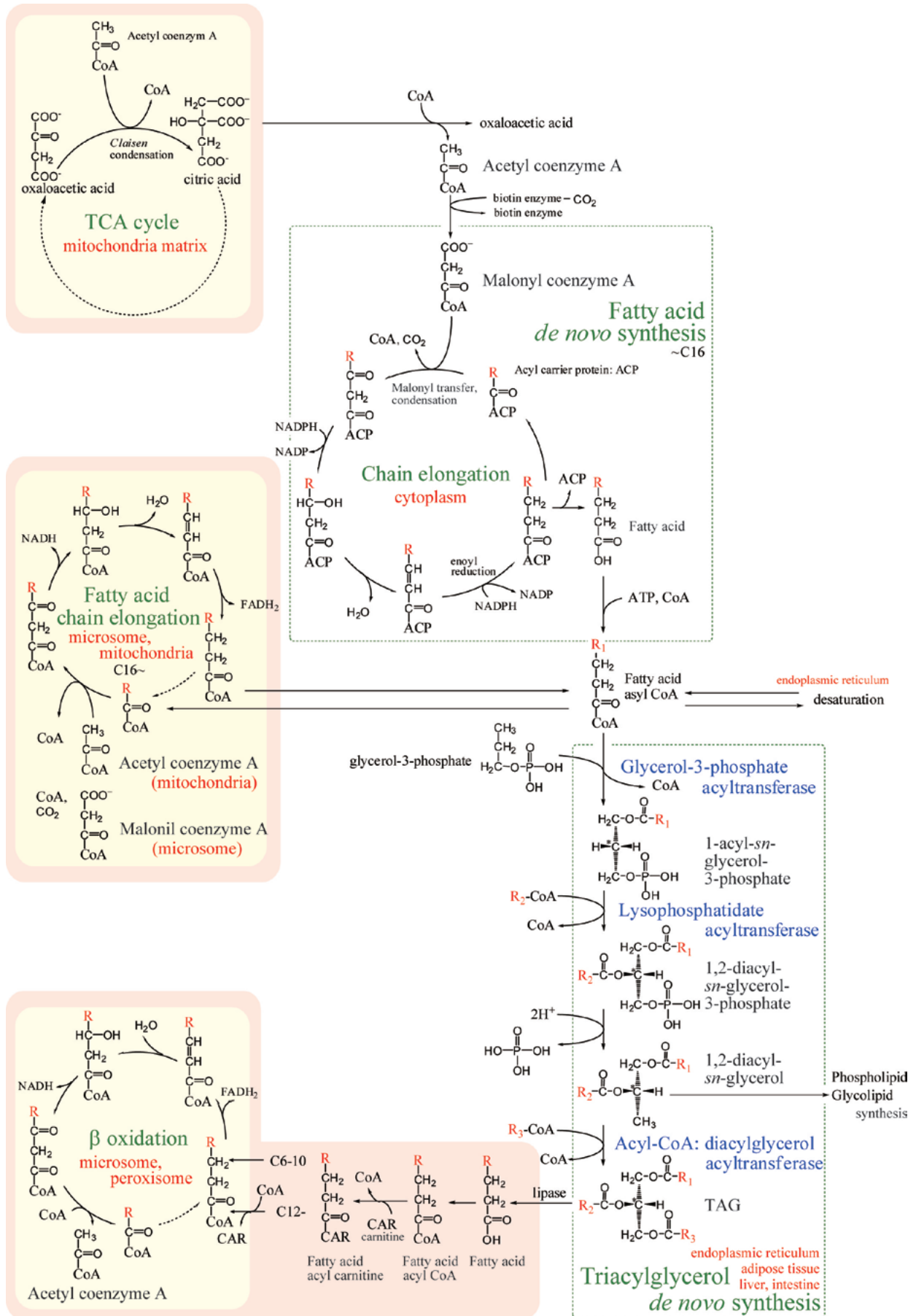


Fig. 5. TAG synthetic and metabolic pathways in a mammalian cell<sup>29)</sup>

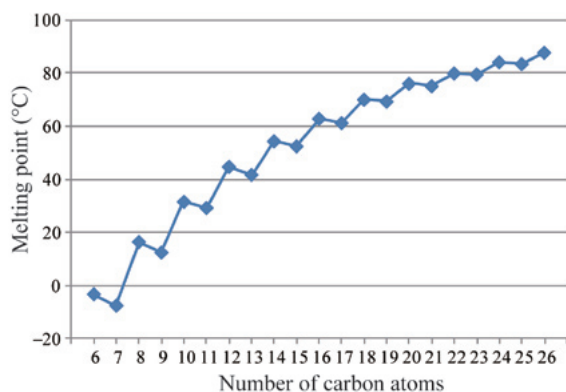


Fig. 6. Relationship between the carbon atom number of saturated fatty acids and their melting points<sup>87)</sup>

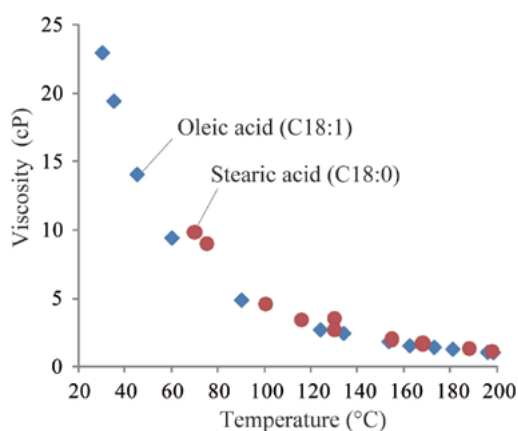


Fig. 7. Viscosities of two fatty acids. Stearic acid: Saturated acid with 18 carbon atoms. Oleic acid: Unsaturated 18-carbon fatty acid with one *cis* C=C<sup>91)</sup>

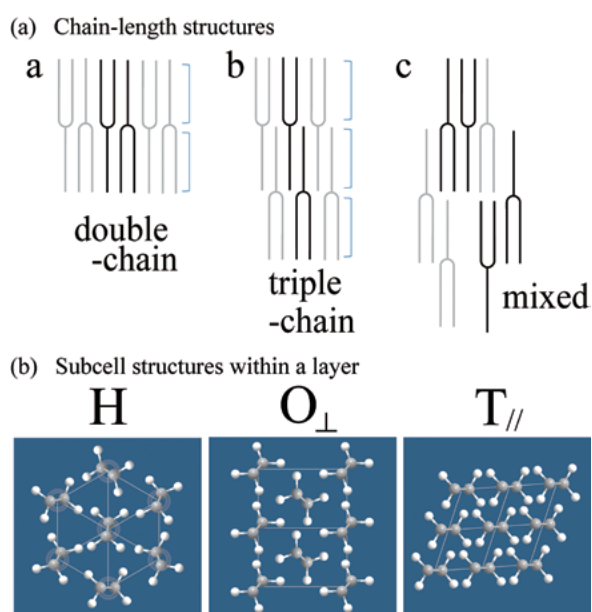


Fig. 8. Two kinds of Structure in TAG crystals. (a): Chain-length structure.<sup>70)</sup> a, double-chains length structure; b, triple-chain lengths structure; c, mixed structure. (b) Subcell structure within a layer. H, hexagonal subcell structure; O<sub>⊥</sub>, orthorhombic perpendicular subcell structure; T<sub>//</sub>, triclinic parallel subcell structure

### Polymorphic phase in TAG crystals

TAG crystals show polymorphism. Just like other long chain molecules, TAGs also form crystals with layer structures. These crystal structures of TAGs are usually classified by two distinctive features: the number of acyl-chain-length structures participating in a layer (Fig. 8a) and the type of subcell structure within the acyl-chain-length structures dictated by the inter-chain orientation (Fig. 8b). The stable crystal of TAGs has double-chain lengths or triple-chain lengths type of structure (Fig. 8a). The common subcell structure within a chain-length structure is known to be hexagonal with no ordered arrangement of the chain planes (H), orthorhombic with every second chain plane is perpendicular to the plane of the rest (O<sub>⊥</sub>) or triclinic with all chain planes are parallel (T<sub>//</sub>) (Fig. 8b).

The possible combination number of the chain-length structures and the subcell structures is large. A given TAG species has at least 36 possible packing manners in theory. In practice, however, only three structures called  $\alpha$ ,  $\beta'$  and  $\beta$ -polymorphs generally exist due to the packing preference which is brought by intermolecular interactions and thermodynamic conditions.

The polymorphic transformation goes monotonically in the order  $\alpha$ ,  $\beta'$  and  $\beta$ , indicated by the arrows in Fig. 9. For most of TAG species, the  $\beta$  polymorph is the most stable polymorph; however,  $\beta'$  is of the most stable one for some TAG species, *e. g.* PPO<sup>81)</sup> and PPM,<sup>46)</sup> M: Myristic acyl. For complex TAG mixtures, *i. e.* natural fats,  $\beta'$  polymorph is often the most stable polymorph.<sup>115)</sup> The structure of the polymorphs and the structural changes associated with polymorphic phase transformation are described as follows (Fig. 9).

$\alpha$ -polymorph: Thermodynamically, this is the least stable phase with the lowest melting point. Its chain-length structure is generally double-chain and the subcell structure is H. The main part of the hydrocarbon chains are oscillating and hexagonally close packed. The methyl end group regions are somewhat more disordered, as in liquid crystals.<sup>27)</sup>

$\beta'$ -polymorph: This is the more stable phase showing the intermediate melting point. Its chain-length structure is double- or triple-chain and the O<sub>⊥</sub> subcell structure exists within all or part of the layer. The acyl chains are

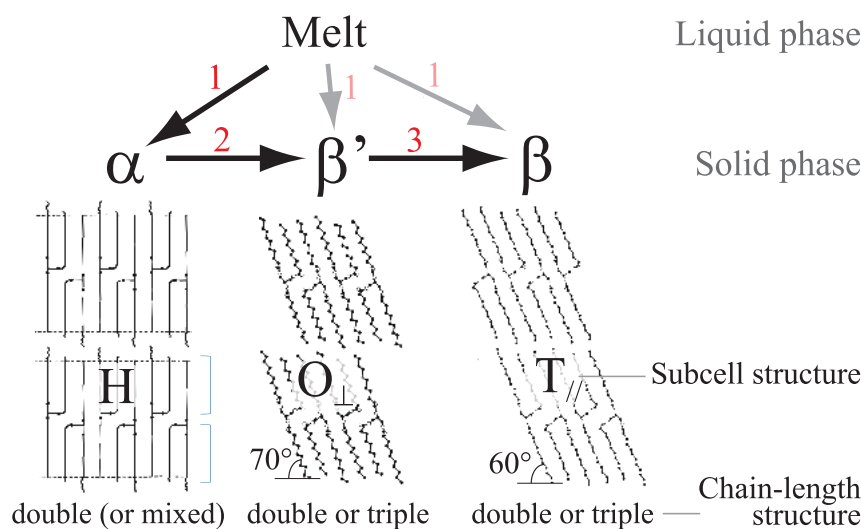


Fig. 9. Polymorphic transformation and structures of polymorphs<sup>27)</sup>

tilted about  $70^\circ$  from the plane formed by methyl end groups.

$\beta$ -polymorph: The most stable phase showing the highest melting point. Hydrocarbon chain planes are arranged in parallel and the subcell structure is generally  $T_{//}$ . The angle of tilt is about  $60^\circ$ .

These polymorphs are often described with subscripts, *e.g.*  $\beta_1$ ,  $\beta_2$ . Only three terms, *i.e.*  $\alpha$ ,  $\beta'$  and  $\beta$ , are not enough to indicate the polymorphism of TAGs containing unsaturated acyls because of its complexity.<sup>82)</sup> It is recommended that they are numbered in the order of decreasing melting points.<sup>53)</sup> These nomenclatures with different subscript need not always indicate independent polymorphs. For example, Kellens *et al.*<sup>36)</sup> reported that the melting point variation between [ $\beta'_1$  and  $\beta'_2$ ] and [ $\beta_1$  and  $\beta_2$ ] of a TAG seemed to be only due to crystal perfection and crystallinity. Mykhaylyk and Martin<sup>70)</sup> also reported that  $\alpha_2$  phase formed in some TAGs species can be characterized as a transient structure. These polymorphs, however, are likely to be isolated and stabilized by cooling immediately after its formation.<sup>46)</sup> To understand polymorphic transformations taking place in TAGs, especially in natural fats, the structure of various unstable phases have to be determined.

The lateral interaction among acyl chains, intermolecular glycerol interactions and the methyl ends interaction are the main driving force of the phase transformation. The associated structural changes can be explained as below.

Melt  $\rightarrow$  solid phase (arrow 1 in Fig. 9): Cooling process. The C–C bonds within acyl chains become *trans* configuration. Crystallization is the least understood phase transition in terms of structural changes. The details are described in the next section.

$\alpha \rightarrow \beta'$  (arrow 2): Hexagonal packing in  $\alpha$ -polymorph likely to change always to the orthorhombic packing.<sup>27)</sup> Which chain-length structure they form (double or triple) is depend on chain sorting which may be related to the conformational disordering of the  $\alpha$  form.<sup>25)</sup> The chains become tilt and the methyl ends become lined up. The methyl-groups overlap develops large intermolecular repulsion. To reduce this large repulsive energy, the perpendicular chain-plane arrangement ( $\perp$ ) is likely to be introduced.<sup>24)</sup>

$\beta' \rightarrow \beta$  (arrow 3): Parallel chain-plane arrangements ( $//$ ) are introduced within all layers. The matching of the terminal methyl groups within the inter-layer space and the conformational order of unsaturated bonds, when such are present, is completed.<sup>14,15,121)</sup>

The polymorph transformation to more stable phase can be melt-mediated process which enables the transformation finish in a shorter time compared to solid-to-solid transformations.<sup>46,84)</sup> This difference can be explained by thermodynamics.<sup>83)</sup>

### Crystallization process

The cooling-down procedure from the TAG melt greatly influence the crystallization of fats. In fats industries, these procedures so-called “annealing” are the important part of the technology to control the polymorph formed. To understand the crystallization of TAG systems, general theories for crystal nucleation and crystal growth have been applied.<sup>20)</sup> However, as been mentioned so far, polymorphism complicates the crystallization of TAGs. Herewith, a rough picture will be given for the crystallization of TAGs.

To describe the crystallization behavior of TAGs, Gibbs free energy ( $G$ ) is the most important. Because crystallization, *i. e.*, phase transition, is the process which changes volume ( $V$ ) and entropy ( $S$ ) of the system; therefore, it is difficult to use the other thermodynamic potentials which have  $V$  and/or  $S$  as their variables:

$$\Delta E = T\Delta S - P\Delta V \quad (E : \text{internal energy})$$

$$\Delta H = T\Delta S + V\Delta P \quad (H : \text{enthalpy})$$

$$\Delta F = -S\Delta T - P\Delta V \quad (F : \text{Helmholtz free energy})$$

where  $T$  is temperature and  $P$  is pressure.

For crystallization from the melt to occur, the activation energy barrier,  $\Delta G^{\ddagger}$ , should be crossed over. The relative  $\Delta G^{\ddagger}$  values for TAG polymorphs were studied by Malkin<sup>57)</sup> and they can be depicted as shown in Fig. 10. The larger  $\Delta G^{\ddagger}$  value indicates the greater difficulty of the formation of crystal nucleus.  $\beta$ -polymorph is most difficult to crystallize due to its largest  $\Delta G^{\ddagger}$ . It is consistent with the observed crystallization rate which decreases in order of  $\alpha$ ,  $\beta'$  and  $\beta$ .<sup>84)</sup>

$\Delta G$  is expressed by the function of temperature and pressure as:

$$\Delta G = -S\Delta T + V\Delta P$$

The Gibbs free energy of one particle is called chemical potential  $\mu$ :

$$\Delta\mu = -s\Delta T + v\Delta P$$

$\mu$  is convenient to use especially when one wants to describe crystallization since some local equilibriums,

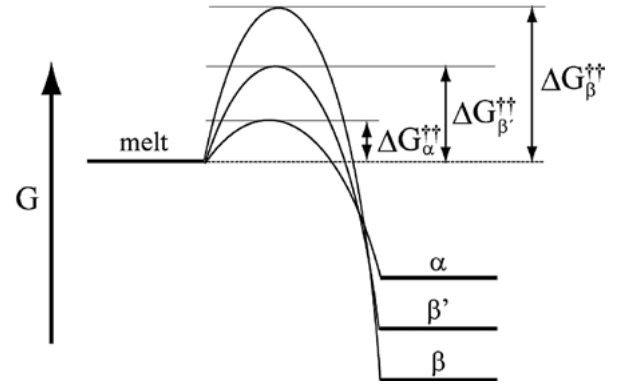


Fig.10. Diagram of the activation Gibbs free energy  $\Delta G^{\ddagger}$ <sup>57,89)</sup> and those of each polymorph

*i. e.* liquid phase and solid phase, are coexisting within a system under crystallization process. The difference in  $\mu$  between the local equilibrium systems ( $\Delta\mu$ ) is the driving force to cross over the activation energy barrier.

When  $\Delta\mu$  is defined as:

$$\Delta\mu \equiv \mu_{\text{liquid}} - \mu_{\text{solid}}$$

$\mu_{\text{liquid}}$ :  $\mu$  of the liquid phase exists at crystallization

$\mu_{\text{solid}}$ :  $\mu$  of the solid phase exists at crystallization

it can be derived:

$$\Delta\mu = -(s_{\text{liquid}} - s_{\text{solid}})\Delta T + (v_{\text{liquid}} - v_{\text{solid}})\Delta P \quad \text{--- eq. 1}$$

It can be supposed that the difference in volume is small between liquid and solid,

$$v_{\text{liquid}} \approx v_{\text{solid}}$$

Therefore, eq. 1 becomes:

$$\Delta\mu = -(s_{\text{liquid}} - s_{\text{solid}})\Delta T$$

where  $\Delta T$  is called the supercooling:

$$\Delta T = T_m - T$$

$T_m$ : melting temperature of the solid phase

$T$ : actual temperature of the system

When larger  $\Delta T$  is induced, the absolute value of  $\Delta\mu$  becomes larger. The larger  $\Delta\mu$  the larger the driving force for crystallization and the driving force cross the activation energy barrier  $\Delta G^{\ddagger}$ , crystal nucleus is formed.

After the nucleation, crystals grow at a certain rate which is proportional to  $\Delta\mu$ . Fig. 11 shows the  $\Delta\mu$  of each polymorph at a temperature  $T$ .  $\Delta\mu$  is larger in the order of  $\Delta\mu_{\alpha} < \Delta\mu_{\beta'} < \Delta\mu_{\beta}$ . This indicates that once the nucleus is formed, the more stable polymorph grows faster.

Structural changes of TAGs on crystallization are proposed by synchrotron radiation X-ray diffraction

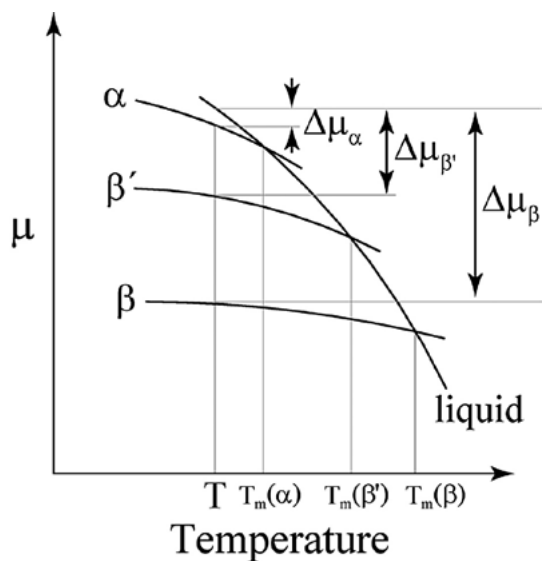


Fig.11. Relationship between chemical potential and temperature for liquid phase and three polymorphs of TAGs.  $\Delta\mu$ , difference in chemical potential between liquid and solid;  $T$ , actual temperature;  $T_m$ , melting temperature <sup>1,19,120,123)</sup>

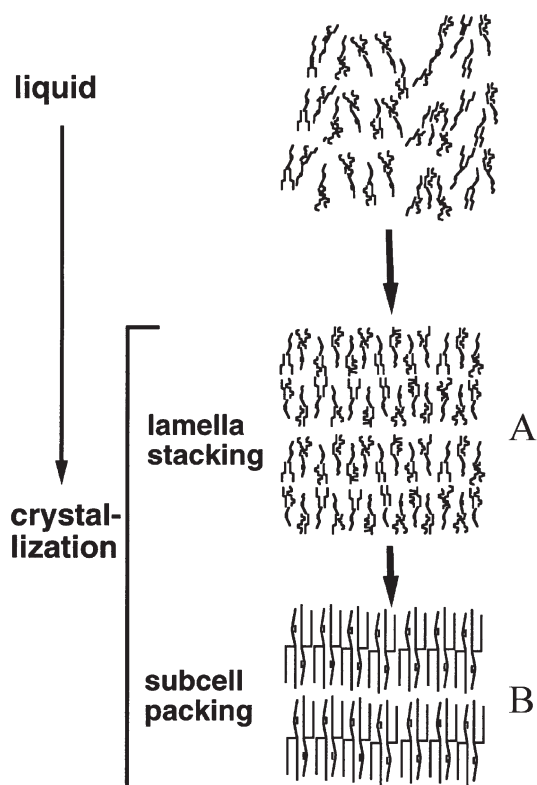


Fig.12. A model of crystallization of fats from neat liquid <sup>80)</sup>

studies (Fig. 12). Lamella stacking is firstly occurred (A in Fig. 12), followed by the detailed subcell packing (B in Fig. 12). <sup>118,119)</sup> It is estimated that the time required for the A to B transformation is of the order of several tens of second for SOS  $\beta'$ -polymorph and 500 second for SOS  $\beta_2$ -polymorph.

Regarding the formation of the lamella structure, Mykhaylyk *et al.* recently proposed the plausible model. <sup>70,71)</sup> Two types of molecular dimers possibly exist in a TAG liquid phase and the stability of these dimers depends on thermal conditions and compatibilities between the TAG acyl moieties (see Fig. 46 on page 49). In a liquid state of TAGs containing solely saturated or unsaturated acyls, only one type of dimers with double-chain-length structure is formed and leading double-chain-length layer. In TAGs with both saturated and unsaturated acyls, a packing incompatibility between these acyls stabilizes both type of dimers and leading the formation of the lamella with random packing of the two dimers. The structural complexity of the latter lamella likely explains the complex phase behavior of TAGs with unsaturated acyls.

#### “Molecular compound” formation

It has been reported that a third component exists in some TAG binary systems. This third component is known as the “molecular compound”.

It is generally accepted that the liquid phase of a TAG mixed system may be treated as a close approximation to an ideal mixture. <sup>20)</sup> Once they are crystallized, they are separated and generally form solid solution (Fig. 13a). However, in some TAG binary systems which have “specific interactions”, they form molecular compounds (Fig. 13b). A molecular compound behaves like a new, pure TAG species with unique phase behavior that differ from those of its component TAGs.

The first report on the molecular compound was made in 1963 by Moran. <sup>66)</sup> He conducted DSC thermal analysis on several TAG binary systems and found unexpected melting behaviors in POP-OPO binary system. The observed phase diagram of POP-OPO system was likely to be made up of two binary systems, in juxtaposition, of POP-compound and compound-POP (Fig. 14). He thus proposed that the “molecular compound”

is formed in POP-OPO binary system and it would not be chemically bonded as in true compound, but merely a highly-favored crystal packing.

After this report, several studies have reported on the molecular compound formation in TAG binary systems using thermal analysis and powder X-ray diffraction. The formations of a molecular compound have also been observed in POP-PPO,<sup>63,66</sup> SOS-OSO<sup>48</sup>) and SOS-SSO systems.<sup>18,62</sup> It must to note that oleoyl acyls (O) are present in both component TAGs of the above systems. Therefore, the intermolecular interactions at oleoc acyl moieties, including  $\pi$ - $\pi$  interaction among olefinic groups, are thought to be the driving force for the molecular

compound formation. It is quite interesting how such a van der Waals type interaction can enable the formation of the stable compound. However, the structure and the driving force for the compound formation are not well understood yet, despite numerous attempts.

With emphasis on the recent developments, the fundamental knowledge of polymorphism and molecular compound formation of TAG systems have been summarized in relation to the factor influencing these phenomena, such as TAG chemical structures and crystallization conditions. Since the phase behavior of a multicomponent TAG system is thought to be able to be obtained by summing all the behavior of the component TAGs,<sup>20</sup>) it is important to understand these fundamentals of TAG structure and phase behavior.

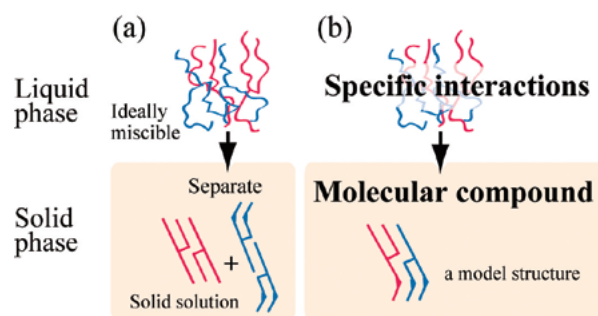


Fig.13. Illustration of "molecular compound" formation

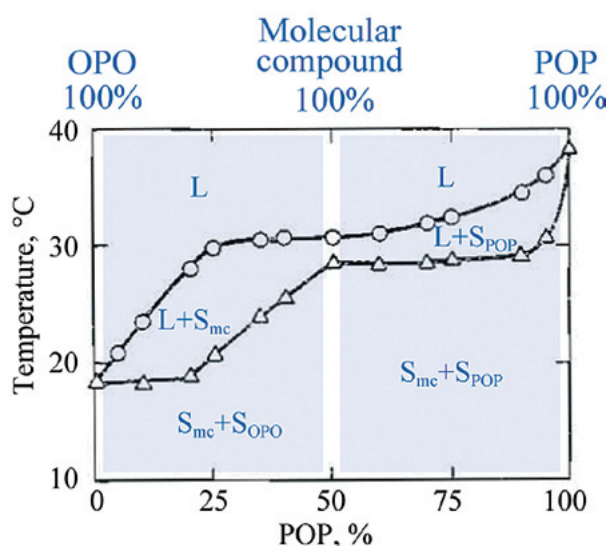


Fig.14. Melting behavior of POP-OPO binary systems.<sup>66</sup> Sample crystals were prepared as follows: Melts (100 °C) were quenched to 0 °C and then incubated 2-4 weeks at as high a temperature as possible to induce most stable polymorphs. ○, melt point; △, thaw point; L, liquid; S<sub>mc</sub>, solid of molecular compound; S<sub>OPO</sub>, solid of OPO; S<sub>POP</sub>, solid of POP.

## Chapter 3

### Raman Spectra of Triacylglycerols

#### Abstract

The total number of the atoms of a TAG molecule is about 170, hence it has approximately 500 normal modes. Some of them are selected to be observed as a vibrational spectrum, "a letter from the TAG molecule".

Vibrational spectroscopy is the suitable method to investigate TAG structural changes during phase transition because they can be applied not only the crystals but also the liquid phases. Since the conformational changes of TAGs are usually accompanied with large polarizability changes, their Raman spectra reflect these changes with high sensitivity and are particularly useful in this respect.

In this chapter, the Raman spectra of TAGs will be interpreted on the basis of the previous studies on polyethylene, paraffines, *n*-alkanes and fatty acids. Firstly, the vibrational modes of polyethylene will be briefly introduced because their spectra are understood well and they dominate the TAG composition. The assignments of Raman bands (1800–700cm<sup>-1</sup>) observed in several TAG phases will be then illustrated with respect to each spectral region. Spectral differences among the phases will be explained in relation to their structures.

## Introduction

TAGs are one of the well known molecules which give strong Raman scattering, since their acyl moieties that dominate the composition have large polarizability volumes. The structural changes during TAG phase transition are reflected with high sensitivity in the Raman spectra. In order to understand the complicated TAG spectra, the spectrum of polyethylene is the good reference. Polyethylene chains are the model compound of lipids, and their spectra are studied extensively for a long time.

A polyethylene chain, an infinite *trans* zigzag chain, is constructed by repeating  $-\text{CH}_2-$  units which have nine proper vibrations: three atoms with three degree of freedom ( $x$ ,  $y$  and  $z$ ) for each. These vibrations are depicted in Fig. 15. Although the Bravais unit cell of polyethylene chains is  $-\text{CH}_2\text{CH}_2-$ , the dispersion curve of polyethylene is often expressed taking  $-\text{CH}_2-$  as the unit because of simplicity (Fig. 16). There are nine branches ( $\nu_1, \nu_2, \dots, \nu_i, \dots, \nu_9$ ) and the  $\delta$  indicates the phase difference between two adjacent  $-\text{CH}_2-$  units. Optical active vibrations have the value 0 or  $\pi$  for the  $\delta$ ; therefore, they can be expressed as  $\nu_i(\delta=0)$  or  $\nu_i(\delta=\pi)$ . Among these modes, the Raman active modes are  $\nu_1(\delta=0)$ ,  $\nu_2(\delta=0)$ ,  $\nu_3(\delta=\pi)$ ,  $\nu_4(\delta=0)$ ,  $\nu_4(\delta=\pi)$ ,  $\nu_6(\delta=\pi)$ ,  $\nu_7(\delta=0)$  and  $\nu_7(\delta=\pi)$ .<sup>88)</sup>

In crystalline polyethylene, there are inter-chain interactions, which influence the above described vibrational modes. The dispersion curve for the crystal has been also acquired.<sup>109,113)</sup> Polyethylene crystals have orthorhombic perpendicular ( $O_{\perp}$ ) unit cell structure (Fig. 17a) and the Bravais unit contains two polyethylene chains (Fig. 17b). Therefore, every dispersion curve is split into two curves: One is for the vibration attributed to symmetric displacement of the adjacent-polyethylene chains; the other is for that of asymmetric (Fig. 18). This separation can be accounted for reasonably well using a model based on a short-range hydrogen atom-atom repulsive potential.<sup>113)</sup> Because of the interaction between the two chains within a Bravais unit, the Raman spectra of the crystal become complicated. TAG polymorphs show similar types of crystal subcell structure; therefore, this effect should be kept in one's mind.

Another factor complicates TAG polymorph spectra is the band progression. Just as described above, the bands observed in polyethylene spectra are limited in the in-phase vibrations ( $\delta=0$  or  $\delta=\pi$ ). On the other hand, finite chains show a series of progression bands ( $0 \neq \delta \neq \pi$ ).<sup>104)</sup> The spectral pattern of the progression bands reflects very sensitively the chain length of the *trans*-zigzag chain. TAGs consisting of the acyls with different chain length will have a few series of progression.<sup>126)</sup>

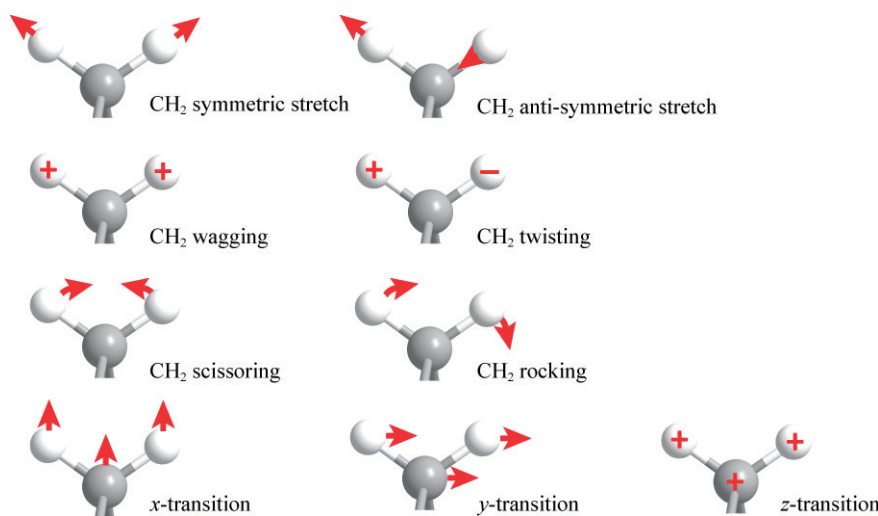


Fig. 15. Nine normal modes of  $-\text{CH}_2-$

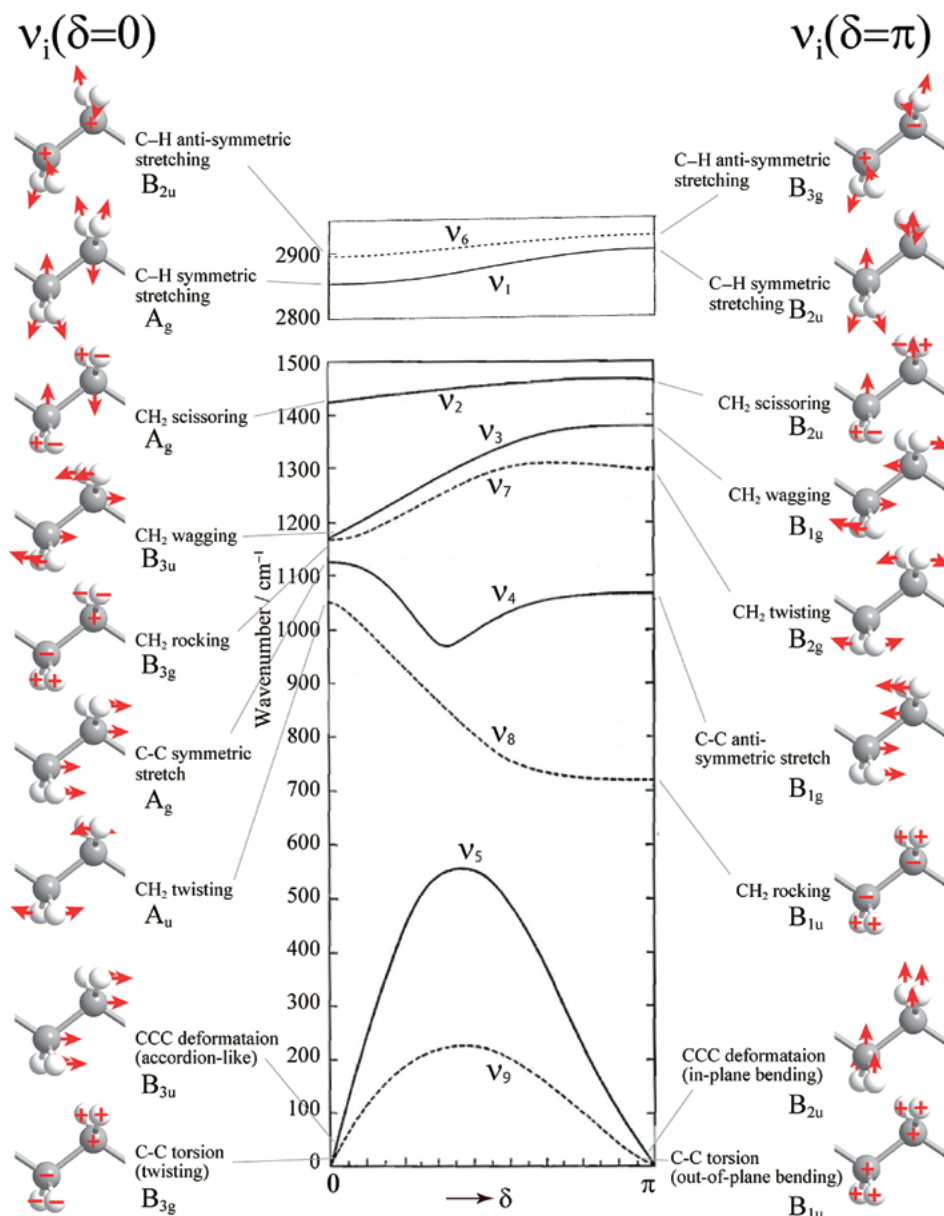


Fig.16. Dispersion curve of single polyethylene chain. <sup>49,88,111,112)</sup>  $\delta$  is the phase difference between two adjacent units ( $-\text{CH}_2-$ ). Solid lines indicate in-plane vibrations, dashed lines indicate out-of-plane vibrations. CH<sub>2</sub> twisting and CH<sub>2</sub> rocking are coupled in  $v_7$  and  $v_8$ .

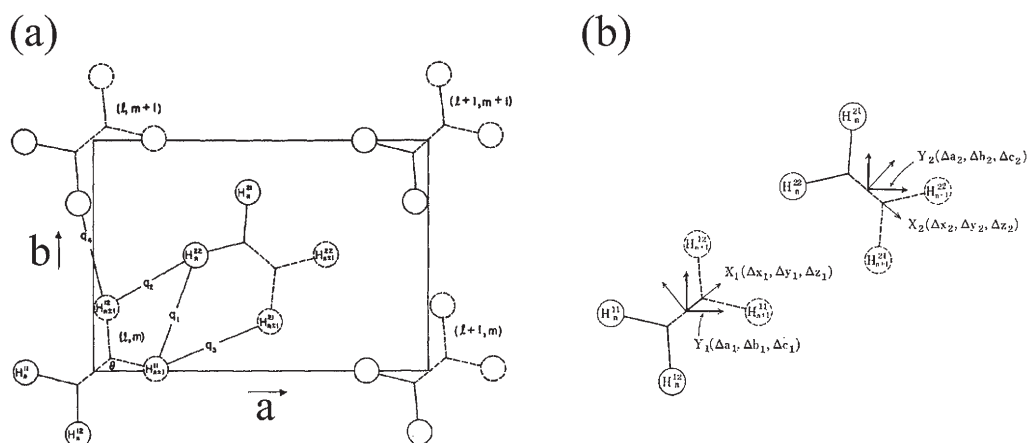


Fig.17. Crystal structure and the Bravais cell of crystal polyethylene. <sup>113)</sup> (a), orthorhombic perpendicular ( $O_{\perp}$ ) structure. <sup>94)</sup> (b), Bravais unit cell and the coordinate system along the crystal axis

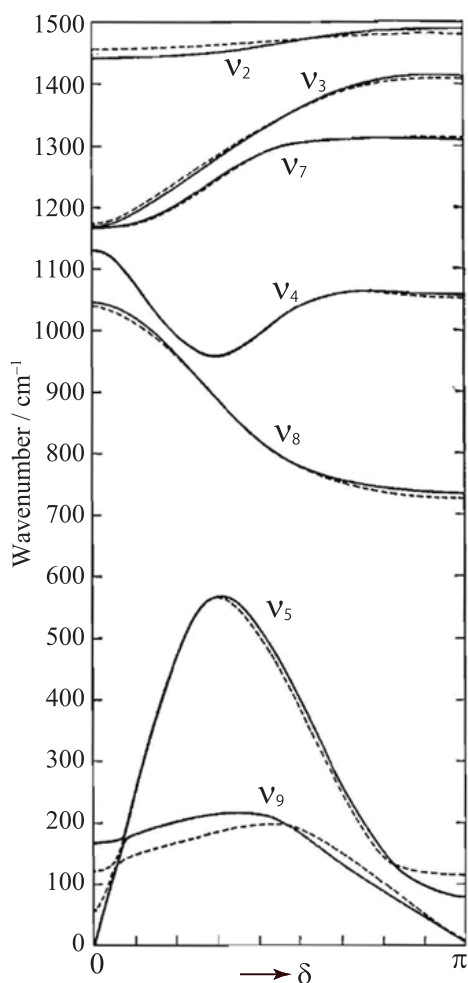


Fig.18. Dispersion curve of crystal phase of polyethylene.<sup>109,113)</sup>  $\delta$  is the phase difference between two adjacent units ( $-\text{CH}_2-$ ). Solid lines indicate the vibrations attributed to symmetric displacement of the adjacent-polyethylene chains; dashed lines indicate those of asymmetric

During TAG phase transition, especially in solid to liquid transition, their spectra change drastically. For a random chain (not a *trans* zigzag), every normal mode would become more or less active due to the breakdown of selection rules.<sup>114)</sup> Band progressions also affect the spectral changes during solid-liquid phase transition. In going from solid to liquid, *trans* zigzag chains introduce some *gauche* conformations into them and they are segmented into some shorter *trans* chains with a variety of length. The progressions reflecting their chain length are developed and layered as a consequence in the broad band features of liquid phase. Mizushima and Shimanouchi suggested that all-*trans* zigzag chain shorter

than  $\text{C}_{16}\text{H}_{34}$  are likely exist in liquid state of *n*-alkanes.<sup>65)</sup> Long chain molecule acts as segments of *trans* zigzag chains in the liquid phase.

The introduction of *gauche* conformation has another effect. The spectrum of a all-*trans* chain, *e.g.* polyethylene, distributes all its intensity to the in-phase bands ( $\delta=0$  or  $\delta=\pi$ ). For the liquid, however, the intensity distribution tends to be more even for all the modes in the progression.<sup>100)</sup> The *gauche* conformations in the liquid affect the degree of coupling between adjoining oscillators which is determined by their relative orientation, and is reflected in the intensities of all the modes in the progression.<sup>100)</sup> The progression bands which do not have intensities in all-*trans* conformation become apparent with some observable intensities in the liquid phase. Such 'density-of-states progression' explains the observed progression in liquid *n*-alkanes.<sup>8)</sup>

It has not been explained explicitly; however, there is a general concept that a TAG spectrum is the superposition of that of each acyl-chain length structure (Fig. 19). This is probably based on the fact that the acyl chains are isolated by the glycerol moiety. It can be supposed that there is no vibrational coupling among the layers. This concept provides the basis for the vibrational spectroscopic studies on TAGs. Previous studies<sup>64,125)</sup> have reveals acyl chain structures standing on this basis.

## Experiment

### Preparation of TAG samples

Three TAG species constituted of palmitic and oleic acyls were purchased from Sigma-Aldrich (St. Louis, MO, USA): tripalmitin (PPP,  $\approx 99\%$  purity), 1,3-dipalmitoyl-2-oleoyl-*sn*-glycerol (POP,  $\approx 99\%$ ) and 1,3-dioleoyl-2-palmitoyl-*sn*-glycerol (OPO,  $\approx 99\%$ ). Their liquid- and polymorphic-phases were prepared as follows;

Approximately 2-mg PPP sample was put on a cover glass and kept  $>70^\circ\text{C}$  to acquire liquid phase. It was cooled down to  $45^\circ\text{C}$  and crystallized to  $\alpha$ -polymorph, and then heated up to  $50^\circ\text{C}$  to transform  $\alpha$ -polymorph to  $\beta'$ -polymorph. 3  $\mu\text{L}$  of POP and OPO melts were put on cover glasses and kept at  $50^\circ\text{C}$  to maintain in liquid phase. They were rapidly cooled down to  $4^\circ\text{C}$  to acquire  $\alpha$ -polymorph, then incubated at  $20^\circ\text{C}$  for 11 days to transform the POP and OPO samples to more stable

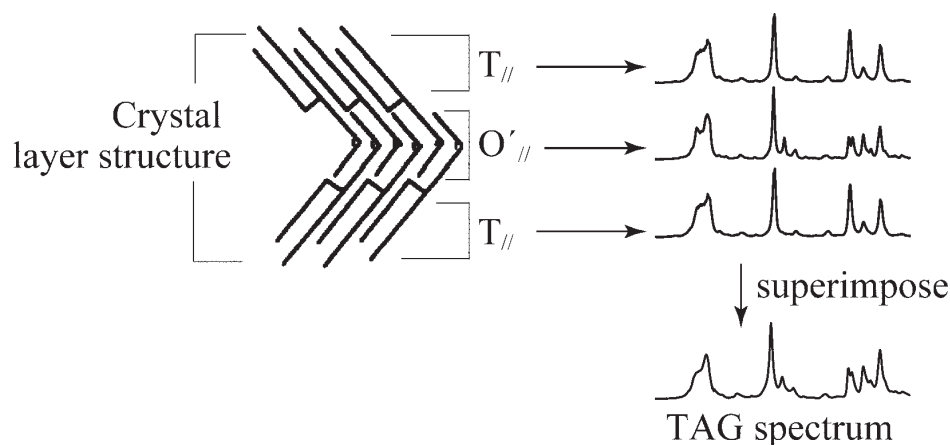


Fig.19. The concept to understand the spectra of TAGs which have acyl-chain length subcell structure.

polymorphs.

In addition to the TAG samples, polyethylene sheet (50-  $\mu\text{m}$  thickness) produced by blown-extrusion method was acquired at a retail market.

#### Raman spectroscopic measurement

For PPP samples, Raman scattering was excited with the 785-nm line of a Ti-sapphire laser (Spectra Physics 3900S, Newport, Santa Clara, CA, USA). The back-scattered Raman light from the sample was collected by an objective lens (LUCPlanFLN20x, Olympus, Tokyo, Japan) and measured with a spectrometer (Chromex 250i, Bruker Optik GmbH, Ettlingen, Germany) and a CCD detector ( $400 \times 1340$  pixels, Spec-10 400BR(LM), Roper, Sarasota, Florida, USA). The laser power was 17 mW at the sample point and the exposure time was 30 s. Spectral resolution was  $\sim 3 \text{ cm}^{-1}$ .

For other samples, the 532-nm line of a Nd:YVO<sub>4</sub> laser (Verdi, Coherent, Santa Clara, CA, USA) was used as the excitation source. The back-scattered Raman light was collected by above mentioned objective lens and measured with a spectrometer (Shamrock, Andor, Belfast) and an EMCCD detector (Newton, Andor). The laser power was 3 mW at the sample point. Four measurements with 300 s exposure time were accumulated. Spectral resolution was  $\sim 2 \text{ cm}^{-1}$ .

The integrated Raman intensities of almost all the polarization components were measured. During the

measurement, sample temperatures were controlled by a cryostat (Linkam 10021, Tadworth, Surrey, UK) in order to maintain desired phases.

#### Result — Raman band assignments

The acquired Raman spectra were shown in Fig. 20. In this section, the assignments of bands observed in the TAG finger-print spectra will be described on the basis of the spectroscopic data of basic molecules such as polyethylene, paraffins, *n*-alkanes and fatty acids. They are summarized in Fig. 20 with comparison to a crystal polyethylene spectrum. As described in the introduction section, the bands observed in a TAG Raman spectrum are mostly related to those originating from polyethylene chain structures. For these bands, the notation of branch which the band belongs to ( $\nu_i$ ) has been added.

#### Region 1760 – 1720 $\text{cm}^{-1}$

The bands observed in this region originate from ester C=O stretching modes.<sup>68)</sup> These bands contain information regarding the geometry of the ester region of TAGs.<sup>4,5,128)</sup> TAGs have three ester linkages (Fig. 1); therefore, one can logically expect three vibrational bands in this region. Actually, the existence of three bands in the TAG liquid phase has been reported.<sup>13)</sup>

The  $\alpha$ -polymorph of TAGs does not show a clear feature with three bands.<sup>1)</sup> This is likely to be due to its ambiguous configuration in the vicinity of the linkages.

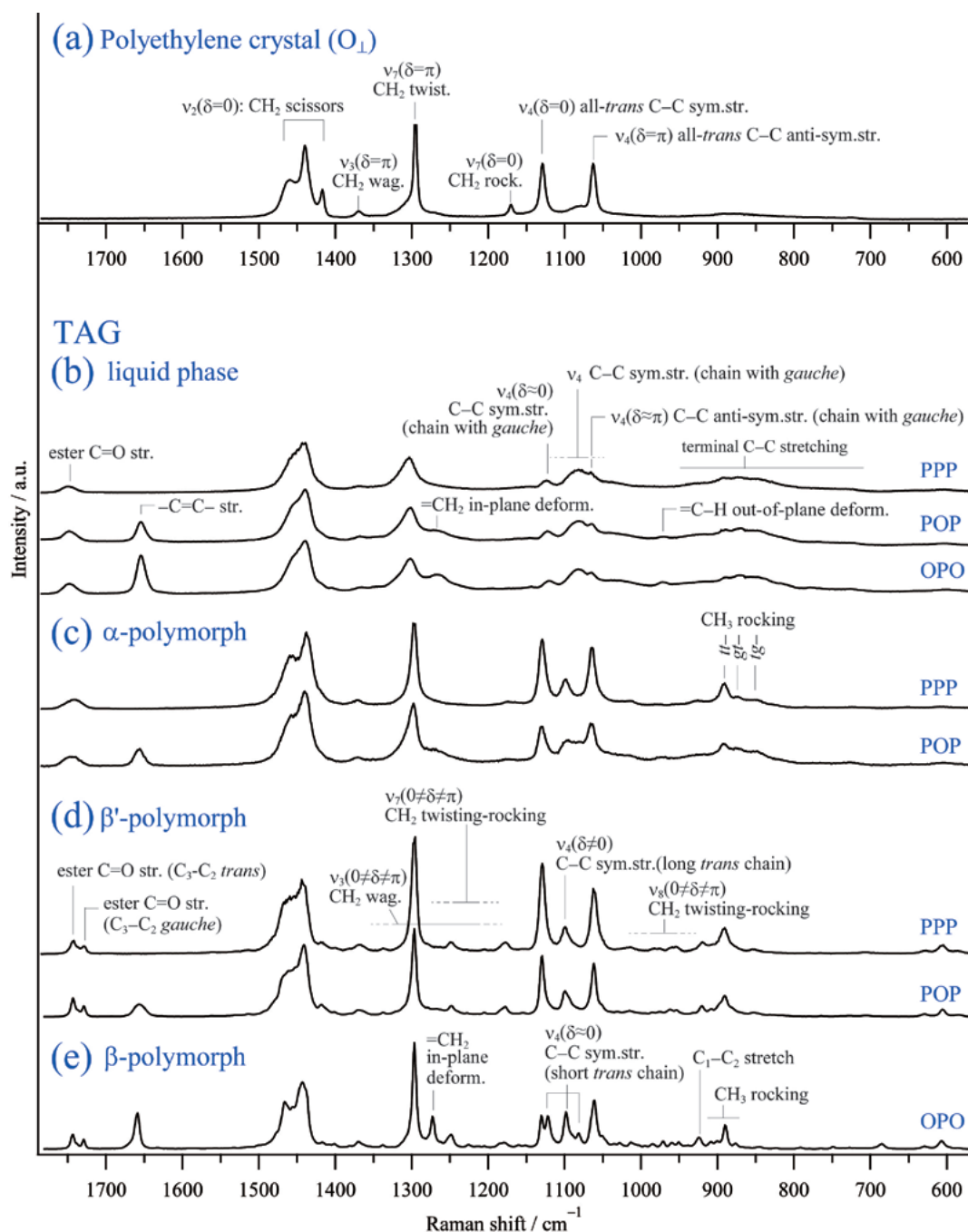


Fig.20. Assignments for TAG Raman bands

During the phase transition from  $\alpha$ -polymorph to more stable phases, TAGs tend to configure 'h' conformer (see page 22) introducing a *gauche* configuration around  $C_2 - C_3$  bond in *sn*-3 acyl chain (Fig. 21). This change significantly affects in the frequency of the ester C=O stretching of the chain. From the previous studies, the band at  $\sim 1728 \text{ cm}^{-1}$  corresponds this *sn*-3 C=O vibration, while the band at  $\sim 1743 \text{ cm}^{-1}$  corresponds to *sn*-1 and -2 acyls' C=O with *trans*  $C_2 - C_3$  configuration.<sup>1,69)</sup> Using

these assignments, Sprunt *et al.* suggest the following approximate conformations for  $C_2 - C_3$  of three acyls of SOS in different polymorphic forms:  $\beta_1$ , two *trans*, one *gauche*;  $\beta_2$  two *trans*, one *gauche*;  $\beta'$ , three *gauche*;  $\gamma$ , one *trans*, two *gauche*;  $\alpha$ , three disordered.

Between these two bands, a weak band  $\sim 1737 \text{ cm}^{-1}$  is observed.<sup>13)</sup> Bicknell-Brown *et al.* reported that ester C=O stretching frequency is sensitive to rotation about the  $C_2 - C_1$  bond in some phospholipids.<sup>2)</sup> It is likely the

reason for the existence of  $1737\text{ cm}^{-1}$  band, and also for the band broadening of  $\alpha$ -polymorph. On the other hand, da Silva and Rousseau speculated that the observation of three bands might be related to the presence of trace amounts of moisture in the samples that would interact with C=O bond of the esters, leading to a slightly altered conformation.<sup>13)</sup>

#### Region $1680 - 1630\text{ cm}^{-1}$

The band due to C=C stretching is seen at  $\sim 1655\text{ cm}^{-1}$  in the Raman spectra of TAGs which contain unsaturated acyl chains (Fig. 20). The frequencies of this vibrational mode depend sensitively on its conformation. The C=C bond existing in natural TAGs is normally in *cis* configuration. The conformation around *cis* C=C bond determines the overall shape of acyl chains and

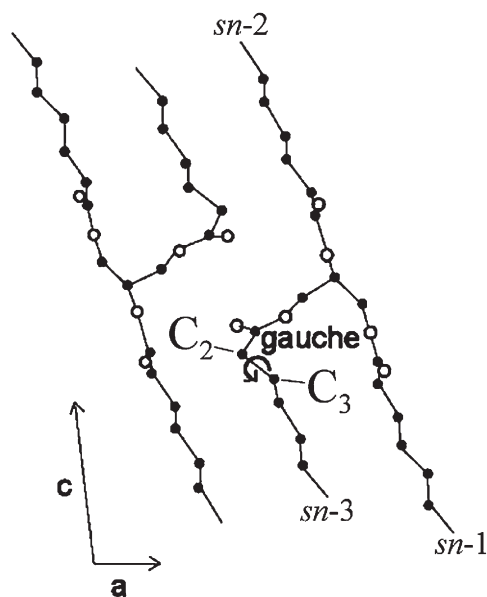


Fig.21. Molecular packing in the vicinity of the glycerol backbone in the  $\beta$  phase of TAGs<sup>1,31,51)</sup>

has a strong influence on the lateral packing and dynamic properties of the acyl chains, eventually affecting the overall TAG phase properties.

Kobayashi *et al.*<sup>40)</sup> reported in a study of oleic acid that the bands at  $1661$ ,  $1657$  and  $1642\text{ cm}^{-1}$  are associated with the olefinic *skew-cis-skew'*, *skew-cis-trans*, *trans-cis-trans* conformations, respectively (Fig. 22). Koyama and Ikeda reported that  $\sim 1657\text{ cm}^{-1}$  is observed in amorphous forms of fatty acid with a *cis* olefin group.<sup>47)</sup>

Additionally, a weak band at around  $1633\text{ cm}^{-1}$  is observed (Fig. 20). This band can be found in some previous reports on TAGs, but the assignment of this band seems to be uncertain. This band is likely to be a mode other than  $-\text{CH}_2-$  ones, since the vibrational modes from polyethylene moiety do not appear in this frequency region (Fig. 18). There are some possible origins of this band. Firstly, the carboxyl C=O stretching mode of impurities, such as diacylglycerols, monoacylglycerols and fatty acids, seems to be explainable. The purity of the commercially available TAG samples is less than 99%, >1% of impurities are therefore contained. Second, the C=C configuration other than shown in Fig. 22 is probably related. It has been reported that *skew-cis-skew'* configuration exists in some fatty acids containing *cis* C=C bond.<sup>85)</sup> The third possibility is the stabilization of  $\pi$  orbital of C=C bonds. In the spectra of TAGs having conjugated C=C bonds show such a low frequency band<sup>107)</sup> because of the stabilization by  $\pi$ - $\pi$  resonances. However, the TAGs shown in Fig. 20 do not have any C=C conjugation. Speculatively, it can be related to the intermolecular  $\pi$ - $\pi$  stacking interaction because this band becomes clearer in the solid phase where the  $\pi$ - $\pi$  stacking is expected to occur. Further investigation is needed for the conclusive assignment.

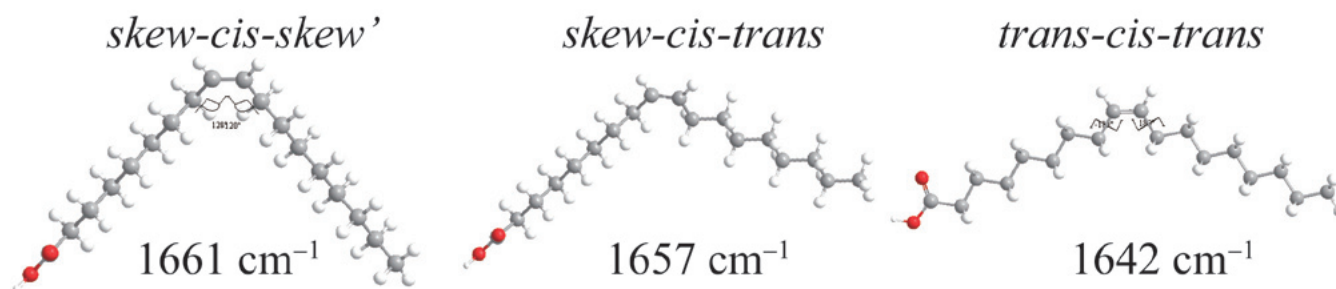


Fig.22. The configurations around *cis* C=C, overall shape of the oleic acid and their frequencies of Raman bands<sup>40)</sup>

### Region 1440 $\text{cm}^{-1}$

Interpretation of this  $\text{CH}_2$  scissors mode region ( $\nu_2$ ) is complex for two main reasons. First, interactions between the vibrational modes whose symmetries are the same lead to Fermi resonances (Fig. 23a).<sup>102</sup> The Fermi resonances arise between the Raman active fundamental,  $\nu_2(\delta=0)$  and the overtone of  $\nu_8(\delta=\pi)$ , and results in a doubling of the band in this region.

The second reason is that these modes are involved in strong inter-chain interactions within crystals.<sup>102,113</sup> For example the orthorhombic perpendicular structure ( $\text{O}_\perp$ ) of polyethylene crystal,<sup>113</sup> which is the only case studied in any detail, the separation of the dispersion curve into a- and b-axis polarized components should be taken into account (Fig. 23b, also see page 31). In the Raman spectra of polyethylene, the band splitting originating from this polarization difference is observed only for  $\nu_2(\delta=0)$  because the value of splitting for this mode is relatively large compared with other modes (Fig. 18).<sup>113</sup> The splitting of these two components is about  $35 \text{ cm}^{-1}$  at  $\delta=0$  (Fig. 23b). As the result, the band  $\sim 1417 \text{ cm}^{-1}$  is

prominent in polyethylene  $\text{O}_\perp$  crystals (Fig. 20a).

In TAGs, the band around  $1460\text{-}1470 \text{ cm}^{-1}$  shifts higher frequency region as the phase transforms into more stable one, *i. e.* liquid  $\rightarrow \alpha \rightarrow \beta' \rightarrow \beta$  (Fig. 20). It is likely due to the increase in inter-chain interaction which affects not only the frequency of  $\nu_2(\delta=0)$  but also the one of  $\nu_8(\delta=\pi)$ . The frequency interval between  $\nu_2(\delta=0)$  and the overtone of  $\nu_8(\delta=\pi)$  reflects in the degree of Fermi resonance interaction.

The band splitting due to the crystal-field effect is distinctive at  $\sim 1417 \text{ cm}^{-1}$  in  $\beta'$ -polymorph which has  $\text{O}_\perp$  subcell structure (Fig. 20d).<sup>38</sup> It is, however, much weaker than that observed in polyethylene  $\text{O}_\perp$  crystal (Fig. 20a). These are some possible reasons; namely crystal defects and imperfect perpendicular arrangements. In  $\beta'$ -polymorph of POP, the incomplete perpendicular arrangement occurs because their palmitoyl (extended) and oleoyl (bent) chains are packed in the same acyl-chain-length structure.<sup>128</sup> In the TAG  $\beta$ -polymorph having the  $\text{T}_{//}$  subcell, in which polyethylene chains are parallel to each other, this band splitting is not apparent.<sup>127</sup>

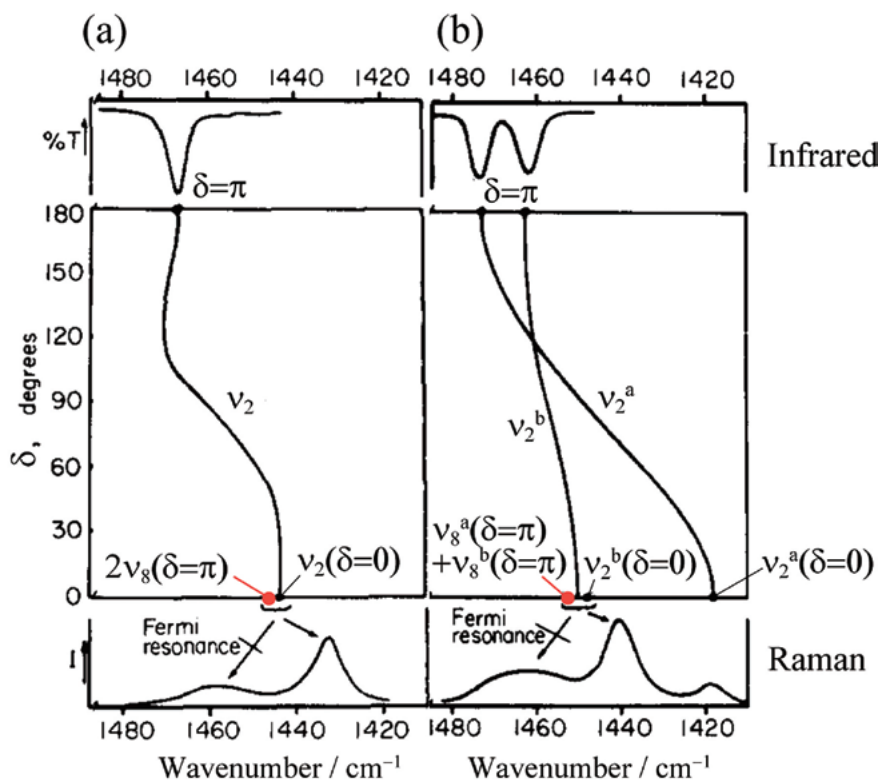


Fig.23. The  $\text{CH}_2$  scissors mode frequencies dispersed in the perpendicular direction, plotted as a function of  $\delta$ .<sup>102</sup>  $\delta$  is the phase difference between two adjacent units  $-\text{CH}_2-$ . (a), the mode of extended isolated polyethylene chain. The doubling of Raman bands due to the Fermi resonance between  $\nu_2(\delta=0)$  and the overtone of  $\nu_8(\delta=\pi)$ ; (b), the modes of polyethylene orthorhombic crystals which are involved in strong intermolecular interactions.

In the melt and  $\alpha$ -polymorph, the splitting can be detected although it is very weak. It may indicate that the acyl-chain planes are arranged not in the totally random way but in somehow biased one. To investigate the structure in TAG melt, it will be interesting to compare the strength of the band splitting between TAG melt and TAG molecules in solution where TAG acyl chains are arranged in the completely random distribution.

#### Region 1370–1180 $\text{cm}^{-1}$

The  $\text{CH}_2$  wagging fundamental,  $\nu_3(\delta = \pi)$ , is prominent in this region. In the polyethylene crystal, this band appears at  $1370 \text{ cm}^{-1}$  (Fig. 20a). It originates from all-*trans* conformation of the extended chains.

In the TAG spectra, this band becomes broader as the chains become more and more conformationally disordered, *i. e.*  $\beta \rightarrow \beta' \rightarrow \alpha \rightarrow$  liquid (Fig. 20). However, the band intensity does not change much, in contrast to some other bands, *e. g.*  $1180 \text{ cm}^{-1}$  (see page 37) and  $\sim 1130 \text{ cm}^{-1}$  (see page 38). Generally, band intensities may undergo drastic changes in going from a *trans* to a *gauche* bond. This intensity constancy is probably due to the orientation of the local polarizability derivative in the disordered chain. Cates, Strauss and Snyder (1994) reported that this band in liquid *n*-alkanes was assigned to the *gauche-trans-gauche*' configuration (Fig. 24).<sup>8)</sup> This sequence has a local center of symmetry that allows this mode to appear in the Raman spectra. Therefore, the conformational change does not change the intensity very much.

The  $\nu_3$  mode shows its progressions in the region of  $1370\text{--}1180 \text{ cm}^{-1}$ .<sup>95)</sup> They sensitively reflect the length and parity (odd/even) of the *trans* chain. The band observed at  $1340 \text{ cm}^{-1}$  in TAG  $\beta'$ - and  $\beta$ -polymorphs

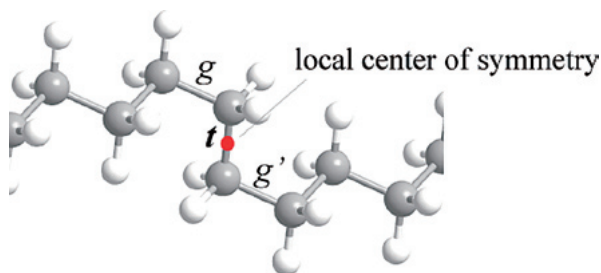


Fig.24. *Gauche-trans-gauche*' conformation observed in liquid phase

may be one of the progression bands (Fig. 20). This  $\nu_3$  progression bands are also appeared in infrared spectra, and Yano *et al.* used these bands as the reference to analyze the *trans* chain length of the acyls of TAGs.<sup>126,127)</sup>

It should be noted that another type of  $\nu_3$  progressions has been reported in a study on *n*-alkanes.<sup>8)</sup> These progressions can be observed also in the liquid phase. It is suggested that their origin lies in the density of vibrational states. For the liquid, the intensity distribution tends to be more even. The progression bands are much broader than those of the ordered chain and usually appear superimposed on a continuous background in the region  $1370\text{--}1180 \text{ cm}^{-1}$ .<sup>8)</sup>

#### Region 1300–1180 $\text{cm}^{-1}$

The strong band at  $\sim 1300 \text{ cm}^{-1}$  is the  $\text{CH}_2$  twisting mode,  $\nu_7(\delta = \pi)$ . The most stable polymorph,  $\beta$ , shows a sharp band at  $1296 \text{ cm}^{-1}$ . On the other hand, liquid phase of TAGs give a strong but relatively broad band around  $1305 \text{ cm}^{-1}$ . Substantial conformational disorder in the liquid phase increases the frequency to around  $1305 \text{ cm}^{-1}$ .<sup>122,129)</sup> The band observed in  $\alpha$  or  $\beta'$  polymorphs is likely to be the superposition of these two bands.

At around  $1170 \text{ cm}^{-1}$ , the zone-center mode of the other side of  $\nu_7$  branch,  $\nu_7(\delta = 0)$ , appears in polyethylene crystal (Fig. 20a). This is the  $\text{CH}_2$  rocking mode. In TAG spectra, this band appears  $\sim 1180 \text{ cm}^{-1}$ . As shown in Fig. 20, this band intensity reflects the conformational disorder in crystals. The  $\beta'$ - and  $\beta$ -polymorphs have higher intensity of this band compare to  $\alpha$ -polymorphs. In the liquid phase, this band smears out. It is known that the infrared rocking mode frequency of a  $\text{CD}_2$  group substituted in a polyethylene chain is sensitive to *trans-gauche* rotational isomerization of the chain.<sup>58)</sup> This sensitivity forms the basis of a commonly used infrared method for determining site-specific conformation in polyethylene systems, and applied to some model biological systems to investigate their conformational disorder.<sup>60,61)</sup> Unlike these  $\text{CD}_2$  rocking bands, the Raman  $\text{CH}_2$  rocking band is not independent of other polyethylene bands; however, it is likely that this is a possible Raman probe for the degree of TAG crystal disorder.

In-between the two bands described above,  $\nu_7$  progression bands ( $0 \neq \delta \neq \pi$ ,  $\text{CH}_2$  twisting-rocking modes)

appear in  $1300-1180\text{ cm}^{-1}$ . The band at  $\sim 1250\text{ cm}^{-1}$  is probably one of these bands because it broadens out in synchronization with  $1180\text{ cm}^{-1}$  ( $\nu_7(\delta=0)$ ) (Fig. 20). The band observed at  $1275\text{ cm}^{-1}$  (Fig. 20e) has been assigned to the same origin;<sup>106)</sup> however, it is more likely to have a different origin because this band does not appear in the spectra of  $\beta'$ -polymorph which show  $1180$  and  $1250\text{ cm}^{-1}$  bands. The assignment of this  $1275\text{ cm}^{-1}$  band is described in the next section. There are several other bands with relatively small intensity in this region. They can be assigned with high possibility to the  $\nu_7$  progression bands or the  $\nu_3$  progressions which overlap in this region.

#### Region $1280-1260\text{ cm}^{-1}$

A broad band  $\sim 1265\text{ cm}^{-1}$  appears in the liquid phase of TAGs containing unsaturated acyl chains (Fig. 20b). The intensity of this band increase when the number of olefinic group increases. The origin of this band is the olefinic  $=\text{CH}$  in-plane deformation.<sup>47)</sup> In the TAG crystals whose olefinic group are stacked (Fig. 25a), this band becomes narrower. From the study of fatty acid with *cis* olefinic group, this band is most intense for the *skew-cis-skew'* conformation of the  $-\text{C}=\text{C}-$  bond (Fig. 25b).<sup>47)</sup> The observed bands in OPO  $\beta$ -polymorph could then be indicative of the *skew-cis-skew'* conformation. On the other hand, the  $\beta'$ -polymorph of POP does not show any distinctive band in this region. This observation supports the FT-IR study of Yano *et al.* (1993) where they reported the  $-\text{C}=\text{C}-$  conformation in  $\beta'$ -polymorph of POP should be deformed from *skew-cis-skew'*.<sup>128)</sup>

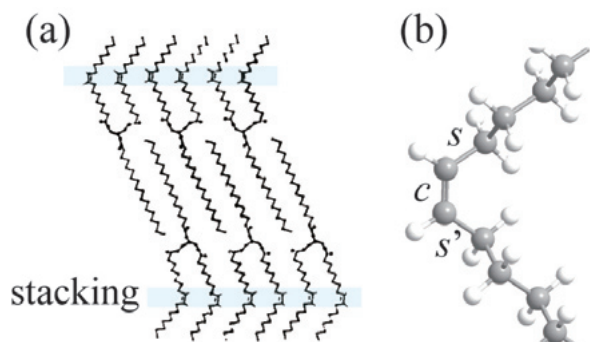


Fig.25. Structures around  $\text{C}=\text{C}$  bonds observed in TAG crystals. (a), Crystal structure of  $\beta$ -polymorph of OSO.<sup>44)</sup>  $\text{C}=\text{C}$  bonds are stacked. (b), *skew-cis-skew'* conformation.

#### Region $1140-1050\text{ cm}^{-1}$

The bands derived from  $\nu_4$  branch, the  $\text{C}-\text{C}$  skeletal stretching modes are observed in this region.<sup>112)</sup> They are one of the most important bands in the Raman spectroscopic study of polyethylene chain structure. Since the chain backbone is directly involved in these vibrations, substantial spectral changes are expected whenever the conformation of the backbone changes. Their band features are applied to investigate the conformational order of lipid bilayer<sup>56,76,122)</sup> and TAGs<sup>13,46,54,55,77)</sup>.

In the Raman spectrum of polyethylene crystal where almost every  $\text{C}-\text{C}$  bond is in *trans* configuration, two sharp and strong bands are observed at  $1130$  and  $1061\text{ cm}^{-1}$  in this region (Fig. 20a). They are the  $\text{C}-\text{C}$  symmetric stretching ( $\nu_4(\delta=0)$ ) and the anti-symmetric stretching ( $\nu_4(\delta=\pi)$ ) modes, respectively (Fig. 16). These two bands are prominent in the spectra of TAG solid phases (Fig. 20c, d and e) and indicating that they contain *trans* zigzag chains.

Between these two prominent bands, some sharp bands can be observed in TAG polymorphs. These bands have been assigned to the  $\nu_4(\delta \approx 0)$  of *trans* zigzag chain.<sup>40)</sup> The frequency of the band is affected by the chain length and chain boundary condition. A fundamental study was conducted by Kobayashi *et al.* using a number of mono-unsaturated fatty acids crystals.<sup>40)</sup> The backbone of these mono-unsaturated fatty acids are separated into two *trans*  $\text{C}-\text{C}$  chains by the  $\text{C}=\text{C}$  bond, one being the methyl-side chain and the other the carboxyl-side chain (Fig. 26). These two chains are different in their boundary

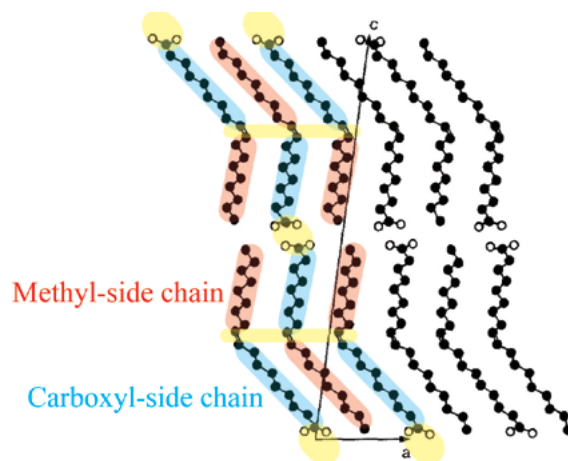


Fig.26. Crystal structure of oleic acid.<sup>33)</sup> Yellow-shaded region indicate the parts where the intermolecular interaction is relatively strong.

condition. For methyl-side chain, one end is free and the other is fixed by inter-molecular interactions at C=C bond (Free-Fixed chain), whereas for the carboxyl-sided chain both ends are fixed because dimerization of the carboxyl groups (Fixed-Fixed chain).

Kobayashi *et al.* used the approximation of the simple coupled oscillators model for the chains with different carbon number ( $n$ ), which for these two types of chain boundary conditions gives the following allowed phase angles ( $\delta$ ) :

$$\delta_k = (2k-1)\pi/2(n-1) \quad (\text{for Free-Fixed chain}) \text{ --- eq.1}$$

$$\delta_k = k\pi/(n-1) \quad (\text{for Fixed-Fixed}) \text{ --- eq.2}$$

where  $k=1, 2, \dots, n-1$

As with polyethylene, the smallest  $k$  value ( $k=1, \delta \approx 0$ ) corresponds to the C-C symmetric stretching vibration and the largest ( $k=n-1, \delta \approx \pi$ ) to the anti-symmetric stretching. Based on the above consideration, they have fitted experimental data of the mono-unsaturated fatty acids using the dispersion curve of the all-*trans* polyethylene  $\nu_4$  mode, leading to the assignment of Raman bands of oleic acid at 1125 and 1095  $\text{cm}^{-1}$  to the C-C symmetric stretching mode of the methyl-side ( $n=9$ , Free-Fixed) and carboxyl-side chains ( $n=9$ , Fixed-Fixed) respectively (Fig. 27).<sup>40)</sup>

It is shown that this assignment is maintained in a TAG, SOS.<sup>106)</sup> The structural arrangement in the oleoyl

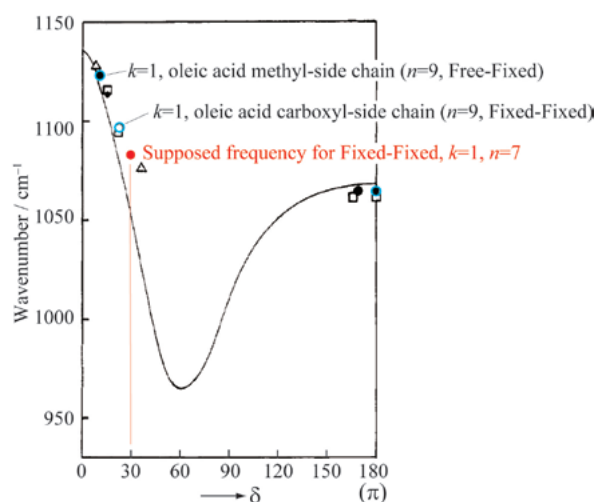


Fig.27. Frequencies of C-C stretching modes for mono-unsaturated fatty acids.<sup>40)</sup> ○, oleic acid; □, palmitic acid; △, petroselinic acid, and ●, erucic acid.

chains of SOS may be seen as similar to the above, since in SOS the fixed-fixed part of the chain will be between the C=C bond and the polar ester groups of the glycerol backbone where intermolecular attraction is relatively strong. The free end of the free-fixed chain will be at the non-polar bilayer interface region.

In the spectrum of  $\beta$ -polymorph of OPO, there is an extra band at 1080  $\text{cm}^{-1}$  in addition to the above mentioned 1125 and 1095  $\text{cm}^{-1}$  bands (Fig. 20). This probably originates from the glycerol-side *trans* chain of *sn*-3 acyl of OPO which is the Fixed-Fixed chain with  $n=7$  (Fig. 28). In TAG  $\beta$ -polymorph, it is known that the *sn*-3 chain is bent in the vicinity of glycerol (Fig. 21). As a consequence, that *trans* chain has a chain length shorter by two, compare to that of *sn*-1 (Fig. 28). Following eq.2, the  $k=1$  mode of Fixed-Fixed chain with  $n=7$  should have  $\delta=30^\circ$ , and likely to have a frequency around 1080  $\text{cm}^{-1}$  (Fig. 27).

In the spectrum of solid phase of PPP, a band exists  $\sim 1100 \text{ cm}^{-1}$  (Fig. 20c and d). This band origin must be a different from  $k=1$  mode. PPP does not have any C=C bond; therefore, it contains only long *trans* chains. For larger  $n$ , the value of  $\delta$  for  $k=1$  becomes smaller near to 0 (eq. 1). Such small  $\delta$  does not explain the frequency of  $\sim 1100 \text{ cm}^{-1}$ . Vogel and Jahnig assigned this band to a  $\nu_4$  progression mode with  $k=3$  of *trans* C-C chain.<sup>122)</sup> PPP contain  $n=16$ , Free-Fixed *trans* chains. The  $\delta$  of  $k=3$  mode for the chain can be calculated from eq. 1, and it is

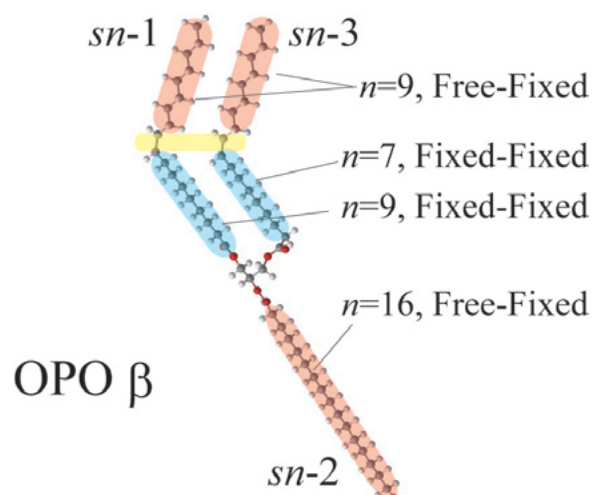


Fig.28. Structure of OPO  $\beta$ -polymorph with indicating each *trans* chain length and its boundary condition

$30^\circ$ . This  $\delta$  value is reasonable to explain this band origin.

The Raman spectra of TAG liquid phase show a characteristic broad band at  $\sim 1080\text{ cm}^{-1}$  (Fig. 20b). This is related to the increased number of *gauche* configuration in the liquid;<sup>13,26,27</sup> however, this band is not directly attributable to *gauche* bond stretching.<sup>98</sup> The broad band shape is probably due to the *trans* chain segmentation and the density-of-states progressions induced by the increased *gauche* configurations (see also page 32).

#### Region $980 - 960\text{ cm}^{-1}$

The band due to *cis* = C - H out-of-plane deformation<sup>56</sup> is seen at  $\sim 970\text{ cm}^{-1}$  in the Raman spectra of liquid TAGs containing unsaturated acyl chains (Fig. 20b).

In the spectra of TAG  $\beta'$ - and  $\beta$ -polymorphs, a series of small bands can be observed. These are likely to be  $\nu_8$  progression bands.<sup>95</sup> In crystals, the  $\nu_8$  branch splits into two components which are polarized along crystal a- and b-axis (Fig. 18). Therefore, each of the progression bands tend to split into two components in the crystals.

#### Region $930 - 700\text{ cm}^{-1}$

The bands observed in  $900 - 875\text{ cm}^{-1}$  region originate from the  $\text{CH}_3$  terminal rocking mode of hydrocarbon chains.<sup>86</sup> This mode is consist of several vibrational modes, principally of in-plane methyl rocking,  $\text{C}_{\omega-1} - \text{C}_\omega$  (the bond between the terminal methyl C atom and the next C) stretching, and CCC deformation which is localized in the end of chains. For a chain longer than about ten carbon atoms, their in-phase and out-of-phase frequencies differ by only a few  $\text{cm}^{-1}$  (Fig. 29).

For a chain shorter than ten, these vibrations which are essentially degenerate in long chains, interact and lead to separated bands as shown in Fig. 29.

The bands observed in OPO  $\beta$ -polymorph spectrum in this region (Fig. 20), *i. e.* 909, 900, 890 and  $877\text{ cm}^{-1}$ , are satisfactorily explained by Fig. 29. However, less stable polymorphs show other bands whose frequencies differ from those in Fig. 29. These bands can be explained by the acyl chain packing imperfections at the crystal layer surface (Fig. 30).<sup>130</sup> TAGs need not always consisting of the set of acyl chains with the best packing compatibility; therefore, it is likely to have some surplus part as shown in Fig. 30. These surplus parts tend to introduce *gauche* rotational configuration, and this change influences on the  $\text{CH}_3$  rocking frequency. The *gauche-trans* configuration from the methyl ends (*gt-*) results in the frequency of

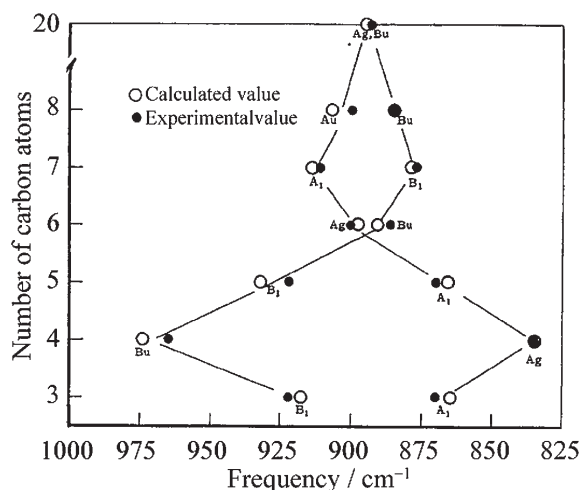


Fig.29. The frequencies of the in-plane methyl rocking mode of *n*-alkanes<sup>86</sup>

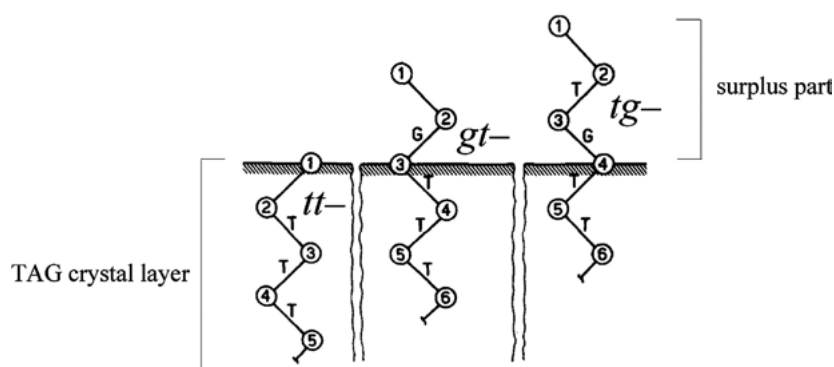


Fig.30. Depiction of the chain packing imperfection at the crystal layer surface.<sup>130</sup> *t*, *trans*; *g*, *gauche*.

879  $\text{cm}^{-1}$ .<sup>37,130</sup> Likewise, *gg*- and *tg*- result in 862 and 850  $\text{cm}^{-1}$ , respectively. These end-*gauche* configurations explain the weak bands in this region (Fig. 20).

It should also be noted here that there are also the bands of  $\text{C}_1-\text{C}_2$  (the bond between the ester C atom and the next C) stretching mode in the region 920–850  $\text{cm}^{-1}$ .<sup>3,72</sup> The band at around 920  $\text{cm}^{-1}$  is probably assigned to this mode.<sup>83</sup> Also, the broad band that contribute the background in the 950–700  $\text{cm}^{-1}$  region which is remarkable in TAG liquid phase spectra (Fig. 20a) is probably due to the delocalized C–C stretching modes at a chain terminal.<sup>98</sup>

On the basis of the accumulated spectroscopic data, Raman spectroscopy has contributed to reveal the detailed structure of TAG polymorphs. The spectral regions other than described in this chapter, *i. e.* low-frequency and  $\sim 3000 \text{ cm}^{-1}$  regions, are also very informative. Raman spectroscopy is really instrumental in elucidating the structure and phase behavior of TAG systems.

## Chapter 4

### Investigation of Molecular Compound Formation in a TAG Binary System

#### Abstract

Raman spectroscopy has been applied to characterize physical mixtures of TAGs. Solid phase and liquid phase of the 1,3-dipalmitoyl-2-oleoyl-*sn*-glycerol (POP) and 1,3-dioleoyl-2-palmitoyl-*sn*-glycerol (OPO) binary system, which is thought to be a molecular compound forming system, were investigated. The obtained Raman spectra were subjected to singular value decomposition (SVD) for extracting the spectrum and the concentration profile for each phase existing in the system. As the result, the existence of the POP-OPO molecular compound is shown spectrometrically in the crystal sample set. The compound is apparently formed at the molar ratio of POP:OPO = 1:2 with deformed C=C configuration, and it is inconsistent with the previous reports. This inconsistency may be due to the difference in thermal treatment of crystal preparation. In the liquid samples, no evidence relating to the compound formation is observed. It is likely that the molecular compound does not exist in the liquid phase and it is the dynamically formed phase being influenced

by crystallizing procedure. The factors affecting the structure of molecular compound are discussed.

#### Introduction

It has been reported that a third component exists in some TAG binary systems. This third component is known as the “molecular compound” and behaves like a new, pure TAG species with unique phase behavior that differs from those of its component TAGs (see also page 28). Specific molecular interactions are thought to be operating between the component TAGs leading to the compound formation. Minato *et al.* (1997) investigated on POP-OPO system by thermal analysis and have clearly shown the formation of molecular compound at POP:OPO = 1:1 ratio.<sup>63</sup> The molecular compound has a stable phase,  $\beta$ -polymorph, with a distinct melting point which is different from that of either of POP or OPO.

The structure model for the POP-OPO molecular compound is proposed by powder X-ray analysis and polarized-infrared spectroscopy.<sup>63,64</sup> Because of the bent geometrical structure of oleoyl chains, it is assumed that compact packing of oleoyl and palmitoyl chains in the same leaflet may arouse serious steric hindrance. Consequently, the structure model with a double chain length structure shown in Fig. 31a is most plausible.<sup>63</sup> This structure is in contrast to the triple chain length structure of corresponding polymorph of each component TAG,  $\beta$ -polymorphs of POP and OSO (Fig. 31b).<sup>44,128</sup> These results indicate that the intermolecular interaction at olefinic groups play a key factor in the formation of a molecular compound.

Despite these quite interesting indications, no precise structural data from single crystal X-ray diffraction techniques on molecular compounds are available. The major reason for this lack of data can be ascribed to difficulties in obtaining single crystals of TAGs containing unsaturated fatty acyls. The crystallinity is often not adequate for crystal X-ray diffraction study.

It is believed that the POP-OPO molecular compound is formed immediately after mixing POP and OPO in their liquid phase.<sup>117</sup> It is based on the readily constructed model structure with supposed of the stacking of olefinic groups (Fig. 31a). If this supposition is correct, oleoyl chain interactions can additionally arise in the liquid

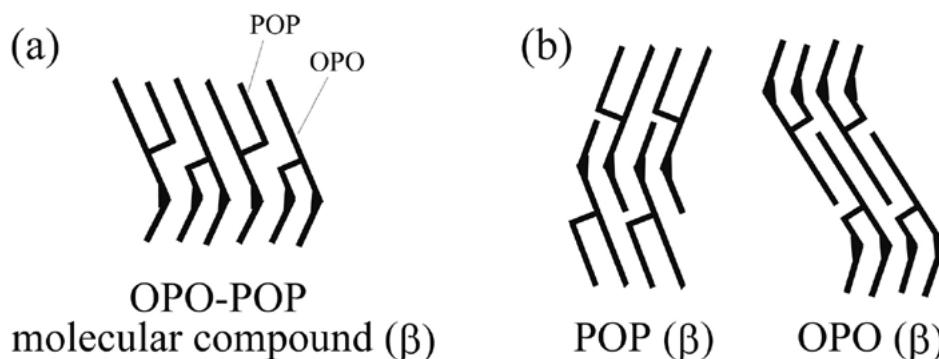


Fig.31. Structure model of the  $\beta$ -polymorph of POP–OPO compound (a),<sup>63)</sup> and the structures of its component TAGs (b).<sup>44,128)</sup>

phase when mixing the component TAGs. To investigate such interaction, Raman spectroscopy is the suitable method. In contrast to X-ray diffraction analysis, Raman spectroscopy can be applied to the liquid phase to study its structure, and indeed, it has revealed the structure formed on TAG crystal nucleation.<sup>26)</sup>

In this chapter, the combination of Raman spectroscopy and singular value decomposition analysis (SVD) has been applied to address the problem of molecular compound formation in the TAG binary system. SVD is useful for extracting physically meaningful components from two-dimensional data dependent on a physical variable. It is obvious that this technique helps to extract the qualitative (spectrum) and quantitative (concentration) information on the molecular compound from a set of Raman spectra of POP-OPO mixture with different concentration of the component TAGs. By using this technique, the structure and the mechanism of the compound formation have been studied.

## Experiment

### Samples

POP and OPO were purchased from Sigma-Aldrich (St. Louis, MO, USA). The purity of the samples was verified by the following gas chromatography and it was about 99%. Both samples were used without further purification. They were completely melted at 50 °C and mixed with a vortex mixer to prepare the eleven samples with different molar ratio of POP and OPO in 10% increments. The concentration of each TAG molecule in the binary mixture was confirmed by gas chromatography. 0.5 mg of the sample was

dissolved into ~50  $\mu$ L of *n*-heptane to make ~10 mg/ml sample solution. 0.5- $\mu$ L solution was injected into a gas chromatograph (Shimadzu GC-17A, Kyoto, Japan) with an auto-injector (Shimadzu AOC-17). Split injection mode was selected and the ratio was 1:10. Helium was used as the carrier gas with 30-cm/s linear gas rate. The injector and detector temperatures were 320 and 370°C, respectively, the oven temperature was raised from 250 to 365°C at a rate of 5°C/min and hold 365°C for 5 min. The gas-chromatography-capillary column was a Rtx-65TG (15-m length, 0.32-mm i.d. and 0.1- $\mu$ m film thickness) (Restek, Bellefonte, PA, USA). Signals were detected with a flame-ionization detector. The reference material IRMM-801 (IRMM, Geel, Belgium) was used for peak identification and determination the calibration factor of each triacylglycerol. The chromatographic peaks detected after 14-min injection, which corresponded to the TAGs with acyls' -carbon-atoms number >40, were integrated to calculate the total TAG amount. Each TAG quantity was expressed as the ratio to the total. All samples were analyzed in duplicate.

Two sample sets were prepared: One is crystals and the other is melts. Crystal samples were prepared as follows: The samples were heated at 50°C to be completely melted and cooled down to 4°C to crystallize the metastable polymorph. They were then placed in an incubator (IJ201, Yamato Scientific, Tokyo) held at 20°C for 11 days to transform the crystals into more stable forms. Nitrogen atmosphere was provided in order to avoid the autoxidation of TAGs. Melt samples were prepared by heating the sample to 50°C and gradually cooling down to 40°C by a cryostat (Linkam 10021, Tadworth, Surrey, UK).

### Differential scanning calorimetry (DSC)

The polymorph of the sample crystals was checked by DSC using a DSC-60 (Shimadzu, Kyoto, Japan). Approximately 1.5 mg of each sample melt was set in an aluminum pan. The pans were incubated with the same thermal condition described in the sample section. The DSC was set to 10°C and analysis was performed from this temperature up to 60°C at a heating rate of 5°C/min. An empty pan was used as a reference sample.

### Raman spectroscopic measurement

The samples were kept at 15 and 40°C for the crystal and melt samples, respectively, by a cryostat during the measurement (Fig. 32). Dry nitrogen atmosphere was provided in order to keep free of sample autoxidation and condensed moisture. Raman scattering was excited with the 532-nm line of a Nd:YVO<sub>4</sub> laser (Verdi, Coherent, Santa Clara, CA, USA). The back-scattered Raman light from the sample was collected by an objective lens (LUCPlanFLN20x, Olympus, Tokyo) and measured with a spectrometer (Shamrock, Andor, Belfast) and an EMCCD detector (Newton, Andor). The integrated Raman intensities of all the polarization components were measured. The laser power was 3 mW at the sample point. Four measurements with 300 s exposure time were accumulated. Spectral resolution was  $\sim 2.1 \text{ cm}^{-1}$ .

### Extraction of the components in the system using singular value decomposition (SVD)

The Raman spectra were analyzed with SVD for

extracting the concentration profile and spectrum for each independent spectral component (Fig. 33). Details are described as follows.

Firstly, Raman spectra were subjected baseline correction using a line fitting and then normalized with the CH<sub>2</sub>-scissors bands in order to eliminate the effect of laser power fluctuation.

The Raman spectra were assembled to form the matrix  $M$  (Fig. 33). The rows and columns of the matrix were the Raman spectra ( $\lambda$ ) and the sample number (11 in the present study), respectively. Then, SVD was applied to the matrix. SVD is a mathematical treatment to decompose a given matrix  $M$  into a product of three matrices  $U$ ,  $W$  and  $V$  (Fig. 33 eq. 1).  $U$  and  $V$  are orthonormal matrices and  $W$  is a diagonal matrix. Each diagonal element of the matrix  $W$  is a positive real number and is called singular value. The magnitude of singular value  $w_{ii}$  indicates the contribution of the product of row vector  $u_i$  and column vector  $v_i$  to the matrix  $M$  (eq. 2). The  $w_{ii}$  are ordered according to their contribution to the total variance in the observations. Hence, the first few elements,  $w_{1,1} \dots w_{n,n}$ , are associated with the physically significant information in the system, and the remaining elements are primarily associated with the random instrumental and experimental error. The  $n$  is therefore the number of significant components in the data set.

Then, by using the acquired number  $n$ , the spectrum and the concentration profile of each component were isolated under constraints in order to minimize ambiguities. The constraints were as follows:

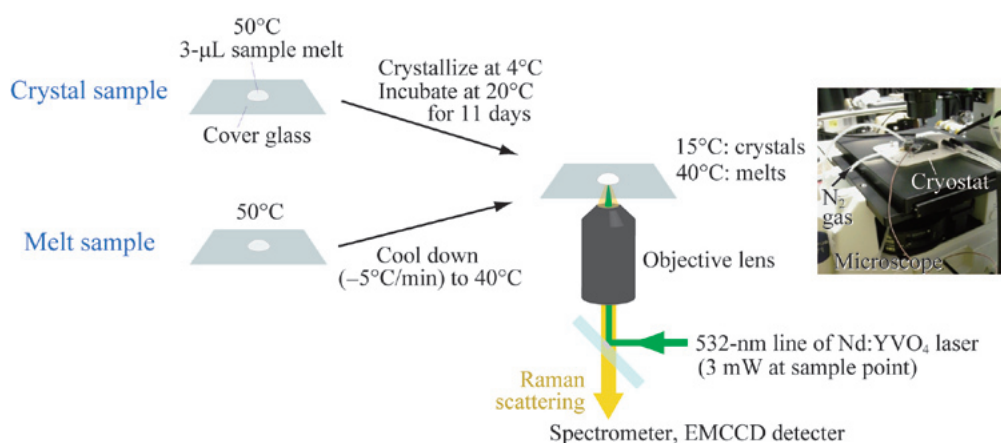


Fig.32. Sample preparation and Raman spectroscopic measurement

$$\begin{aligned}
 \begin{matrix} M \\ \lambda \\ \boxed{\phantom{M}} \end{matrix} &= \begin{matrix} U \\ \lambda \\ \boxed{\begin{matrix} u_1 \\ \vdots \\ u_n \end{matrix}} \end{matrix} \begin{matrix} W \\ n \\ \boxed{\begin{matrix} w_{1,1} \\ \vdots \\ w_{n,n} \end{matrix}} \end{matrix} \begin{matrix} V \\ n \\ \boxed{\begin{matrix} v_1 \\ \vdots \\ v_n \end{matrix}} \end{matrix} & \quad (1) \\
 &= w_{1,1}u_1v_1 + \cdots + w_{n,n}u_nv_n & \quad (2) \\
 &= \underbrace{w_{1,1}u_1v_1 + \cdots + w_{n,n}u_nv_n}_{\text{Significant components}} + \underbrace{w_{n+1,n+1}u_{n+1}v_{n+1} + \cdots + w_{11,11}u_{11}v_{11}}_{\text{error}} & \quad (3) \\
 &= \begin{matrix} U' \\ \lambda \\ \boxed{\begin{matrix} u_1 \\ \vdots \\ u_n \end{matrix}} \end{matrix} \begin{matrix} W' \\ n \\ \boxed{\begin{matrix} w_{1,1} \\ \vdots \\ w_{n,n} \end{matrix}} \end{matrix} \begin{matrix} V' \\ n \\ \boxed{\begin{matrix} v_1 \cdots v_n \end{matrix}} \end{matrix} + \boxed{\text{error}} & \quad (4) \\
 &= \begin{matrix} U' \\ \lambda \\ \boxed{\begin{matrix} u_1 \\ \vdots \\ u_n \end{matrix}} \end{matrix} \begin{matrix} W' \\ n \\ \boxed{\begin{matrix} w_{1,1} \\ \vdots \\ w_{n,n} \end{matrix}} \end{matrix} \begin{matrix} K^{-1} \\ n \\ \boxed{\phantom{K^{-1}}} \end{matrix} \begin{matrix} C \\ n \\ \boxed{\begin{matrix} c_1 \cdots c_n \end{matrix}} \end{matrix} + \boxed{\text{error}} & \quad (5) \\
 &= \underbrace{\begin{matrix} S \\ \lambda \\ \boxed{\begin{matrix} s_1 \\ \vdots \\ s_n \end{matrix}} \end{matrix} \begin{matrix} C \\ n \\ \boxed{\begin{matrix} c_1 \cdots c_n \end{matrix}} \end{matrix}}_{\text{Spectra and concentration profile of the components}} + \boxed{\text{error}} & \quad (6)
 \end{aligned}$$

Fig.33. The scheme of the extraction of the spectra and concentration profiles of the significant components in the data.

- 1) authentic POP and OPO spectra and non-negativity for spectra, and
- 2) non-negativity, unimodality and closure for concentration profiles.

**Results and discussion**

*Properties of the samples*

The concentrations of POP and OPO of the samples were shown in Fig. 34. It is confirmed that the sample set of the present study is composed of the samples with the desired molar ratios of component TAGs in 10% increments.

The DSC heating curves of the samples are shown in Fig. 35. 100%-POP sample shows the endothermic peak at 30.4°C and this corresponds to POP β<sub>2</sub>'-polymorph (Table 3). Likewise, 100%-OPO sample shows the peak at 21.1°C, it is due to the OPO β<sub>1</sub>-polymorph. The samples with any other composition than that of the pure components show an endothermic peak between these two temperatures.

The previous study reported that the melting temperature of POP-OPO molecular compound were 16°C and 32°C for α - and β-polymorph respectively.<sup>63)</sup> From the DSC curves, it is likely that these polymorphs of the POP-OPO molecular compound are not formed in the present study.

*Raman spectra and concentration profiles of the components in the crystal samples*

The Raman spectra of the polycrystals of eleven samples are shown in Fig. 36. Every spectrum shows the sharp conformational-sensitive bands at ~1745, 1296, 1130, ~1100 and 1060 cm<sup>-1</sup> which are characteristic to solid phase of TAGs.

These spectral data are assembled into a matrix and subjected to SVD. The result is shown in Fig. 37. From the first to the third elements have relatively high singular values, while after the fourth elements have small values. This indicates that three distinctive phases exist in the sample set.

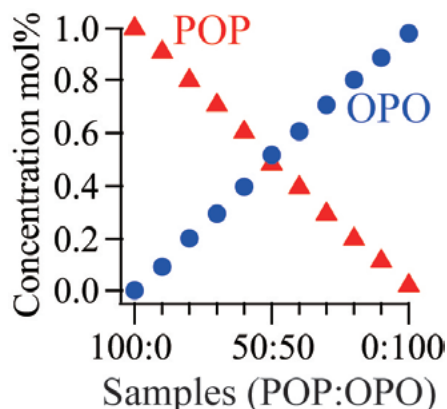


Fig.34. The concentration profiles of POP and OPO of the samples

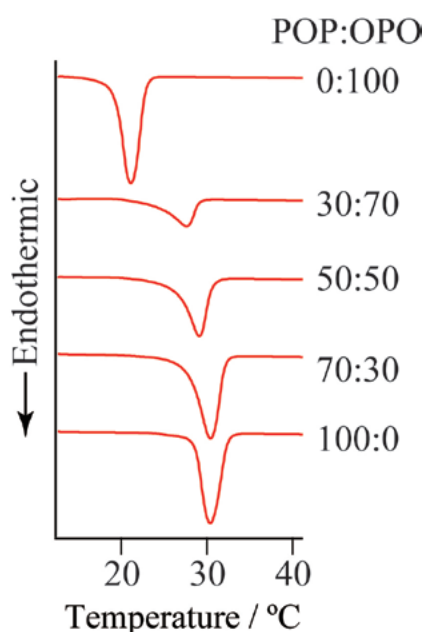


Fig.35. DSC heating thermograms of the crystal samples

Table 3. Melting points of polymorphs of POP<sup>82)</sup> and OPO<sup>63)</sup>

Triacylglycerol	Polymorph	Melting point (°C)
POP	$\alpha$	15.2
	$\gamma$	27.0
	$\delta$	29.2
	$\beta'_2$ (pseudo- $\beta'_2$ )	30.3
	$\beta'_1$ (pseudo- $\beta'_1$ )	33.5
	$\beta_2$	35.1
	$\beta_1$	36.7
OPO	$\alpha$	-18.3
	$\beta'$	11.7
	$\beta_2$	15.8
	$\beta_1$	21.9

Then, the concentration profiles and Raman spectra of these three phases are reconstructed. It is confirmed that two spectral components are not enough to explain the data set. The concentration profiles and spectra show unreasonable features (data not shown). On the other hand, three components successfully explain the data set. The reconstructed concentration profiles and spectra of the three components are shown in Fig. 38 and Fig. 39. When the sample is 100%-POP, concentration index of the component 1 is 1 (Fig. 38), therefore, the component 1 is POP. The reconstructed Raman spectrum for the component 1 successfully reproduces the spectrum of 100%-POP sample (Fig. 39). Likewise, the component 2 is identified as pure OPO. The spectrum for the component 2 also successfully corresponds to that of 100%-OPO sample. The component 3 is likely to be a phase formed by mixing POP and OPO. It shows a meaningful concentration profile. Also, its reconstructed Raman spectrum shows a natural spectral feature which is composed of Lorentzian curves. From these results, the existence of the third component in the binary system is shown spectrometrically, and its concentration profile and Raman spectrum are successfully determined.

#### Structure of the third component

From the acquired concentration profiles (Fig. 38), it is observed that the component 3 is apparently formed at a molar ratio which is different from the previous studies.<sup>63,66)</sup> Fig. 40 shows the model-concentration profile with supposing the third component is formed at POP:OPO = 1:1 or at 1:2 molar ratio. The latter profile is more similar to the acquired profile (Fig. 38). Therefore, the component 3 is thought to be formed at POP:OPO = 1:2 molar ratio.

One plausible reason for this discrepancy is that the component 3 is a polymorph of the OPO other than  $\beta$  and not a molecular compound. The rationale for this is that the sum of the concentration of component 2 (OPO  $\beta$ -polymorph) and component 3 (Fig. 41) almost reproduce the total amount of OPO shown in Fig. 34. However, the melting point of POP:OPO = 30:70 sample, where component 3 accounts for 80% amount (Fig. 38), is about 27.5°C (Fig. 35). This melting temperature is higher than any polymorph of OPO; therefore, it is difficult to assign

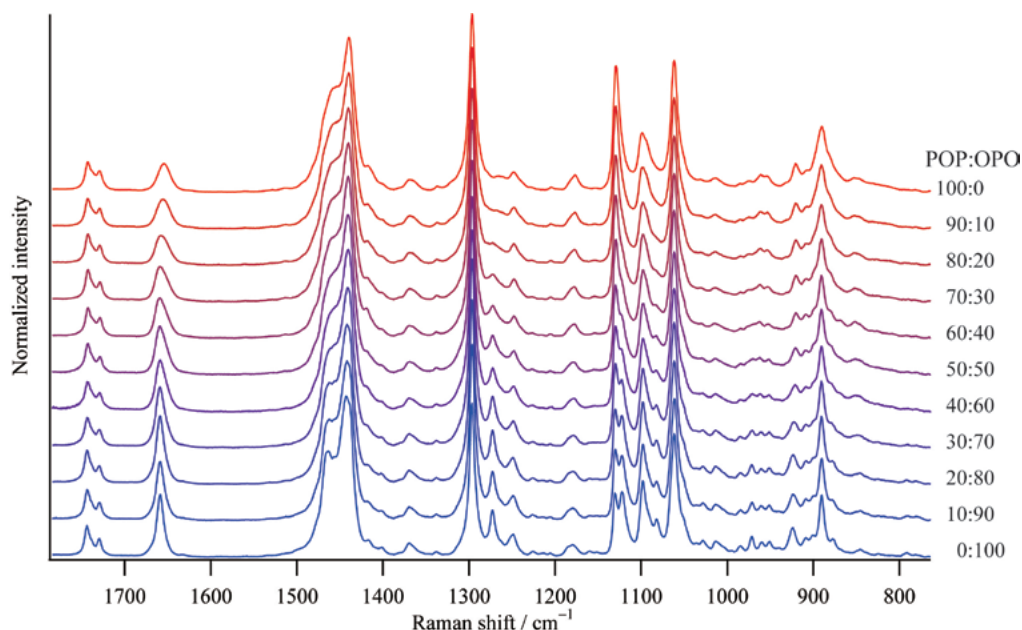


Fig.36. Raman spectra of the polycrystal of eleven POP-OPO binary mixtures

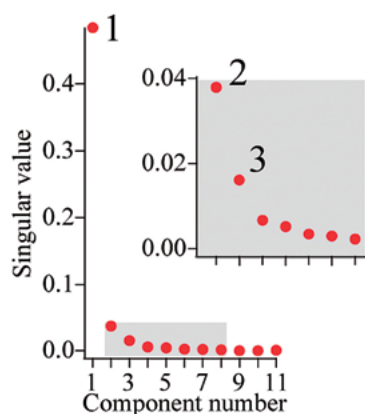
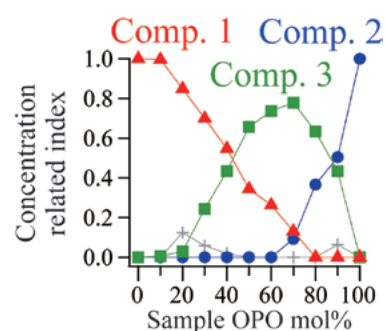


Fig.37. Result of SVD. Three elements are detected as the major ones

Fig.38. Reconstructed concentration profiles of the three components.  $\blacktriangle$ , component 1;  $\bullet$ , component 2;  $\blacksquare$ , component 3; +, residuals.

component 3 to an OPO polymorph. Also, supposing the component 3 as a polymorph of POP is unreasonable in terms of the sum concentration of components 1 and 3. Therefore, the component 3 is more likely to be a phase composed of both TAGs.

To acquire the structural information on the POP:OPO = 1:2 compound, its Raman spectrum is compared to the averaged spectrum of one part of POP  $\beta'$ -polymorph and two parts of OPO  $\beta$ -polymorph ( $1 \times (\text{POP } \beta') + 2 \times (\text{OPO } \beta)$ , Fig. 42). They are both normalized with the  $\text{CH}_2$  scissoring band area ( $\sim 1440 \text{ cm}^{-1}$ ) and their difference spectrum is also shown. The difference spectrum has continuous positive intensities at  $1370\text{--}1230$ ,  $1100\text{--}$

$1000$  and  $880\text{--}800 \text{ cm}^{-1}$ . They are corresponding to the background increases which are characteristic in the spectrum of the less stable polymorphic phase of TAG molecules (see Chapter 3) and indicate the existence of disorder in the crystal especially at the methyl end region of the acyl chains.

The difference spectrum (Fig. 42) shows the  $\sim 1745 \text{ cm}^{-1}$  band broadening to the higher frequency region and the increasing  $\sim 1737 \text{ cm}^{-1}$  band intensity. They are corresponding to the deformations introduced to the vicinity of ester linkages (see Chapter 3). The 1:2 compounds likely to have the conformational ambiguities also at glycerol moieties.

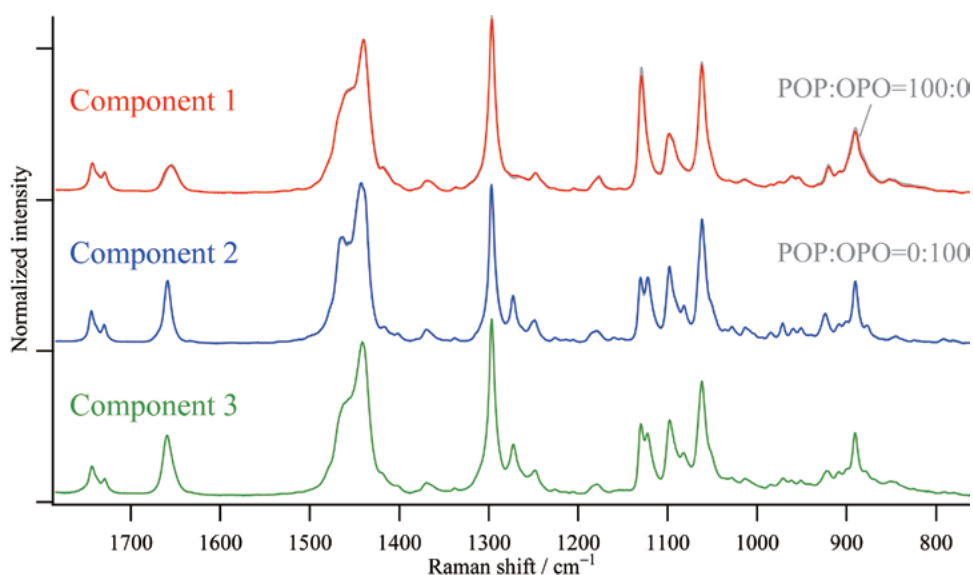


Fig.39. Reconstructed Raman spectra. The spectra of components 1 and 2 almost overlap the spectra of POP-100% and OPO-100% (gray lines), respectively.

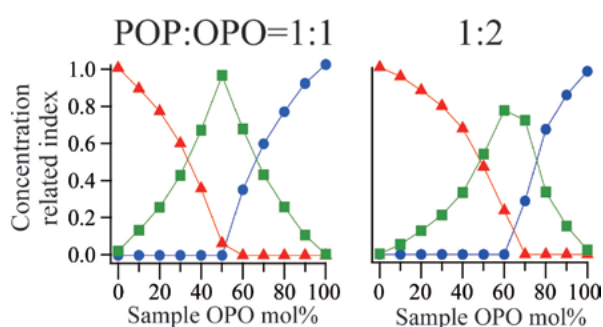


Fig.40. The calculated model concentration profiles with supposing the third component is formed at POP:OPO=1:1 (left) and with supposing 1:2 (right). ▲, component 1; ●, component 2; ■, component 3.

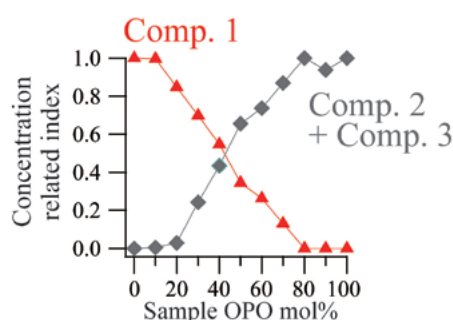


Fig.41. Concentration profiles. ▲, component 1; ◆, component 2 plus component 3.

The sharp feature of  $1272\text{ cm}^{-1}$  band of the 1:2 compound indicates that the compound contains *slew-cis-skew'* configuration at C=C bond (see Chapter 3). However, some other configurations are likely to be also existed since its band intensity and width are smaller and broader than those of OPO  $\beta$ -polymorph (Fig. 39). Fig. 43 shows the C=C stretching band region and the results of the curve fitting by Lorentzian functions. Two bands can be detected at  $\sim 1660$  and  $\sim 1654\text{ cm}^{-1}$  in the 1:2 compound spectrum. The former band is prominent in the OPO  $\beta$ -polymorph and its C=C configuration is assigned to *skew-cis-skew'*.<sup>40)</sup> This C=C configuration leads to a low-angle bend in the oleic acyl and is likely

to play a important role on the intra- and inter-molecular acyl chain stacking as shown in Fig. 44a. The latter band,  $\sim 1654\text{ cm}^{-1}$ , which is observed in POP  $\beta'$ -polymorph corresponds to deformed *slew-cis-skew'* configuration.<sup>128)</sup> Oleoyl and palmitoyl acyls are packed in the same leaflet in POP  $\beta'$ -polymorph (Fig. 44b) and this incomplete stacking of oleoyl acyls deforms the *skew-cis-skew'* configuration. In the 1:2 compound, the existence of  $1654\text{ cm}^{-1}$  band indicates that a significant amount of the deformed configuration exists and the C=C packing is not perfect, it is different from the model proposed by Minato *et al.* (Fig. 31a).<sup>64)</sup>

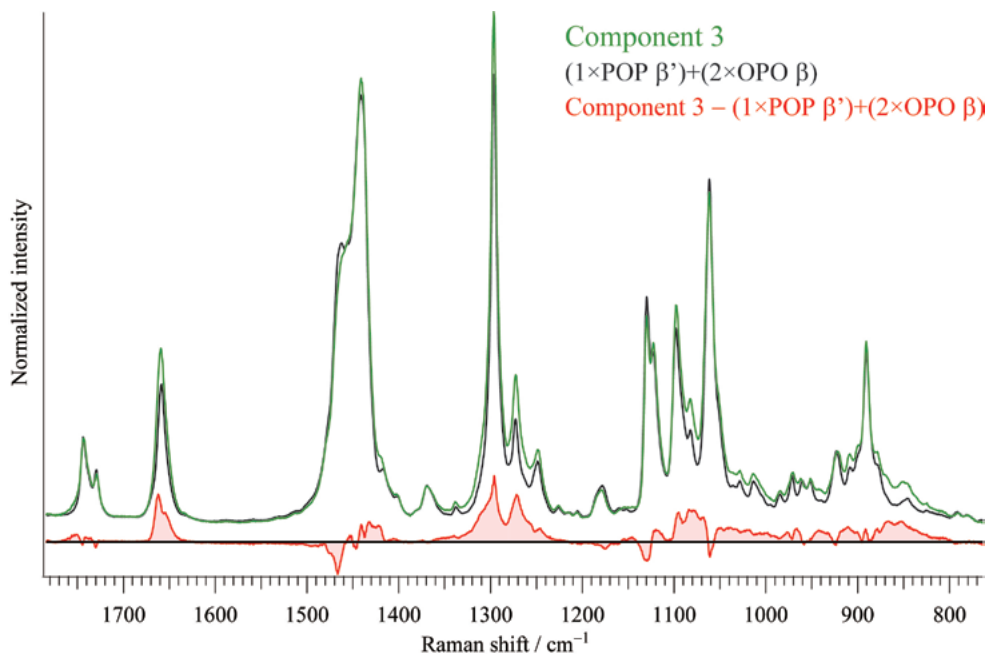


Fig.42. Comparison between the spectra of component 3 and the averaged spectrum of one part of POP  $\beta'$  and two parts of OPO  $\beta$  ( $1 \times \text{POP } \beta' + 2 \times \text{OPO } \beta$ ). The difference spectrum is also shown.

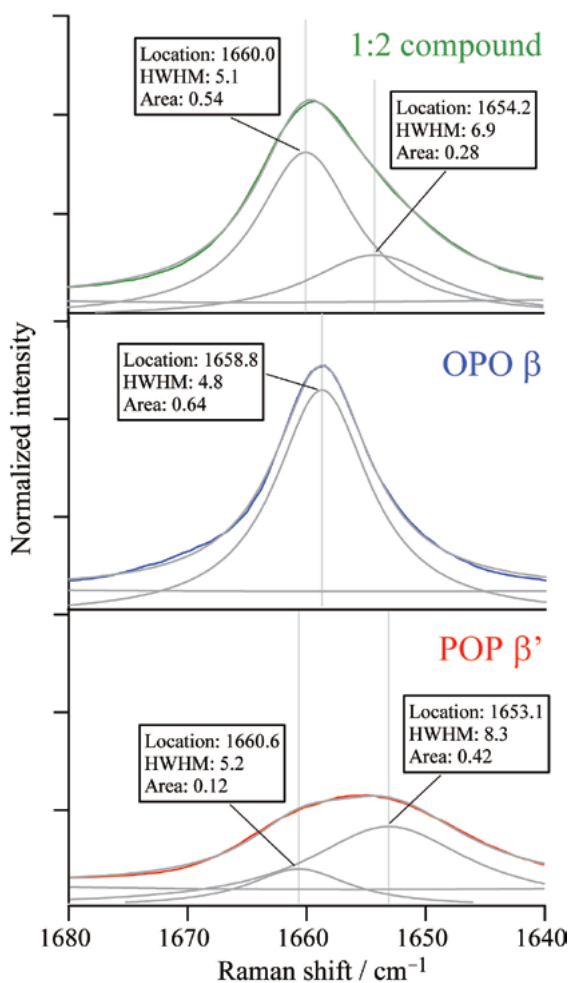


Fig.43. C=C stretching region of the Raman spectra of POP, OPO and 1:2 compound and their curve fitting results.

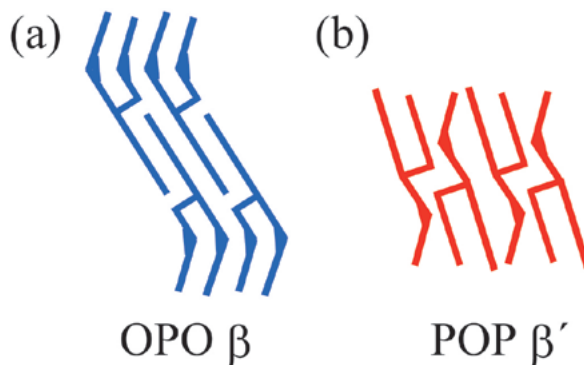


Fig.44. Crystal structures of OPO  $\beta$ -polymorph and POP  $\beta'$ -polymorph<sup>44,128)</sup>

#### Investigation of the compound formation in melt

Regarding the compound formation in liquid phase, Raman spectra of the sample melt were measured at 40°C and analyzed by SVD (Fig. 45). Only two components are detected, corresponding to POP and OPO. This indicates that mixing these two TAG species in the liquid phase does not give rise to intermolecular interactions between POP and OPO similar to those observed in the crystal phase.

In TAG melt, two variants of molecular dimers are considered as stable units (Fig. 46).<sup>70)</sup> They represent different chain length structures with different locations

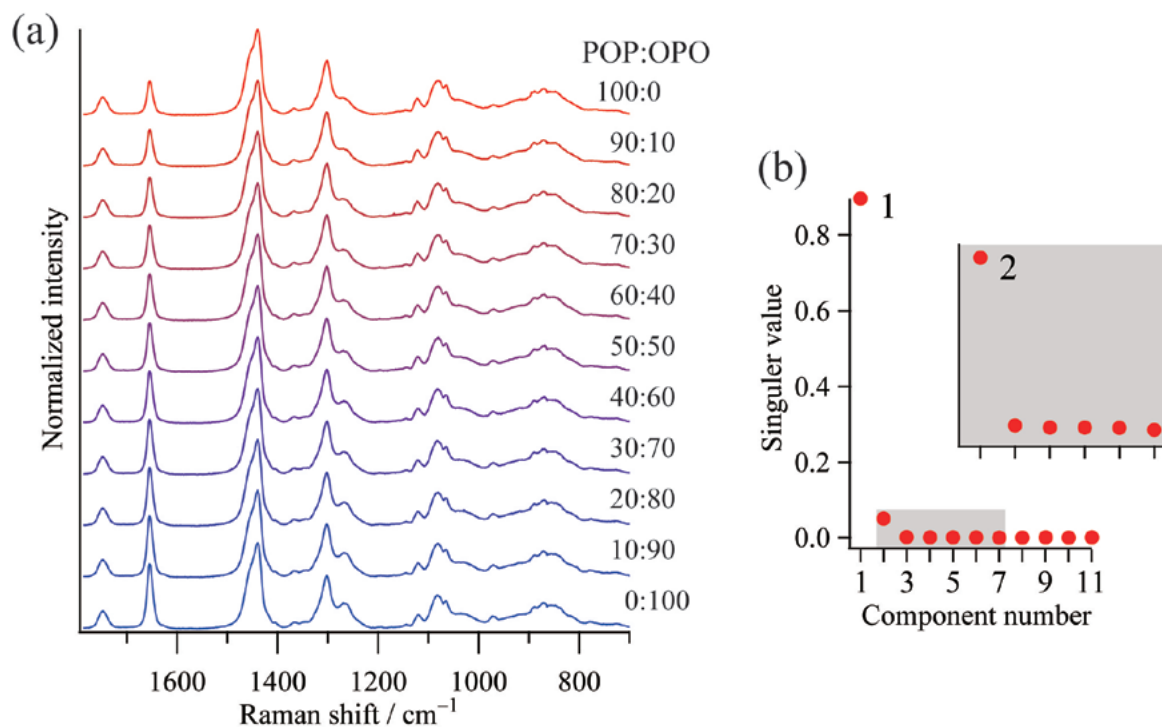


Fig.45. Raman spectra of the melt samples (a) and its SVD result (b)

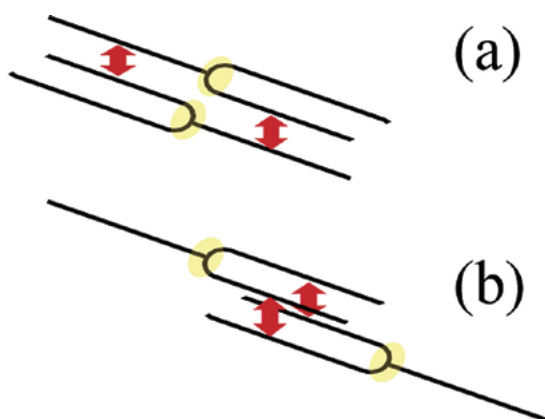


Fig.46. A schematic 3D representation of possible molecular dimers in TAG melts.<sup>70)</sup> (a), glycerol moieties of the adjacent molecules are close to each other and form a dimeric units; (b), glycerol moieties are spaced and form a three-chain length structure.

of the glycerol moieties of adjacent molecules. Both dimers can involve four acyl chain interactions between the two molecules, and the stability of these dimers should be dependent on both the structure of the acyls and the thermodynamic conditions. Regarding the two-chain length structure of the POP-OPO compound model (Fig. 31a), the dimer with the close glycerol moieties

(Fig. 46a) should be more stable in POP-OPO melt. However, any spectral changes ascribed to the increase of this dimer can be detected. It is reported that a packing incompatibility between saturated and unsaturated acyls leads to stabilize both type of dimers in the liquid phase of a TAG consisting of these acyls.<sup>70)</sup> Therefore, both dimers presumably coexist in 100%-POP and 100%-OPO melt, as well as in their mixtures. This is the plausible reason for the any spectral changes observed by mixing.

#### *Factors affecting the structure of molecular compound*

In the present study, the molecular compound is formed at POP:OPO = 1:2 molar ratio which is inconsistent with the previous studies. There are two possible reasons: the difference in the crystal incubation duration and the cooling procedure.

In the study of Minato *et al.*, the binary mixtures of POP and OPO were incubating over one month while the incubation period was eleven days in the present study. Shorter incubation time may generate a metastable structure of the molecular compound other than  $\beta$ -polymorph. This may explain the DSC melting results of this study. However, it is unlikely that the 1:2 compound

will be broken and reconstructed into 1:1 compound after some incubation period.

Regarding the latter possibility, Koyama and Ikeda conducted an interesting study on fatty acids and phospholipids containing C=C bonds.<sup>47)</sup> They reported that the *skew-cis-skew'* configuration dominates in the sample with annealing treatment (slow cooling) while little exists in the samples with rapid cooling. The POP:OPO=1:2 molecular compound have significant amount of the configuration different from *skew-cis-skew'*. This indicates that the crystallizing condition in the present study is somehow faster than those in the previous studies. It was an annealing treatment in the previous study (crystallizing at 20 or 29°C).<sup>63)</sup> More recently, Mykhaylyk and Martin observed a transient mesophase,  $\alpha_2$ -polymorph, after a rapid cooling from melt.<sup>71)</sup> The  $\alpha_2$ -polymorph is specifically observed for TAGs consisting of both saturated and unsaturated acyls. They suggest that the structural incompatibility between saturated and unsaturated acyl chains equalizes the stability of the two molecular pairs in melt (Fig. 46), and results in the  $\alpha_2$ -polymorph where the two pairs coexist.<sup>70)</sup> This is likely to be the reason for the formation of the 1:2 compound, since  $\alpha$ -polymorphs are considered to have large influence on the polymorph which will be formed next. Fig. 47 summarizes the putative mechanism for the formation of

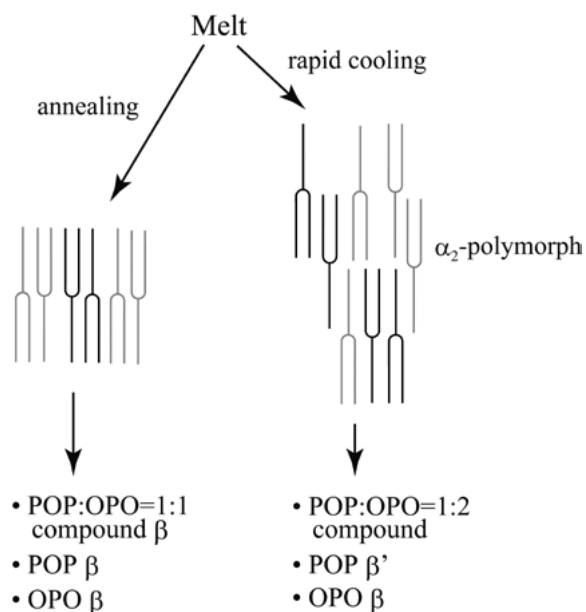


Fig.47. Illustration of the relation between the cooling treatments and the resulting phases

1:1 and 1:2 compounds. An annealing treatment induces the molecular pair with two-chain length structure in the melt, and it will readily form 1:1 compound. On the other hand, a rapid cooling introduces the  $\alpha_2$ -polymorph in the binary system, and its structure provides the decisive difference between the two compound structures. The crystallizing procedure has also modified the POP polymorph. While it is  $\beta$  in the previous study (annealing), it is  $\beta'$  in the present one (rapid cooling).

## Conclusion

The formation of the molecular compound in POP-OPO binary system has been shown spectrometrically. This compound is likely to form at POP:OPO = 1:2 molar ratio, which is different from the previous reports. Since it has been believed that the POP-OPO molecular compound is formed just after mixing the component TAGs in their liquid phase, this observation raises interesting questions. The 1:2 compound shows the deformed C=C configuration which indicates that the compound is formed by a rapid cooling process. The rapid cooling probably introduces the specific phase,  $\alpha_2$ -polymorph, in the POP-OPO system and its structure provides the fundamental difference in the molecular compound structure (1:1 or 1:2). It is likely that the molecular compound does not exist in the liquid phase, it is the dynamically formed phase being influenced by crystallizing procedure.

It is quite interesting how the van der Waals type interaction among the acyl moieties can enable the formation of the stable compound. The ratio of POP:OPO = 1:2 appears plausible, because it also corresponds the number of oleoyl acyls they have. Oleoyls have been thought the key factor forming the compound. The conclusion from the present study is in accordance with this empirical evidence.

## Chapter 5 TAG Phase Behaviors in Multicomponent Systems

### Abstract

Naturally occurring TAGs are present in multicomponent systems which consist of more than 30

TAG species. It is empirically known that the mixing of these multicomponent systems, accompanied by a large TAG compositional change, would indicate a transition to a completely different fat with different phase behavior. However, because of the complexity, the underlying causes are not known so far.

Adopting bovine and porcine fats as the instance of TAG multicomponent systems, the influence of the difference in TAG composition on their phase behavior and phase behavior of their mixture are investigated. From their Raman spectra, it is shown that porcine fats contain  $\beta'$ -polymorphs, while bovine fats do not contain them. The difference arises due to the TAG compositional difference between the two fats. The major TAG species in porcine fats (OSatO) is likely to form  $\beta'$ -polymorphs in the present experimental condition. In bovine-porcine mixture systems, however,  $\beta'$ -polymorphs scarcely exist even in the presence of porcine fat upto 50%. The SatOSat-OSatO type “molecular compound” formation is the most likely reason why the addition of the bovine fat disturbs the  $\beta'$ -polymorph formation. The empirically known drastic changes of phase behavior which are caused by mixing multicomponent systems seem to be due to “molecular compound” formation.

The feasibility of Raman spectroscopy to differentiate the origin of animal fats is also discussed.

## Introduction

The most familiar multicomponent TAG system is probably cocoa butter which chocolates are made of (Fig. 48). This system has been studied extensively for a long time (*e.g.* Peschar *et al.*)<sup>75)</sup> because of its importance in food industry. However, its phase behavior and the underlaid mechanisms have still many secrets.

### “Multicomponent TAG system”



Its phase behavior still remains unclear.

Fig.48. The most familiar multicomponent TAG system

Natural fats are generally made up of TAGs.<sup>6,87)</sup> They contain about more than 30 TAG species<sup>32)</sup> and it is known that these multicomponent TAG systems also exhibit polymorphism.<sup>20,79,115)</sup> The phase behavior varies depending on the TAG composition.

The TAG composition of biological systems is genetically determined. Even though their fatty-acid compositions of the systems do not have much difference (Table 4), their TAG compositions are diverged. This diversity is due to the substrate specificity of the enzymes involved in the TAG biosynthesis (Fig. 5).<sup>89)</sup> This specificity difference is appearing as the difference in *sn*-specific fatty acid composition, *i.e.* TAG composition (Table 5).

As shown in Table 5, bovine fat and porcine fat, which are both widely used in food industry, have different TAG composition. Bovine fats have high concentration of TAGs with oleoyl acyls in their *sn*-2 position. On the other hand, porcine fats have ones with oleoyls in their *sn*-1 and *sn*-3 positions. Saturated fatty acyl chains (*e.g.* palmitic and stearic acyls) occupy the positions other than those mentioned above. They can be depicted as Fig. 49. Such difference in TAG composition may bring about polymorphic difference between these two fats.

It is said that small TAG compositional changes could be explained as the natural variations in the properties of the fats, however, large compositional changes of multicomponent TAG systems would indicate a transition to a completely different fat with different phase behavior.<sup>116)</sup> For example, mixing of porcine fat and palm oil at 1:1 ratio produces the fat containing relatively more solid phase (Fig. 50).<sup>66)</sup> It is suggested that the compound formation is the reason for the change in phase behavior; however, no evidence for the molecular

Table 4. Fatty-acid composition of bovine and porcine fats<sup>124)</sup>

Fatty acid	Bovine	Porcine
Myristic acid (C14:0)	3.7	1.6
Palmitic acid (C16:0)	26.1	23.9
Palmitoleic acid (C16:1)	6.2	2.4
Stearic acid (C18:0)	12.2	12.8
Oleic acid (C18:1)	35.3	35.8
Linoleic acid (C18:2)	1.1	14.3
Linolenic acid (C18:3)	0.5	1.4

Table 5. *Sn*-specific fatty acid composition of bovine <sup>11)</sup> and porcine fats <sup>10)</sup>

Fatty acid	Bovine fat			Porcine fat		
	<i>sn</i> -1	<i>sn</i> -2	<i>sn</i> -3	<i>sn</i> -1	<i>sn</i> -2	<i>sn</i> -3
Myristic acid (C14:0)	2.9	1.5	5.7	0.7	3.5	0.6
Palmitic acid (C16:0)	42.0	24.6	21.9	9.8	72.1	5.4
Palmitoleic acid (C16:1)	2.1	0.8	2.9	1.7	3.7	2.1
Stearic acid (C18:0)	34.4	11.3	32.4	38.8	3.8	11.3
<b>Oleic acid (C18:1)</b>	14.9	<b>55.3</b>	34.6	<b>42.7</b>	14.0	<b>65.4</b>
Linoleic acid (C18:2)	0.2	3.9	0.3	6.3	2.9	15.2
<b>Saturated-acid total</b>	<b>79.3</b>	37.4	<b>60.0</b>	49.3	<b>79.4</b>	17.3
Total	96.5	97.4	97.8	100.0	100.0	100.0

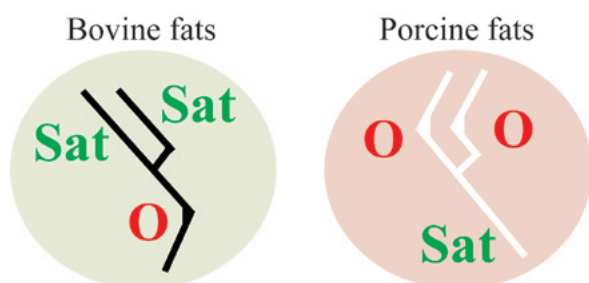
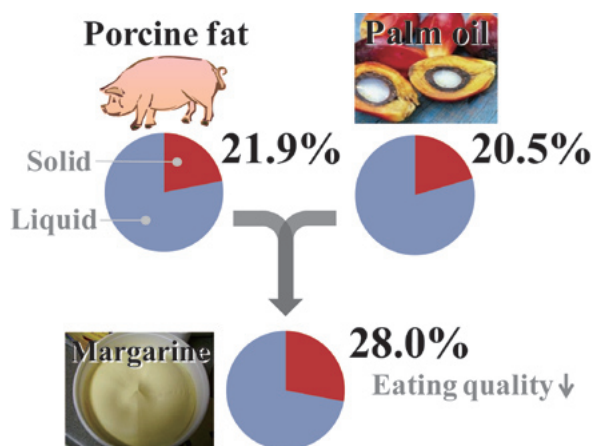


Fig.49. Illustration of the major TAGs of bovine and porcine fats. Sat: Saturated acyl chain. O: Oleoyl chain

Fig.50. After crystallizing at 4°C for 1.5 hours and then incubating at 20°C for 1 week, porcine fat and palm oil contain 21.9% and 20.5% solid phase, respectively. After mixing these two fats, it becomes to contain more solid phase (28.0%). Such a high solid content often deteriorates eating quality. <sup>66)</sup>

compound formation in the mixed multicomponent system has been shown so far.

The objective of this chapter is to investigate the phase behavior of TAG multicomponent systems,

adopting bovine and porcine fats as the instances of such systems. Especially, the influence of the difference in TAG composition on their phase behavior and the phase behavior of their mixture fats are focused. The feasibility of Raman spectroscopy to differentiate the origin of fats is also discussed.

## Experiment

### *Samples and TAG profile analysis*

Seven bovine fats (Bovine tallow A-G) and nine porcine fats (Porcine fat A-I) were used (Table 6). All fats were unfractionated and commercially available. They were used without further purifications. The TAG profiles of the 16 sample fats were analyzed by gas-chromatography (see the experimental section of Chapter 4, page 42).

### *Raman spectroscopic measurement and analysis*

The samples were thoroughly melted at 50°C and 5-μL melt was put on a CaF<sub>2</sub>-slide glass (0.3-mm thickness). The slide glass was set in a cryostat (Linkam 10021, Tadworth, Surrey, UK) and nitrogen atmosphere was provided in order to avoid autoxidation. Firstly, the sample was heated at 80°C for 1 min to erase any crystal memories. Then crystals were prepared by cooling down to incubation temperatures (10, 0, -10 and -20°C) at a rate of -20°C/min and hold for 5 min. Raman spectra were measured after the incubation and the samples were kept at the incubation temperature in a cryostat during the measurements.

Raman scattering was excited with the 785-nm line

of a Ti-sapphire laser (Spectra Physics 3900S, Newport, Santa Clara, CA, USA) (Fig. 51). The back-scattered Raman light from the sample was collected by an objective lens (LUCPlanFLN20x, Olympus, Tokyo, Japan) and measured with a spectrometer (Chromex 250i, Bruker Optik GmbH, Ettlingen, Germany) and a CCD detector ( $400 \times 1340$  pixels, Spec-10 400BR(LM), Roper, Sarasota, Florida, USA). The laser power, measured by a power meter with a photodiode sensor (PD300, Ophir Optronics, Jerusalem, Israel), was 30 mW at the sample point. Three measurements with 60 s exposure time were accumulated.

Spectral resolution was  $3.8 \text{ cm}^{-1}$ . The laser focal point was about  $11 \mu\text{m}$  in diameter with  $60\text{-}\mu\text{m}$  spatial resolution in the horizontal direction.

Raman measurements were made in duplicate. The spectra were averaged, baseline subtracted and deconvoluted with the slit function of the spectrometer (a Gaussian function, the half width at half maximum was  $1.9 \text{ cm}^{-1}$ ) with the use of a triangular apodizing function. The deconvoluted spectra were normalized with the  $\text{CH}_2$ -scissors bands ( $1410 - 1480 \text{ cm}^{-1}$ ) in order to eliminate the effect of laser power fluctuation. The intensity of

Table 6. Samples and their detailed information

Sample name	Product name	Identity
Bovine fat	A "Beef tallow"	Sigma-Aldrich, 03-0660
	B "Edible beef tallow"	Manufacturer 1, product A, lot. A
	C "Edible beef tallow"	Manufacturer 1, product A, lot. B
	D "Refined beef tallow"	Manufacturer 2, product A
	E "Edible refined beef tallow", JAS*	Manufacturer 3, product A, lot. A
	F "Edible refined beef tallow", JAS	Manufacturer 3, product A, lot. B
	G "Hett"	Manufacturer 4, product A
Porcine fat	A "Pork fat"	ERM <sup>†</sup> -BB444
	B "Pork fat"	ERM-BB446
	C "Pork fat"	BCR <sup>‡</sup> -430
	D "Refined lard", JAS	Manufacturer 1, product B, lot. A
	E "Refined lard", JAS	Manufacturer 1, product B, lot. B
	F "Refined better lard", JAS	Manufacturer 3, product B, lot. A
	G "Refined better lard", JAS	Manufacturer 3, product B, lot. B
	H "Refined lard"	Manufacturer 4, product D, lot. A
	I "Refined lard"	Manufacturer 4, product D, lot. B

\*JAS: Japanese Agricultural Standard

<sup>†</sup>ERM: European Reference Material

<sup>‡</sup>BCR: Community Bureau of Reference

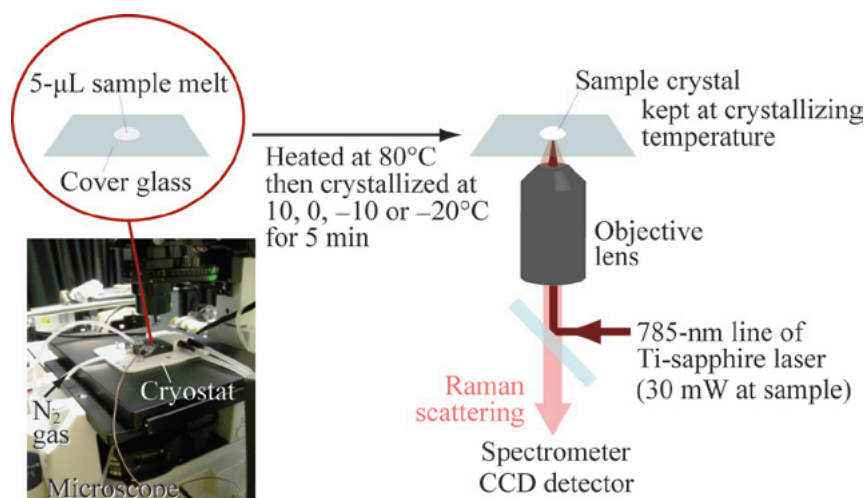


Fig.51. Sample preparation and Raman spectroscopic measurement

the  $1417\text{ cm}^{-1}$  band was acquired by band fitting using a Lorentzian function and the data were assessed with Welch's analysis of variance and the *t*-test.

## Results and discussion

Fatty acyls are abbreviated: Myristic acyl, M; palmitic acyl, P; oleic acyl, O; stearic acyl, S; linoleic acyl, L; arachidic acyl, A. TAG molecular species are expressed with three-letters notation using the abbreviated letters, *e.g.* POS. "POS" can include six TAG species: *Sn*-POS, *sn*-PSO, *sn*-OPS, *sn*-OSP, *sn*-SPO and *sn*-SOP, while "*sn*-POS" means the specific TAG species: *Sn*-1-palmitoyl-2-oleoyl-3-stearoylglycerol.

### TAG profile of the samples

The TAG profiles of tested samples are presented in Table 7. Though variances among previous studies exist, the overall tendency of the profile of the present study is in agreement with these reports.<sup>17,32)</sup> In reference to these studies, *sn*-OPO is the most abundant TAG species in the present-sample set of porcine fats. Its concentration is estimated to be approximately 22% (w/w) of the total TAG; *sn*-OPO accounts for more than 95% of POO in porcine fats<sup>32)</sup> and the POO concentration of the present study is about 23%. This POO concentration (23%) has been derived by using its relative amount (77%, Dugo *et al.*, 2006) to POO+PLS (30.1% of the total TAG, Table 7). On the other hand, *sn*-POO/OOP is the major component in the bovine fats. Its concentration is estimated to be approximately 22% (w/w) of the total TAG; *sn*-POO/OOP

accounts for ~86% of POO<sup>32)</sup> that corresponds to 25.1% of POO+PLS in bovine fats.<sup>17)</sup> The second major TAG in the bovine fats is *sn*-POS/SOP whose concentration is estimated to be ~7% (w/w) of the total TAG; *sn*-POS/SOP accounts for 61%<sup>32)</sup> of POS (11.3% of the total TAG, Table 7).

### Raman spectra of fat crystals

On cooling, melts of bovine- and porcine-fats begin to crystallize when the temperature becomes approximately  $20^{\circ}\text{C}$ . Both fats show granular morphologies composed of a large number of small crystals. It is difficult to identify polymorphic forms only by microscopic images because a polymorphic form could appear in different crystal sizes and different crystal shapes.<sup>35)</sup>

Fig. 52 shows the optical image of bovine and porcine fats. They show polycrystalline morphology. By the use of an objective lens with a small numerical aperture (N.A. = 0.45), the size of focal point ( $11\text{ }\mu\text{m}$  in diameter with  $60\text{ }\mu\text{m}$  in depth) is set enough larger than those of crystals. This helps in acquiring the Raman spectra of a polycrystal with more randomized arrangement.

The Raman spectra of bovine fat A and porcine fat A, which have moderate compositions within each fat group (Table 7), at different incubation temperatures are compared in Fig. 53a. Though these Raman spectra largely resemble one another, the porcine fat shows a shoulder at  $1417\text{ cm}^{-1}$  (Fig. 53b), while the bovine fat does not exhibit this band at the incubation temperature of  $\geq 0^{\circ}\text{C}$ . This band is assigned to the  $\text{CH}_2$ -scissors mode characteristic of the orthorhombic perpendicular ( $\text{O}_{\perp}$ ) subcell structure.

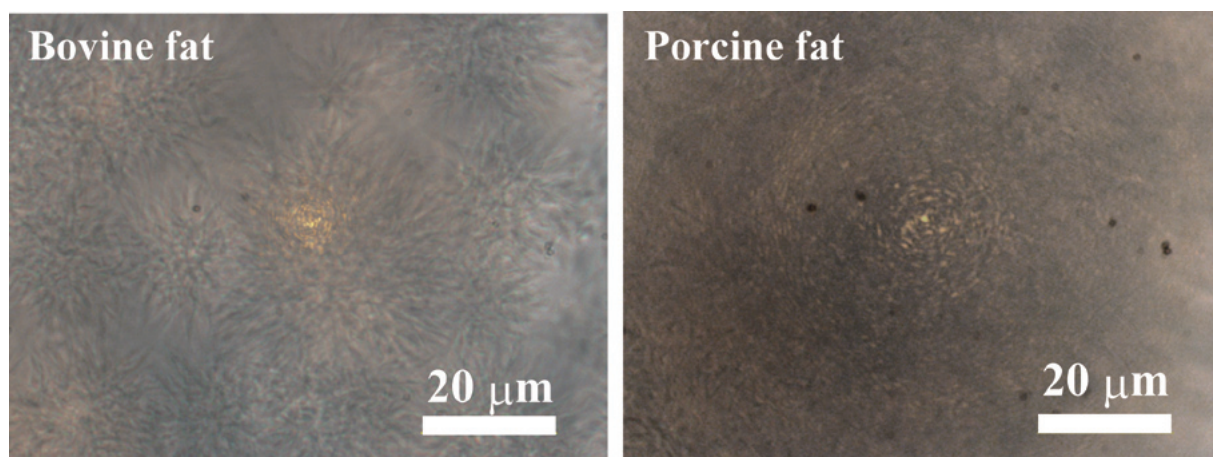


Fig.52. Crystals of bovine and porcine fats at  $5^{\circ}\text{C}$

Table 7. TAG profiles of the samples. Unit: g/100-g total TAG.

		TAG molecule*							
		PPP	MOP	PPS	POP	PLP	PSS	POS	POO (OPO) +PLS
Bovine fat	A	2.0 ± 0.0 <sup>†</sup>	4.2 ± 0.1	2.5 ± 0.0	9.4 ± 0.1	0.9 ± 0.1	1.6 ± 0.0	12.3 ± 0.0	25.9 ± 0.1
	B	3.6 ± 0.0	4.1 ± 0.0	2.4 ± 0.0	10.7 ± 0.0	1.1 ± 0.2	1.4 ± 0.0	10.1 ± 0.1	23.3 ± 0.1
	C	3.8 ± 0.0	4.4 ± 0.0	2.6 ± 0.0	11.6 ± 0.0	1.3 ± 0.2	1.5 ± 0.0	10.6 ± 0.0	25.1 ± 0.0
	D	6.1 ± 0.0	4.4 ± 0.0	2.8 ± 0.1	12.4 ± 0.2	1.2 ± 0.2	1.3 ± 0.0	10.2 ± 0.1	23.4 ± 0.1
	E	2.5 ± 0.0	4.5 ± 0.0	2.9 ± 0.0	9.8 ± 0.0	1.1 ± 0.1	2.2 ± 0.0	12.1 ± 0.0	25.2 ± 0.1
	F	2.1 ± 0.0	4.8 ± 0.1	2.6 ± 0.1	9.4 ± 0.1	1.1 ± 0.0	1.9 ± 0.0	11.3 ± 0.2	24.9 ± 0.4
	G	1.6 ± 0.0	3.7 ± 0.1	2.3 ± 0.0	8.8 ± 0.0	1.0 ± 0.2	1.7 ± 0.0	13.1 ± 0.2	26.8 ± 0.2
Median		2.5	4.4	2.6	9.8	1.1	1.6	11.3	25.1
Porcine fat	A	0.7 ± 0.0	1.7 ± 0.1	2.1 ± 0.1	9.0 ± 0.1	1.2 ± 0.1	1.9 ± 0.0	20.3 ± 0.0	30.5 ± 0.0
	B	0.7 ± 0.0	1.8 ± 0.0	2.1 ± 0.0	9.2 ± 0.0	1.2 ± 0.2	1.9 ± 0.0	20.2 ± 0.0	30.6 ± 0.1
	C	0.5 ± 0.0	1.7 ± 0.1	1.6 ± 0.1	7.5 ± 0.1	1.8 ± 0.1	1.5 ± 0.0	18.6 ± 0.0	30.1 ± 0.1
	D	1.0 ± 0.0	2.2 ± 0.0	2.4 ± 0.0	8.9 ± 0.1	2.0 ± 0.2	2.2 ± 0.0	19.8 ± 0.1	29.0 ± 0.0
	E	1.0 ± 0.0	2.2 ± 0.0	2.4 ± 0.0	8.9 ± 0.1	1.8 ± 0.1	2.2 ± 0.0	19.5 ± 0.0	28.7 ± 0.2
	F	0.9 ± 0.0	2.1 ± 0.1	2.4 ± 0.0	9.1 ± 0.1	1.6 ± 0.1	2.1 ± 0.0	20.1 ± 0.1	29.3 ± 0.1
	G	0.9 ± 0.0	2.2 ± 0.0	2.4 ± 0.0	9.1 ± 0.1	2.0 ± 0.2	2.1 ± 0.0	19.6 ± 0.1	29.2 ± 0.1
	H	0.7 ± 0.0	1.9 ± 0.0	1.9 ± 0.0	8.4 ± 0.0	1.0 ± 0.2	1.6 ± 0.0	18.9 ± 0.1	30.9 ± 0.1
	I	0.8 ± 0.0	1.8 ± 0.0	2.3 ± 0.0	8.5 ± 0.0	1.3 ± 0.0	2.3 ± 0.0	19.9 ± 0.1	30.1 ± 0.1
Median		0.8	1.9	2.3	8.9	1.6	2.1	19.8	30.1

*continued*

		TAG molecule*							
		PLO	SSS	SOS	SOO	OOO+SLS	SLO	SOA	AOO
Bovine fat	A	4.0 ± 0.1	1.0 ± 0.0	3.8 ± 0.1	8.3 ± 0.1	4.9 ± 0.3	1.0 ± 0.2	0.1 ± 0.0	–
	B	4.4 ± 0.1	0.8 ± 0.0	2.6 ± 0.1	6.0 ± 0.1	4.4 ± 0.2	0.9 ± 0.2	6.2 ± 0.1	0.1 ± 0.0
	C	4.7 ± 0.0	0.9 ± 0.0	2.8 ± 0.0	6.5 ± 0.0	4.5 ± 0.2	1.0 ± 0.1	0.1 ± 0.1	–
	D	4.5 ± 0.1	0.8 ± 0.0	2.6 ± 0.0	5.9 ± 0.0	4.7 ± 0.1	0.9 ± 0.1	–	–
	E	4.7 ± 0.1	1.2 ± 0.0	2.9 ± 0.0	6.6 ± 0.1	4.3 ± 0.0	1.2 ± 0.1	–	–
	F	4.4 ± 0.1	1.1 ± 0.0	3.2 ± 0.1	7.2 ± 0.1	4.5 ± 0.1	1.2 ± 0.0	–	–
	G	4.2 ± 0.0	1.0 ± 0.0	4.0 ± 0.1	8.8 ± 0.0	5.1 ± 0.0	1.0 ± 0.1	0.1 ± 0.0	–
Median		4.4	1.0	2.9	6.6	4.7	1.0	0.1	–
Porcine fat	A	8.8 ± 0.0	0.5 ± 0.0	1.2 ± 0.0	3.7 ± 0.1	3.3 ± 0.0	1.9 ± 0.0	–	–
	B	8.9 ± 0.0	0.5 ± 0.0	1.2 ± 0.0	3.5 ± 0.0	3.3 ± 0.0	2.0 ± 0.1	–	–
	C	11.1 ± 0.1	0.5 ± 0.0	1.1 ± 0.0	3.5 ± 0.0	3.2 ± 0.0	2.2 ± 0.0	0.1 ± 0.0	–
	D	8.5 ± 0.1	0.5 ± 0.0	1.5 ± 0.1	4.1 ± 0.1	3.3 ± 0.0	1.9 ± 0.1	–	–
	E	8.3 ± 0.1	0.5 ± 0.0	1.6 ± 0.0	4.1 ± 0.0	3.6 ± 0.1	1.9 ± 0.0	–	–
	F	8.5 ± 0.1	0.4 ± 0.1	1.4 ± 0.0	3.9 ± 0.1	3.4 ± 0.2	1.9 ± 0.1	–	–
	G	8.3 ± 0.1	0.5 ± 0.0	1.4 ± 0.0	3.7 ± 0.1	3.5 ± 0.0	1.9 ± 0.2	–	0.1 ± 0.0
	H	8.8 ± 0.1	0.5 ± 0.1	1.5 ± 0.0	4.4 ± 0.0	3.9 ± 0.1	2.2 ± 0.0	–	–
	I	8.9 ± 0.1	0.5 ± 0.0	1.5 ± 0.0	4.1 ± 0.0	3.5 ± 0.0	2.2 ± 0.1	–	–
Median		8.8	0.5	1.4	3.9	3.4	1.9	–	–

\* TAGs shown are the identifiable major species present

<sup>†</sup> Values represent the mean value of two replicates with standard deviation

<sup>39)</sup> In terms of TAG, it is the  $\beta'$ -polymorph that has the  $O_{\perp}$  subcell structure to give rise to this band. <sup>82)</sup> It is therefore shown that the porcine fat contains the  $\beta'$ -polymorph under the present experimental conditions. It is widely known that porcine fats tend to be crystallized in  $\beta$ -form. <sup>20,115)</sup> Due to the highly-biased distribution of palmitic acyl at *sn*-2 position in porcine fats, they are easy to pack and

reorder to the most orderly and stable polymorphic form,  $\beta$ . The metastable  $\beta'$ -polymorph formation in the present study is most likely to be caused by the rapid cooling rate and short incubation time. Campos and co-workers also reported that a rapid cooling induced  $\beta'$  in a porcine fat. <sup>7)</sup> Nucleation and growth of the metastable form normally predominate in fat crystallization and reformation to the

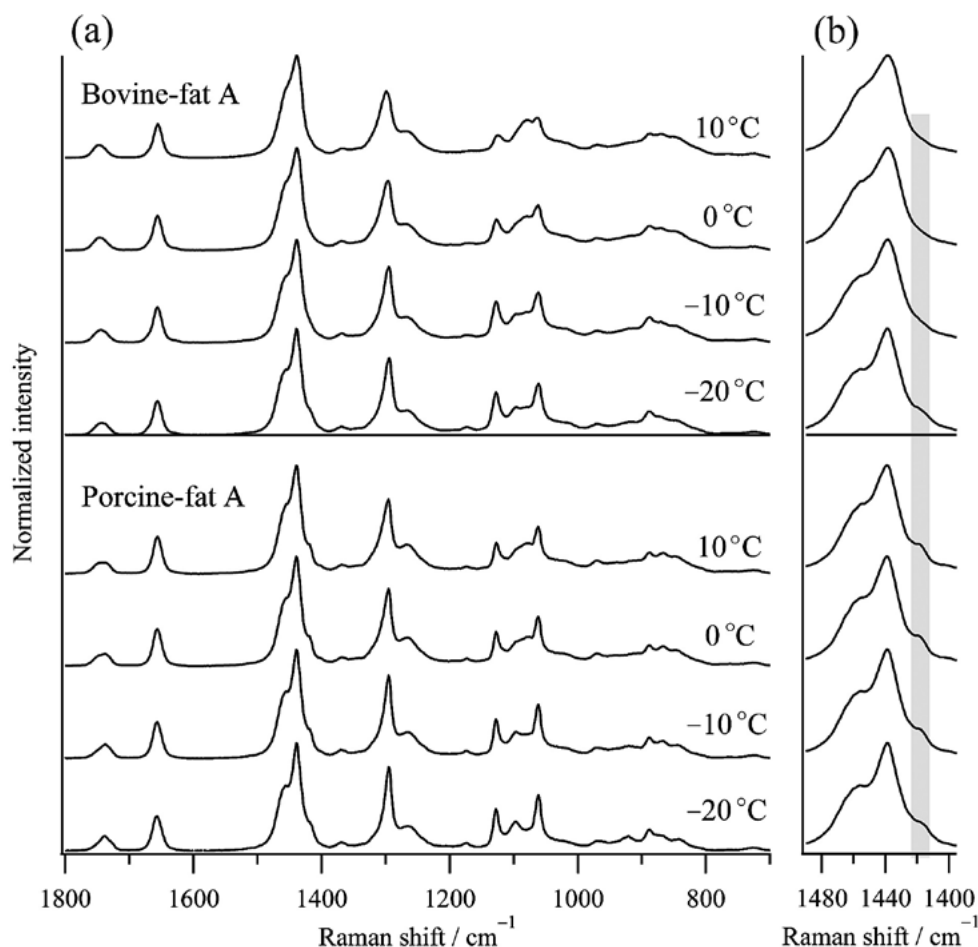


Fig.53. Raman spectra of bovine- and porcine-fats at each incubation temperature. (a) Spectra of bovine-fat A and porcine-fat A. These two fats have the medium TAG composition within each animal-fat group (see Table 2). (b) Enlarged spectra of the CH<sub>2</sub>-scissors region corresponding to each left-hand-side spectrum. Shaded region indicates the position  $\sim 1417 \text{ cm}^{-1}$ .<sup>67)</sup>

most stable polymorph is the kinetic process that takes time. The reformation seems to be uncompleted within the 5-min incubation period in the present study.

In the bovine fat, cooling to  $-20^\circ\text{C}$  produces the  $\beta'$ -polymorph (Fig. 53b). This observation is in accordance with the previous study that has reported the rapid cooling to  $-25^\circ\text{C}$  produces the  $\beta'$ -polymorph in bovine fat.<sup>79)</sup> On the contrary the incubation temperatures of 10, 0 and  $-10^\circ\text{C}$  induce small amount of  $\beta'$ -polymorph formation even though the melting point of  $\beta'$ -polymorph in bovine fats is higher than these temperatures.<sup>79)</sup> It might be because the cooling to above  $-20^\circ\text{C}$  provided insufficient supercooling for the bovine fat to crystallize in the  $\beta'$  form. For TAG crystallization, it is known that melts should be cooled well below the melting point because of the free energy penalty associated with crystal formation.<sup>59)</sup> More

stable polymorphs have higher free energy penalty and therefore they need more supercooling to crystallize. The incubation temperatures above  $-20^\circ\text{C}$  are likely to form less stable  $\alpha$ -polymorph in the bovine fat and this is confirmed by the Raman spectra.

This difference in crystallization is due to the difference in  $\Delta G^{\ddagger}$  (see Chapter 2, page 27). The values of  $\Delta G^{\ddagger}$  for bovine and porcine fats are almost impossible to measure because these fats do not express distinctive melting points. They melt over a wide range of temperature rather than at a distinctive temperature as would be the case for pure TAGs. However, the melting points ( $T_m$ ) of SatOSat and OSatO TAGs have been studied in details (Fig. 54).<sup>14)</sup> OSatO type TAGs, which are the major components in porcine fats, have relatively low melting temperature than SatOSat. It means that

OSatO has higher Gibbs free energy, therefore,  $\Delta G^{\ddagger}$  is smaller in OSatO. The difference in free energy is likely to be the reason for the formation of more stable polymorph ( $\beta'$ ) in porcine fats (Fig. 55).

The differences, other than the  $1417\text{ cm}^{-1}$  band between the spectra of the bovine fat and those of the porcine fat, are not sensitive to the polymorphic difference. Relatively large differences are observed in the C–C stretch- ( $1140\text{--}1040\text{ cm}^{-1}$ ) and the C=O stretch-region ( $1770\text{--}1720\text{ cm}^{-1}$ ). The intensities of these

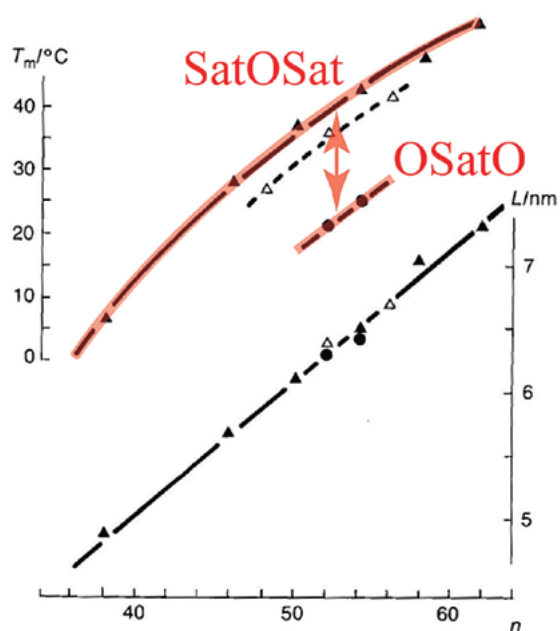


Fig. 54. Difference in melting point ( $T_m$ ) of  $\beta$ -polymorphs of SatOSat and OSatO type TAGs.  $n$ : the number of acyl chain carbon atoms.  $\blacktriangle$ , SatOSat;  $\bullet$ , OSatO;  $\triangle$ , SatO(Sat+2).<sup>14)</sup>

conformation-sensitive bands have been employed as a measure of conformational order of TAG.<sup>5,128)</sup> However, the significant amount of liquid TAG (*i. e.* TAG in random form) within the sample masks the band features due to the crystal polymorphs. At the temperature range of the present experiment, bovine fats and porcine fats are in the form of crystalline suspensions in liquid-form TAG.

The  $1417\text{ cm}^{-1}$ -band intensities ( $A_{1417\text{ cm}^{-1}}$ ) of both fats are acquired by band fitting (Fig. 56a) and their dependence on incubation temperatures is shown (Fig. 56b). The difference in  $A_{1417\text{ cm}^{-1}}$  between the porcine and bovine fats is most remarkable when the incubation temperature is  $-10\sim 0^\circ\text{C}$ .

Fig. 57a shows the Raman spectra of the seven bovine fats and the nine porcine fats measured at the incubation temperature of  $0^\circ\text{C}$ . The  $1417\text{ cm}^{-1}$  band is easily detected in all porcine fats, while it is very weak in bovine fats. The  $A_{1417\text{ cm}^{-1}}$  value of each sample is acquired by the band fitting and plotted for each fat group in Fig. 57b. The variances of the  $A_{1417\text{ cm}^{-1}}$  values of these two groups are unequal; therefore, Welch's *t*-test is conducted to find whether the averages are significantly different. The average  $A_{1417\text{ cm}^{-1}}$  value of porcine fats is statistically higher than that of bovine fats at a significance level of  $P < 0.0001$  (Fig. 57b). It is therefore shown that this Raman band discriminates the origins of the present sample sets. The difference in polymorphic features enables Raman spectroscopy to distinguish these two fats by a single band.

In the next step, the crystallization behaviors of

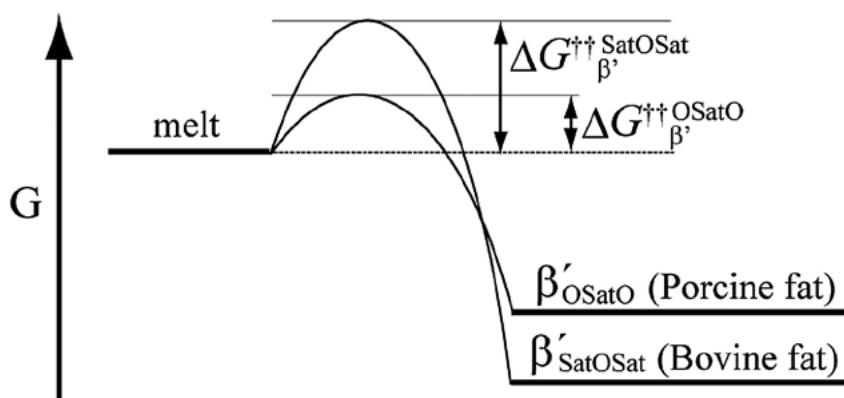


Fig. 55. Schematic diagram for the  $\Delta G^{\ddagger}$  of  $\beta'$ -polymorph of SatOSat and OSatO TAGs

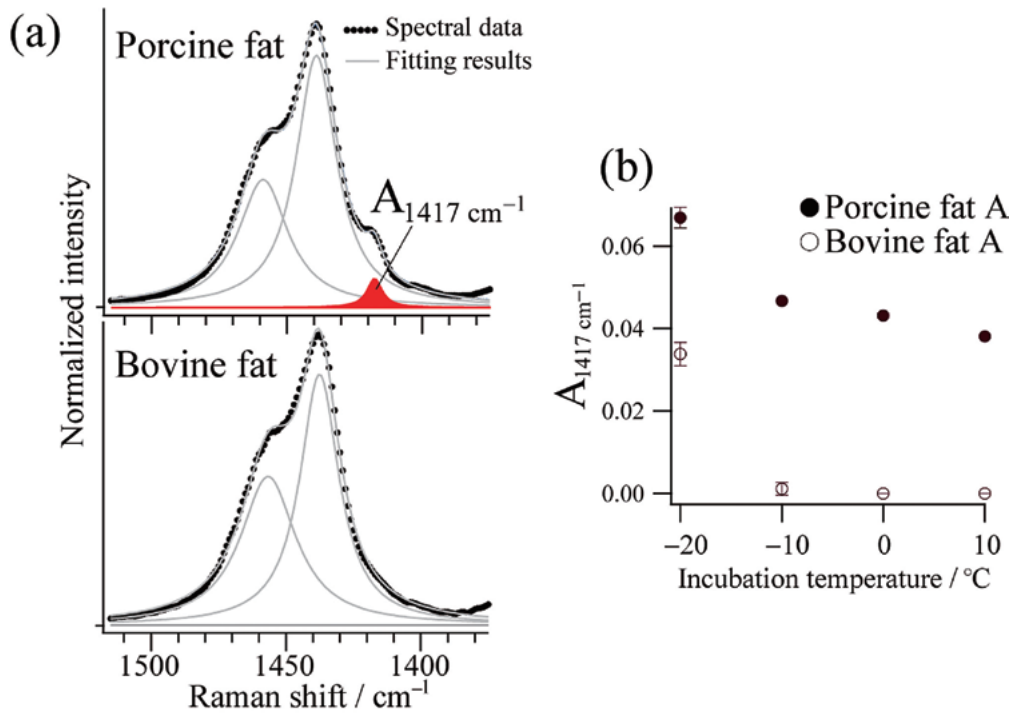


Fig.56. The  $1417 \text{ cm}^{-1}$ -band intensities ( $A_{1417 \text{ cm}^{-1}}$ ) of both fats. (a) Intensities are acquired by Lorentzian-band fitting. (b) Relation between  $A_{1417 \text{ cm}^{-1}}$  and incubation temperatures.<sup>67)</sup>

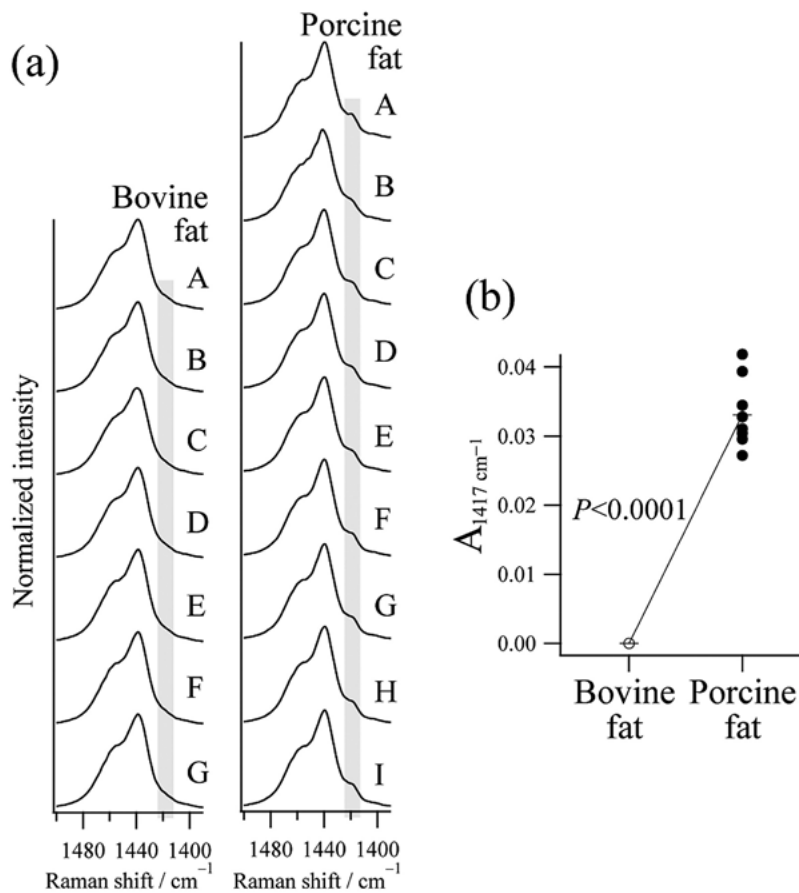


Fig.57. Raman spectra of the  $\text{CH}_2$ -scissors region of all samples after rapid cooling down to and incubation at  $0^{\circ}\text{C}$  (a). The  $1417 \text{ cm}^{-1}$ -band intensity ( $A_{1417 \text{ cm}^{-1}}$ ) of each sample is plotted for each fat group (b). The average  $A_{1417 \text{ cm}^{-1}}$  value of each fat group (indicated by —) is also plotted. The porcine fats have statistically higher  $A_{1417 \text{ cm}^{-1}}$  values than the bovine fats at a significance level of  $P < 0.0001$ .<sup>67)</sup>

bovine-porcine-mixture fats are investigated. Bovine-fat A and porcine-fat A were thoroughly melted and mixed using a vortex mixer to prepare the mixture fats with different porcine-fat concentrations. The  $1417\text{ cm}^{-1}$  band intensities measured for 15-different-mixing ratios are plotted in Fig. 58. When porcine fat concentrations are below 50%, the band intensities at  $1417\text{ cm}^{-1}$  are too small to be detected. It is indicated that the  $\beta'$ -polymorph scarcely exists even in the presence of porcine fat upto 50%. The approximated-straight line of the band intensity ratio does not intersect the point of origin (solid line in Fig. 58). Considering the fact that the porcine fat contains a large amount of  $\beta'$  forming TAGs (*i. e.* OSatO), this line should intersect the point of origin (dashed line in Fig. 58). The addition of the bovine fat markedly disturbs the  $\beta'$ -polymorph formation of these TAGs.

The “molecular compound” formation is the most likely reason why the addition of the bovine fat disturbs the  $\beta'$  formation in the porcine fat (Fig. 59). The porcine fat TAGs (OSatO) are likely to produce “molecular compounds” with the TAGs in added bovine fats (SatOSat). The OSatO/SatOSat-type molecular compound forms  $\alpha$  and  $\beta$  polymorphs but does not form  $\beta'$ .<sup>48,63</sup> “Molecular compounds” are likely to be formed also in multicomponent systems.

## Conclusion

It has been shown that bovine and porcine fats have different crystallization properties. In the present

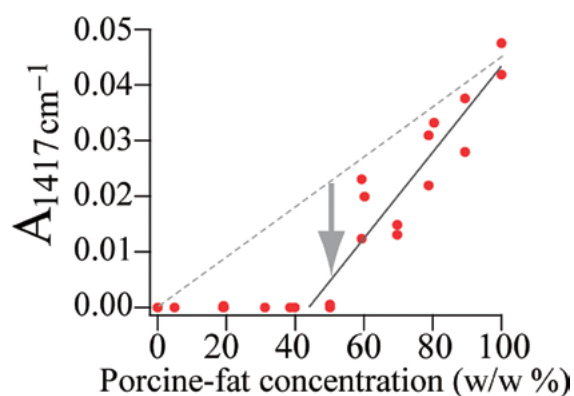


Fig.58. Relation between  $A_{1417\text{ cm}^{-1}}$  and porcine-fat concentration. The dashed line is the approximated-straight line fitted with the data of 60–100% porcine-fat concentrations. The arrow indicates the hindrance of  $\beta'$ -polymorph formation by mixing the fats.

experimental condition, porcine fats contain  $\beta'$ -polymorph, on the other hand, bovine fats contain  $\alpha$  but not  $\beta'$ -polymorph. It is due to their TAG compositional differences: OSatO-type TAG, the major TAG in porcine fats, has smaller  $\Delta G^{\ddagger}$  than SatOSat-type, the major TAG in bovine fats. This difference in crystallization properties is reflected in their Raman spectra. Porcine fats exhibit the band at  $1417\text{ cm}^{-1}$  which is derived from the  $O_{\perp}$  subcell structure of  $\beta'$ -polymorph.

Using above described difference, Raman spectroscopy can differentiate bovine fats and porcine fats by the single band at  $1417\text{ cm}^{-1}$ . In bovine-porcine fat mixture, however, this band is not detected even in the presence of porcine fat upto 50%; an addition of bovine fat to porcine fat is likely to produce SatOSat-OSatO type molecular compound in the mixture, and they do not form polymorph.

Food safety requires the development of reliable techniques that ensure the origin of animal fats. In 2007, a food processing company added porcine fats to its bovine products, such as minced beef, for getting unfair profit.<sup>50</sup> The detection sensitivity of the present method will be higher in bovine-porcine adipose tissue mixture than in extracted fat mixture; because the porcine fat tends to exist within cells and avoid complete mixing with the bovine fat. Also, Raman spectroscopy is not too sensitive to water which is contained in biological tissues. This is the advantage of this method. The possibility of application of this Raman spectroscopic method to adipose tissues will be investigated.

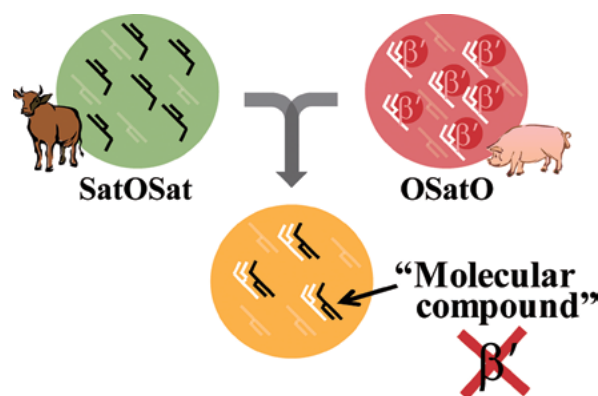


Fig.59. Description for the reduction in  $\beta'$ -polymorph in the mixture fats

The thermal history is the key factor that makes this method feasible. If an appropriate incubation temperature is found, other fats can also be discriminated by their polymorphic features. This new idea of using polymorphic features to discriminate the fat origin will contribute to refine the existing spectroscopic methods. IR spectroscopy can also employ this idea: IR absorption bands of the  $\text{CH}_2$ -rock and  $\text{CH}_2$ -scissors modes also show distinctive bands derived from orthorhombic-subcell structure of the  $\beta'$ -polymorph.<sup>39)</sup> Raman spectroscopy which is sensitive to fats crystal structure has high potential as the powerful tool for the quality control of fats.

## Chapter 6

### Conclusion

With a view to understand the complicated phase behavior of natural fats, I have investigated on the physical mixtures of TAGs by Raman spectroscopy. The results indicate that a third component, the molecular compound, is formed in a model binary TAG system and its structure seems to be influenced decisively by crystallizing procedures. The molecular compound may be the phase dynamically formed by crystallization rather than existing stationary in the liquid phase as previously considered. In addition, the present study implies that the molecular compound may exist not only in a model binary system but also in multicomponent systems. It is also shown that one can differentiate the origin of natural fats by detecting the difference in their polymorphic phases by using Raman spectroscopy.

For a deeper understanding on TAG structures and phase behaviors, Raman spectroscopy is a promising method which can contribute to solutions of the remaining issues described below:

#### 1. Structures formed during initial stages of TAG crystallization.

It has been suggested that the structure of the polymorph that appears first on crystallization works decisively to influence the overall phase behavior. Revealing the mechanism of formation of this first-appearing polymorph is important from the application point-of-view, since it has a potential to program TAG

phase behavior for producing better industrial products. The polymorph which appears first on crystallization is an unstable phase; therefore, the fast methods which can trace the phase transition are required. Raman spectroscopy has already fulfilled this requirement. Most recently, Raman spectrum of low-frequency region that is sensitive to crystal structures can be obtained less than one second.<sup>73)</sup> It is, thus, fast enough to trace the TAG phase transition.

#### 2. Conformation of glycerol moieties

Glycerols are the backbone of TAGs and also of other lipids, and influence the overall structure of these molecules. It has been suggested that the glycerol moieties adopt specific configurations in each TAG polymorphs. However, there is little information on the conformation of the glycerol moieties. It is not only due to the lack of precise structural data from single-crystal XRD but probably also due to the lack of the information of the vibrational spectrum of glycerol moieties. Raman spectroscopy can provide the fundamental information on this backbone structure.

#### 3. Characteristics of TAGs in a living system

TAGs are the form of energy storage of a living system. Therefore, their characteristics such as content, unsaturation degree, acyl chain length and turnover speed should reflect the condition of a cell. Since Raman spectroscopy can measure such quantities of TAGs *in situ*, it has a potential to dynamically monitor the condition of a living cell based on its lipid profile.

On the basis of the accumulated spectroscopic data, Raman spectroscopy has contributed to reveal the structure and the phase behavior of TAG model systems. The three Raman spectroscopic studies described above will provide the new insights of TAG systems. Recent developments on the spectrometer enable to acquire the spectra with high sensitivity. They offer bright future prospects for the Raman spectroscopic studies on multicomponent TAG systems. Raman spectroscopy helps us to draw the whole picture of the phase behavior of natural fats.

## References

- 1) Akita, C., Kawaguchi, T. and Kaneko, F. (2006). Structural study on polymorphism of *cis*-unsaturated triacylglycerol: Triolein, *Journal of Physical Chemistry B*, 110(9), 4346-4353.
- 2) Bicknell-Brown, E., Brown, K.G. and Person, W.B. (1980). Configuration-dependent Raman bands of phospholipid surfaces. 1. Carbonyl stretching modes at the bilayer interface, *Journal of the American Chemical Society*, 102(17), 5486-5491.
- 3) Bicknell-Brown, E., Brown, K.G. and Person, W.B. (1981). Configuration-dependent Raman bands of phospholipid surfaces. 2. Head group and acyl stretching modes in the 800–900  $\text{cm}^{-1}$  region, *Journal of Raman Spectroscopy*, 11(5), 356-362.
- 4) Bresson, S., El Marssi, A. and Khelifa, B. (2005). Raman spectroscopy investigation of various saturated monoacid triglycerides, *Chemistry and Physics of Lipids*, 134(2), 119-129.
- 5) Bresson, S., El Marssi, M. and Khelifa, B. (2006). Conformational influences of the polymorphic forms on the C=O and C–H stretching modes of five saturated monoacid triglycerides studied by Raman spectroscopy at various temperatures, *Vibrational Spectroscopy*, 40(2), 263-269.
- 6) Buchgraber, M., Ullberth, F., Emons, H. and Anklam, E. (2004). Triacylglycerol profiling by using chromatographic techniques, *European Journal of Lipid Science and Technology*, 106(9), 621-648.
- 7) Campos, R., Narine, S.S. and Marangoni, A.G. (2002). Effect of cooling rate on the structure and mechanical properties of milk fat and lard, *Food Research International*, 35(10), 971-981.
- 8) Cates, D.A., Strauss, H.L. and Snyder, R.G. (1994). Vibrational modes of liquid *n*-alkanes: Simulated isotropic Raman spectra and band progressions for  $\text{C}_5\text{H}_{12}$ - $\text{C}_{20}\text{H}_{42}$  and  $\text{C}_{16}\text{D}_{34}$ , *Journal of Physical Chemistry*, 98(16), 4482-4488.
- 9) Chan, J.W., Motton, D., Rutledge, J.C., Keim, N.L. and Huser, T. (2005). Raman spectroscopic analysis of biochemical changes in individual triglyceride-rich lipoproteins in the pre- and postprandial state, *Analytical Chemistry*, 77(18), 5870-5876.
- 10) Christie, W.W. and Moore, J.H. (1970). A comparison of structures of triglycerides from various pig tissues, *Biochimica et Biophysica Acta-Lipids and Lipid Metabolism*, 210(1), 46-56.
- 11) Christie, W.W., Nikolovadamyanova, B., Laakso, P. and Herslof, B. (1991). Stereospecific analysis of triacyl-*sn*-glycerols via resolution of diastereometric diacylglycerol derivatives by high performance liquid chromatography on silica. *Journal of the American Oil Chemists' Society*, 68(10), 695-701.
- 12) Da Silva, E., Bresson, S. and Rousseau, D. (2009). Characterization of the three major polymorphic forms and liquid state of tristearin by Raman spectroscopy, *Chemistry and Physics of Lipids*, 157(2), 113-119.
- 13) Da Silva, E. and Rousseau, D. (2008). Molecular order and thermodynamics of the solid-liquid transition in triglycerides *via* Raman spectroscopy, *Physical Chemistry Chemical Physics*, 10(31), 4606-4613.
- 14) De Jong, S., Van Soest, T.C. and Van Schaick, M.A. (1991). Crystal structures and melting points of unsaturated triacylglycerols in the  $\beta$  phase, *Journal of the American Oil Chemists' Society*, 68(6), 371-378.
- 15) De Jong, S.D. and Van Soest, T.C. (1978). Crystal structures and melting points of saturated triglycerides in the  $\beta$ -2 phase, *Acta Crystallographica Section B-Structural Science*, 34, 1570-1583.
- 16) Dohi, K., Kaneko, F. and Kawaguchi, T. (2002). X-ray and vibrational spectroscopic study on polymorphism of trielaidin, *Journal of Crystal Growth*, 237, 2227-2232.
- 17) Dugo, P., Kumm, T., Fazio, A., Dugo, G. and Mondello, L. (2006). Determination of beef tallow in lard through a multidimensional off-line non-aqueous reversed phase-argentation LC method coupled to mass spectrometry, *Journal of Separation Science*, 29(4), 567-575.
- 18) Engstrom, L. (1992). Triglyceride systems forming molecular-compounds, *Fett Wissenschaft Technologie-Fat Science Technology*, 94(5), 173-181.
- 19) Ferguson, R.H. and Lutton, E.S. (1947). The

- polymorphism of triolein, *Journal of the American Chemical Society*, 69(6), 1445-1448.
- 20) Foubert, I., Dewettinck, D., Van de Walle, D., Dijkstra, A.J. and Quinn, P.J. (2007). Section 7, Physical properties: Structural and physical characteristics, In *The Lipid Handbook with CD-ROM* (Gunstone, F.D., Harwood, J.L. and Dijkstra, A.J., eds.), 3rd edition, 471-534, CRC Press, Boca Raton.
- 21) Garti, N. and Sato, K., eds. (1988). *Crystallization and polymorphism of fats and fatty acids*, Surfactant science series, Vol. 31, 450p, Marcell Dekker Inc., New York.
- 22) Goto, M., Kodali, D.R., Small, D.M., Honda, K., Kozawa, K. and Uchida, T. (1992). Single crystal structure of a mixed-chain triacylglycerol: 1,2-dipalmitoyl-3-acetyl-*sn*-glycerol. *Proceedings of the National Academy of Sciences of the United States of America*, 89(17), 8083-8086.
- 23) Gunstone, F.D. and Padley, F.B., eds. (1997). *Lipid Technologies and Applications*, 834p, Marcel Dekker. Inc., New York.
- 24) Hagemann, J.W. (1988). Thermal behavior and polymorphism of acylglycerides, In *Crystallization and polymorphism of fats and fatty acids* (Garti N and Sato, K., eds.), 9-95, Marcel Dekker Inc., New York.
- 25) Hagemann, J.W. and Rothfus, J.A. (1992). Computer modeling of packing arrangements and transitions in saturated-*cis*-unsaturated mixed triglycerides, *Journal of the American Oil Chemists' Society*, 69(5), 429-437.
- 26) Hernqvist, L. (1984). On the structure of triglycerides in the liquid-state and fat crystallization, *Fette Seifen Anstrichmittel*, 86(8), 297-300.
- 27) Hernqvist, L. and Larsson, K. (1982). On the crystal-structure of the  $\beta'$ -form of triglycerides and structural-changes at the phase-transitions LIQ.  $\rightarrow \alpha \rightarrow \beta' \leftarrow \beta$ , *Fette Seifen Anstrichmittel*, 84(9), 349-354.
- 28) Hoerr, C.W. (1964). X-ray diffraction of fats. *Journal of the American Oil Chemists' Society*, 41(7), 4.
- 29) Ishimoto, S. (1996). *Shuyou taisha keirozu*, in *Seibutsugaku jiten* (Yasugi, R., Ozeki, H., Furuya, M. and Hidaka, T., eds.), 4th edition, Iwanami shoten, Tokyo, 1620.
- 30) Jensen, L.H. and Mabis, A.J. (1963). Crystal structure of  $\beta$ -tricaprin, *Nature*, 197(486), 681-682.
- 31) Jensen, L.H. and Mabis, A.J. (1966). Refinement of structure of  $\beta$ -tricaplin, *Acta Crystallographica*, 21, 770-781.
- 32) Kallio, H., Yli-Jokipii, K., Kurvinen, J.P., Sjovall, O. and Tahvonen, R. (2001). Regioisomerism of triacylglycerols in lard, tallow, yolk, chicken skin, palm oil, palm olein, palm stearin, and a transesterified blend of palm stearin and coconut oil analyzed by tandem mass spectrometry, *Journal of Agricultural and Food Chemistry*, 49(7), 3363-3369.
- 33) Kaneko, F., Yano, J. and Sato, K. (1998). Diversity in the fatty-acid conformation and chain packing of *cis*-unsaturated lipids, *Current Opinion in Structural Biology*, 8(4), 417-425.
- 34) Kellens, M., Meeussen, W. and Reynaers, H. (1990). Crystallization and phase-transition studies of tripalmitin, *Chemistry and Physics of Lipids*, 55(2), 163-178.
- 35) Kellens, M., Meeussen, W. and Reynaers, H. (1992). Study of the polymorphism and the crystallization kinetics of tripalmitin - A microscopic approach, *Journal of the American Oil Chemists' Society*, 69(9), 906-911.
- 36) Kellens, M., Meeussen, W., Riekel, C. and Reynaers, H. (1990). Time resolved X-ray diffraction studies of the polymorphic behavior of tripalmitin using synchrotron radiation, *Chemistry and Physics of Lipids*, 52(2), 79-98.
- 37) Kim, Y.S., Strauss, H.L. and Snyder, R.G. (1989). Conformational disorder in the binary mixture  $n\text{-C}_{50}\text{H}_{102}/n\text{-C}_{46}\text{H}_{94}$ : A vibrational spectroscopic study, *Journal of Physical Chemistry*, 93(1), 485-490.
- 38) Kobayashi, M. (1988). Vibrational spectroscopic aspects of polymorphism and phase transition of fats and fatty acids, In *Crystallization and polymorphism of fats and fatty acids* (Garti, N. and Sato, K., eds.), 139-187, Marcel Dekker Inc., New York.
- 39) Kobayashi, M. and Kaneko, F. (1989). Molecular and crystal-structures of lipids and related-compounds, *Journal of Dispersion Science and Technology*, 10(4-5), 319-350.

- 40) Kobayashi, M., Kaneko, F., Sato, K. and Suzuki, M. (1986). Vibrational spectroscopic study on polymorphism and order-disorder phase-transition in oleic-acid, *Journal of Physical Chemistry*, 90(23), 6371-6378.
- 41) Kobayashi, M., Kobayashi, T., Itoh, Y. and Sato, K. (1984). Polytypism in normal-fatty acids and low-frequency Raman-spectra: stearic-acid *B*-form, *Journal of Chemical Physics*, 80(6), 2897-2903.
- 42) Kobayashi, M., Sakagami, K. and Tadokoro, H. (1983). Effects of interlamellar forces on longitudinal acoustic modes of *n*-alkanes, *Journal of Chemical Physics*, 78(11), 6391-6398.
- 43) Kobayashi, M., Uesaka, T. and Tadokoro, H. (1976). Polarized Raman-spectra of single-crystal *n*-C<sub>36</sub>H<sub>74</sub>, *Chemical Physics Letters*, 37(3), 577-581.
- 44) Kodali, D.R., Atkinson, D., Redgrave, T.G. and Small, D.M. (1987). Structure and polymorphism of carbon-18 fatty acyl triacylglycerols — Effect of unsaturation and substitution in the 2-position, *Journal of Lipid Research*, 28(4), 403-413.
- 45) Kodali, D.R., Atkinson, D. and Small, D.M. (1989). Molecular packing of 1,2-dipalmitoyl-3-decanoyl-*sn*-glycerol (PP10): Bilayer, trilayer, and hexalayer structures, *Journal of Physical Chemistry*, 93(11), 4683-4691.
- 46) Kodali, D.R., Atkinson, D. and Small, D.M. (1990). Polymorphic behavior of 1,2-dipalmitoyl-3-lauroyl(PP12)- and 3-myristoyl(PP14)-*sn*-glycerols, *Journal of Lipid Research*, 31(10), 1853-1864.
- 47) Koyama, Y. and Ikeda, K.I. (1980). Raman-spectra and conformations of the *cis*-unsaturated fatty-acid chains, *Chemistry and Physics of Lipids*, 26(2), 149-172.
- 48) Koyano, T., Hachiya, I. and Sato, K. (1992). Phase-behavior of mixed systems of SOS and OSO, *Journal of Physical Chemistry*, 96(25), 10514-10520.
- 49) Krimm, S., Liang, C.Y. and Sutherland, G. (1956). Infrared spectra of high polymers. 2. Polyethylene, *Journal of Chemical Physics*, 25(3), 549-562.
- 50) Kyodo news (2007), Meat Hope chief admits pork was disguised as ground beef, *The Japan Times*, June 21, p. 2.
- 51) Larsson, K. (1965). The crystal structure of  $\beta$ -form of trilaurin. *Arkiv fur Kemi*, 23(1), 1-15.
- 52) Larsson, K. (1966). Alternation of melting points in homologous series of long-chain compounds. *Journal of the American Oil Chemists' Society*, 43(10), 559-562.
- 53) Larsson, K. (1966). Classification of glyceride crystal forms, *Acta Chemica Scandinavica*, 20(8), 2255-2260.
- 54) Larsson, K. (1973). Conformation-dependent features in Raman-spectra of simple lipids, *Chemistry and Physics of Lipids*, 10(2), 165-176.
- 55) Larsson, K. and Rand, R.P. (1973). Detection of changes in environment of hydrocarbon chains by Raman-spectroscopy and its application to lipid-protein systems. *Biochimica et Biophysica Acta-Lipids and Lipid Metabolism*, 326(2), 245-255.
- 56) Lippert, J.L. and Peticola, W.L. (1972). Raman active vibrations in long-chain fatty-acids and phospholipid sonicates, *Biochimica et Biophysica Acta -Biomembranes*, 282, 8-17.
- 57) Malkin, T. (1954). The polymorphism of glycerides, *Progress in the Chemistry of Fats and other Lipids*, 2, 2-14.
- 58) Maroncelli, M., Strauss, H.L. and Snyder, R.G. (1985). On the CD<sub>2</sub> probe infrared method for determining polymethylene chain conformation, *Journal of Physical Chemistry*, 89(20), 4390-4395.
- 59) McClements, D.J. and Decker, E.A. (2007). *Lipids*, In Fennema's food chemistry (Damodaran, S., Parkin, K.L. and Fennema, O.R., eds.), 4th edition, 155-216, CRC press, Boca Raton.
- 60) Mendelsohn, R. and Davies, M.A. (1991). CD<sub>2</sub> rocking modes as quantitative fourier-transform infrared spectroscopic probes of conformational disorder in phospholipid bilayers, In *Fourier Transform Infrared Spectroscopy in Colloid and Interface Science* (Scheuing, D.R., ed.), 24-43, American Chemical Society.
- 61) Mendelsohn, R., Davies, M.A., Schuster, H.F., Xu, Z.C. and Bittman, R. (1991). CD<sub>2</sub> rocking modes as quantitative infrared probes of one-, two-, and three-bond conformational disorder in dipalmitoylphosphatidylcholine and dipalmitoylphosphatidylcholine / cholesterol mixtures, *Biochemistry*, 30(35), 8558-8563.

- 62) Minato, A., Ueno, S., Smith, K., Amemiya, Y. and Sato, K. (1997). Thermodynamic and kinetic study on phase behavior of binary mixtures of POP and PPO forming molecular compound systems, *Journal of Physical Chemistry B*, 101(18), 3498-3505.
- 63) Minato, A., Ueno, S., Yano, J., Smith, K., Seto, H., Amemiya, Y. and Sato, K. (1997). Thermal and structural properties of *sn*-1,3-dipalmitoyl-2-oleoylglycerol and *sn*-1,3-dioleoyl-2-palmitoylglycerol binary mixtures examined with synchrotron radiation X-ray diffraction, *Journal of the American Oil Chemists' Society*, 74(10), 1213-1220.
- 64) Minato, A., Yano, J., Ueno, S., Smith, K. and Sato, K. (1997). FT-IR study on microscopic structures and conformations of POP-PPO and POP-OPO molecular compounds, *Chemistry and Physics of Lipids*, 88(1), 63-71.
- 65) Mizushima, S.I. and Simanouti, T. (1949). Raman frequencies of *n*-paraffin molecules. *Journal of the American Chemical Society*, 71(4), 1320-1324.
- 66) Moran, D.P.J. (1963). Phase behaviour of some palmito-oleo triglyceride systems, *Journal of Applied Chemistry*, 13(2), 91-100.
- 67) Motoyama, M., Ando, M., Sasaki, K. and Hamaguchi, H. (2010). Differentiation of animal fats from different origins: Use of polymorphic features detected by Raman spectroscopy, *Applied Spectroscopy*, 64(11), 1244-1250.
- 68) Muik, B., Lendl, B., Molina-Diaz, A. and Ayora-Canada, M.J. (2005). Direct monitoring of lipid oxidation in edible oils by Fourier transform Raman spectroscopy, *Chemistry and Physics of Lipids*, 134(2), 173-182.
- 69) Mushayakarara, E. and Levin, I.W. (1982). Determination of acyl chain conformation at the lipid interface region: Raman spectroscopic study of the carbonyl stretching mode region of dipalmitoyl phosphatidylcholine and structurally related molecules, *Journal of Physical Chemistry*, 86(13), 2324-2327.
- 70) Mykhaylyk, O.O. and Martin, C.M. (2009). Effect of unsaturated acyl chains on structural transformations in triacylglycerols, *European Journal of Lipid Science and Technology*, 111(3), 227-235.
- 71) Mykhaylyk, O.O., Smith, K.W., Martin, C.M. and Ryan, A.J. (2007). Structural models of metastable phases occurring during the crystallization process of saturated/unsaturated triacylglycerols, *Journal of Applied Crystallography*, 40, S297-S302.
- 72) Oakes, R.E., Beattie, J.R., Moss, B.W. and Bell, S.E.J. (2003). DFT studies of long-chain FAMES: theoretical justification for determining chain length and unsaturation from experimental Raman spectra, *Journal of Molecular Structure: Theochem*, 626, 27-45.
- 73) Okajima, H. and Hamaguchi, H. (2009). Fast low frequency (down to 10 cm<sup>-1</sup>) multichannel Raman spectroscopy using an iodine vapor filter, *Applied Spectroscopy*, 63(8), 958-960.
- 74) Packter, N.M. and Olukoshi, E.R. (1995). Ultrastructural studies of neutral lipid localisation in *Streptomyces*, *Archives of Microbiology*, 164(6), 420-427.
- 75) Peschar, R., Pop, M.M., De Ridder, D.J.A., Van Mechelen, J.B., Driessen, R.A.J. and Schenk, H. (2004). Crystal structures of 1,3-distearoyl-2-oleoylglycerol and cocoa butter in the  $\beta$ (V) phase reveal the driving force behind the occurrence of fat bloom on chocolate, *Journal of Physical Chemistry B*, 108(40), 15450-15453.
- 76) Pink, D.A., Green, T.J. and Chapman, D. (1980). Raman-scattering in bilayers of saturated phosphatidyl cholines — experiment and theory, *Biochemistry*, 19(2), 349-356.
- 77) Pink D.A., Hanna C.B., Sandt, C., MacDonald, A.J., MacEachern, R., Corkery, R. and Rousseau, D. (2010). Modeling the solid-liquid phase transition in saturated triglycerides, *Journal of Chemical Physics*, 132(5), 054502.
- 78) Resources Council, Science and Technology Agency, Japan (1989). Standard tables of food composition in Japan: Fatty acids, cholesterol and vitamin E (tocopherols), Resources Council, Science and Technology Agency, Japan, Tokyo, 208p.
- 79) Riiner, Ü. (1970). Investigation of the polymorphism of fats and oils by temperature programmed X-ray diffraction. *Lebensmittel-Wissenschaft und*

- Technologie -Food Science and Technology, 3, 101-106.
- 80) Sato, K. (1999). Solidification and phase transformation behaviour of food fats - a review. *Fett/Lipid*, 101(12), 467-474.
- 81) Sato, K. (2001). Crystallization behaviour of fats and lipids - a review. *Chemical Engineering Science*, 56(7), 2255-2265.
- 82) Sato, K., Arishima, T., Wang, Z.H., Ojima, K., Sagi, N. and Mori, H. (1989). Polymorphism of POP and SOS. 1. Occurrence and polymorphic transformation, *Journal of the American Oil Chemists' Society*, 66(5), 664-674.
- 83) Sato, K. and Kobayashi, M. (1992). *Sisitsu no kouzou to dainamikku*, Kyouritsu shuppan, Tokyo, 179p.
- 84) Sato, K. and Kuroda, T. (1987). Kinetics of melt crystallization and transformation of tripalmitin polymorphs, *Journal of the American Oil Chemists' Society*, 64(1), 124-127.
- 85) Sato, K., Yano, J., Kawada, I., Kawano, M., Kaneko, F. and Suzuki, M. (1997). Polymorphic behavior of gondoic acid and phase behavior of its binary mixtures with asclepic acid and oleic acid, *Journal of the American Oil Chemists' Society*, 74(9), 1153-1159.
- 86) Schachtschneider, J.H. and Snyder, R.G. (1963). Vibrational analysis of the *n*-paraffins - II. Normal coordinate calculations, *Spectrochimica Acta*, 19(1), 117-168.
- 87) Scrimgeour, C.M. and Harwood, J.L. (2007). Fatty acid and lipid structure, In *The Lipid Handbook with CD-ROM* (Gunstone, F.D., Harwood, J.L. and Dijkstra, A.J., eds.), 3rd edition, 1-36 CRC Press, Boca Raton.
- 88) Shimanouchi, T. (1977). *Sindou bunkougaku. Sono kakuritsu to kagakuteki ouyou* (ed. Jigyoukai STskk), Jigyoukai STskk, Tokyo, 103p.
- 89) Shindou, H. and Shimizu, T. (2009). Acyl-CoA: Lysophospholipid Acyltransferases, *Journal of Biological Chemistry*, 284(1), 1-5.
- 90) Simpson, T.D. (1983). Solid-phase of trimargarin: A comparison to tristearin, *Journal of the American Oil Chemists' Society*, 60(1), 95-97.
- 91) Small, D.M. (1986). Appendix III. Normal fatty acids: Including data for saturated, unsaturated, and dicarboxylic acids, In *The Physical Chemistry of Lipids: From Alkanes to Phospholipids, Handbook of Lipid Research* (Small, D.M., ed.), Vol. 4, 587-601, Plenum press, New York.
- 92) Small, D.M. (1986). Glycerides, In *The Physical Chemistry of Lipids: From Alkanes to Phospholipids, Handbook of Lipid Research* (Small, D.M., ed.), Vol. 4, 345-394, Plenum press, New York.
- 93) Small, D.M., ed. (1986). *The Physical Chemistry of Lipids: From Alkanes to Phospholipids, Handbook of Lipid Research* (Small, D.M., ed.), Vol. 4, 672p, Plenum Press, New York.
- 94) Smith, A.E. (1953). The crystal structure of the normal paraffin hydrocarbons, *Journal of Chemical Physics*, 21(12), 2229-2231.
- 95) Snyder, R.G. (1960). Vibrational spectra of crystalline *n*-paraffins. 1. Methylene rocking and wagging modes, *Journal of Molecular Spectroscopy*, 4(5), 411-434.
- 96) Snyder, R.G. (1961). Vibrational spectra of crystalline *n*-paraffins. 2. Intermolecular effects, *Journal of Molecular Spectroscopy*, 7(2), 116-144.
- 97) Snyder, R.G. (1967). A revised assignment of  $B_{2g}$  methylene methylene wagging fundamental of planar polyethylene chain, *Journal of Molecular Spectroscopy*, 23(2), 224-228.
- 98) Snyder, R.G. (1967). Vibrational study of chain conformation of liquid *n*-paraffins and molten polyethylene, *Journal of Chemical Physics*, 47(4), 1316-1360.
- 99) Snyder, R.G. (1969). Raman spectrum of polyethylene and the assignment of  $B_{2g}$  wag fundamental, *Journal of Molecular Spectroscopy*, 31(3), 464-465.
- 100) Snyder, R.G. (1990). Distribution of infrared intensity in the spectra of conformationally disordered chain molecule assemblies, *Macromolecules*, 23(7), 2081-2087.
- 101) Snyder, R.G., Aljibury, A.L., Strauss, H.L., Casal, H.L., Gough, K.M. and Murphy, W.F. (1984). Isolated C-H stretching vibrations of *n*-alkanes: Assignments and relation to structure, *Journal of Chemical Physics*, 81(12), 5352-5361.

- 102) Snyder, R.G., Hsu, S.L. and Krimm, S. (1978). Vibrational-spectra in C-H stretching region and structure of polymethylene chain, *Spectrochimica Acta Part A: Molecular and Biomolecular Spectroscopy*, 34(4), 395-406.
- 103) Snyder, R.G. and Kim, Y. (1991). Conformation and low-frequency isotropic Raman-spectra of the liquid *n*-alkanes C<sub>4</sub>-C<sub>9</sub>, *Journal of Physical Chemistry*, 95(2), 602-610.
- 104) Snyder, R.G. and Schachtschneider, J.H. (1963). Vibrational analysis of the *n*-paraffins. 1. Assignments of infrared bands in the spectra of C<sub>3</sub>H<sub>8</sub> through *n*-C<sub>19</sub>H<sub>40</sub>, *Spectrochimica Acta*, 19(1), 85-116.
- 105) Snyder, R.G., Strauss, H.L., Alamo, R. and Mandelkern, L. (1994). Chain-length dependence of interlayer interaction in crystalline *n*-alkanes from Raman longitudinal acoustic mode measurements, *Journal of Chemical Physics*, 100(8), 5422-5431.
- 106) Sprunt, J.C., Jayasooriya, U.A. and Wilson, R.H. (2000). A simultaneous FT-Raman-DSC (SRD) study of polymorphism in *sn*-1,3-distearoyl-2-oleoylglycerol (SOS), *Physical Chemistry Chemical Physics*, 2(19), 4299-4305.
- 107) Takai, Y., Masuko, T. and Takeuchi, H. (1997). Lipid structure of cytotoxic granules in living human killer T lymphocytes studied by Raman microspectroscopy, *Biochimica et Biophysica Acta-General Subjects*, 1335(1-2), 199-208.
- 108) Tasumi, M. and Krimm, S. (1967). Crystal vibrations of polyethylene, *Journal of Chemical Physics*, 46(2), 755-766.
- 109) Tasumi, M. and Krimm, S. (1968). Vibrational analysis of chain folding in polyethylene crystals, *Journal of Polymer Science Part A-2: Polymer Physics*, 6(5), 995-1010.
- 110) Tasumi, M., Shimanou, T., Kenjo, H. and Ikeda, S. (1966). Molecular vibrations of irregular chains. I. Analysis of infrared spectra and structures of polymethylene chains consisting of CH<sub>2</sub>, CHD and CD<sub>2</sub> groups, *Journal of Polymer Science Part A-1: Polymer Chemistry*, 4(5), 1011-2021.
- 111) Tasumi, M. and Shimanouchi, T. (1963). A refined treatment of normal vibrations of polymethylene chain, *Journal of Molecular Spectroscopy*, 11(6), 422-432.
- 112) Tasumi, M., Shimanouchi, T. and Miyazawa, T. (1962). Normal vibrations and force constants of polymethylene chain, *Journal of Molecular Spectroscopy*, 9(4), 261-287.
- 113) Tasumi, M. and Shimanouchi, T. (1965). Crystal vibrations and intermolecular forces of polymethylene crystals, *Journal of Chemical Physics*, 43(4), 1245-1258.
- 114) Tasumi, M. and Zerbi, G. (1968). Vibrational analysis of random polymers, *Journal of Chemical Physics*, 48(8), 3813-3820.
- 115) Timms, R.E. (1984). Phase-behavior of fats and their mixtures, *Progress in Lipid Research*, 23(1), 1-38.
- 116) Timms, R.E. (2003). *Confectionary fats handbook: Properties, production and application*, 441p, The Oily Press, Bridgewater, UK.
- 117) Ueno, S. (2010 July 7). Personal communication.
- 118) Ueno, S., Minato, A., Seto, H., Amemiya, Y. and Sato, K. (1997). Synchrotron radiation X-ray diffraction study of liquid crystal formation and polymorphic crystallization of SOS (*sn*-1,3-distearoyl-2-oleoylglycerol), *Journal of Physical Chemistry B*, 101(35), 6847-6854.
- 119) Ueno, S., Minato, A., Yano, J. and Sato, K. (1999). Synchrotron radiation X-ray diffraction study of polymorphic crystallization of SOS from liquid phase, *Journal of Crystal Growth*, 198, 1326-1329.
- 120) Uwaha, M., ed. (2002). *Kesshou seichou no shikumi wo saguru — sono butsuriteki kiso —*. *Kesshou seichou no dainamikkusu* (Nishinaga, S., Miyazaki, S. and Sato, K., eds.), Vol. 2, Kyoritsu shuppan, Tokyo, 166p.
- 121) Van Langevelde, A., Van Malssen, K., Hollander, F., Peschar, R. and Schenk, H. (1999). Structure of mono-acid even-numbered β-triacylglycerols, *Acta Crystallographica Section B-Structural Science*, 55, 114-122.
- 122) Vogel, H. and Jahnig, F. (1981). Conformational order of the hydrocarbon chains in lipid bilayers. A Raman spectroscopic study, *Chemistry and Physics of Lipids*, 29(1), 83-101.
- 123) Wheeler, D.H., Riemenschneider, R.W. and

- Sando, C.E. (1940). Preparation, properties, and thiocyanogen absorption of triolein and trilinolein, *Journal of Biological Chemistry*, 132(2), 687-699.
- 124) Wood, J.D., Enser, M., Fisher, A.V., Nute, G.R., Sheard, P.R., Richardson, R.I., Hughes, S.I. and Whittington, F.M. (2008). Fat deposition, fatty acid composition and meat quality: A review, *Meat Science*, 78(4), 343-358.
- 125) Yano, J., Kaneko, F., Kobayashi, M., Kodali, D.R., Small, D.M. and Sato, K. (1997). Structural analyses and triacylglycerol polymorphs with FT-IR techniques. 2.  $\beta'_1$ -form of 1,2-dipalmitoyl-3-myristoyl-*sn*-glycerol, *Journal of Physical Chemistry B*, 101(41), 8120-8128.
- 126) Yano, J., Kaneko, F., Kobayashi, M. and Sato, K. (1997). Structural analyses of triacylglycerol polymorphs with FT-IR techniques. 1. Assignments of CH<sub>2</sub> progression bands of saturated monoacid triacylglycerols, *Journal of Physical Chemistry B*, 101(41), 8112-8119.
- 127) Yano, J. and Sato, K. (1999). FT-IR studies on polymorphism of fats: molecular structures and interactions, *Food Research International*, 32(4), 249-259.
- 128) Yano, J., Ueno, S., Sato, K., Arishima, T., Sagi, N., Kaneko, F. and Kobayashi, M. (1993). FT-IR study of polymorphic transformation in SOS, POP, and POS, *Journal of Physical Chemistry*, 97(49), 12967-12973.
- 129) Zerbi, G., Conti, G., Minoni, G., Pison, S. and Bigotto, A. (1987). Premelting phenomena in fatty acids: An infrared and Raman study, *Journal of Physical Chemistry*, 91(9), 2386-2393.
- 130) Zerbi, G., Magni, R., Gussoni, M., Moritz, K.H., Bigotto, A. and Dirlikov, S. (1981). Molecular mechanics for phase-transition and melting of *n*-alkanes: A spectroscopic study of molecular mobility of solid *n*-nonadecane, *Journal of Chemical Physics*, 75(7), 3175-3194.
- 131) Zweytick, D., Athenstaedt, K. and Daum, G. (2000). Intracellular lipid particles of eukaryotic cells, *Biochimica et Biophysica Acta-Reviews on Biomembranes*, 1469(2), 101-120.

### Acknowledgements

I would like to take this opportunity to express my sincere gratitude to Professor Hiro-o HAMAGUCHI. He has taught me not only the basics of spectroscopy but also the fundamental philosophy of research. Professor said, "If it is painful, it is not a research" and "Be honest with what has been observed". These are the most precious words for me. His thoughtful words have always encouraged me and will help me enormously in the future as well.

I would also like to mention gratefully Associate-Professor Hideaki KANO, Assistant-Professor Rintaro SHIMADA, Assistant-Professor Hajime OKAJIMA, Professor Koichi IWATA (of Gakushuin University), Assistant-Professor Tomohisa TAKAYA (of Gakushuin University) and Dr. Young-kun MIN for their invaluable advice on my research. Also, Dr. Keisuke SASAKI, Ms. Yumiko ENDO, Dr. Masaru NOMURA and Dr. Katsuhiro AIKAWA (of Institute of Livestock and Grassland Science, National Agriculture and Food Research Organization) are gratefully acknowledged for their constant support to me. I also owe a deep sense of gratitude to the late Dr. Mitsuru MITSUMOTO and Dr. Sayuki NIKKUNI.

The successful completion of this thesis was possible only with the assistance of all the members in Hamaguchi Laboratory, of all the members in Animal Products Research Team and of all the family, friends, well-wishers who have been supporting me throughout the PhD tenure. Finally, my special thanks will go to Mr. Masahiro ANDO for his help with great expertise in Raman instrumentation and to Dr. Shraeddha TIWARI for her cheerful support in writing the manuscript.

# ラマン分光法によるトリアシルグリセロールの構造および相挙動解析

本山三知代

農研機構畜産草地研究所 畜産物研究領域, つくば市, 305-0901

## 摘 要

トリアシルグリセロール (TAG) は生体における主要なエネルギー貯蔵物質である。その多成分系である天然油脂は、食品や医薬品、化粧品などの工業製品に広く用いられる。工業的要請から TAG 多成分系の相挙動については長い間研究が行われてきたが、その全貌は未だ明らかでない。天然油脂の複雑な相挙動について新たな知見を得るために、ラマン分光法を用いて TAG 多成分系の相挙動解析をおこなった。

はじめに、本研究の背景について述べた (第一章)。ラマン分光法は TAG の構造解析に最適の手法であり、多成分系を対象とするときにもその威力を発揮する。次に、TAG の構造と相挙動について最近の知見に重点を置いてまとめた (第二章)。結晶多形現象や“分子性化合物”形成などの TAG の興味深い相挙動について紹介し、それらの現象に影響を及ぼす結晶化条件などの要因についても言及した。また、TAG の各結晶多形より得られたラマンスペクトルについて、各相に特徴的な分子・結晶構造と関係付けながら詳述した (第三章)。長年に渡り蓄積された分光学的知見に基づき、ラマン分光法により TAG 結晶多形の詳細な構造解析が可能である。以上の章において述べた知見に基づき、TAG 多成分系の構造と相挙動に関する二つの研究をおこなった。一つは分子性化合物を形成すると言われている TAG 二成分系について (第四章)、もう一つは広く工業的に利用されているいくつかの天然油脂について (第五章) である。

これらの研究の結果、用いた TAG 二成分系における分子性化合物の形成が確かめられ、その構造は過去の報告と異なるものであった (第四章)。このことは、分子性化合物の構造は結晶化条件の影響を決定的に受けていることを示唆し、これまで液相においても存在すると考えられてきた分子性化合物は、おそらく結晶化の過程で動的に生成する構造であるためと考察された。また分子性化合物は、これまでその形成が確認されているモデル二成分系においてだけでなく、天然油脂においても形成されていることを示唆する結果が得られた (第五章)。また、ラマン分光法を用いて相挙動の違いを検出することで、天然油脂の由来を判別できることを明らかにした (第五章)。

最後に、TAG の構造および相挙動についてさらに理解を深めるためのラマン分光法を用いた研究の展望について述べた (第六章)。近年の分光器の発達には TAG 多成分系の研究に明るい可能性をもたらしており、ラマン分光法が天然油脂の相挙動の全貌解明に大いに貢献すると期待される。

キーワード：結晶多形, トリアシルグリセロール多成分系, 豚脂, 牛脂, 判別法

© 2012 NARO Institute of Livestock and Grassland Science

All rights reserved. No part of this publication may be reproduced without the permission of the copyright holder.

Published by Institute of Livestock and Grassland Science,  
National Agriculture and Food Research Organization (NARO)  
Ikenodai 2, Tsukuba, Ibaraki 305-0901 Japan

編集委員会事務局  
企画管理部情報広報課  
児玉正文  
飛鳥井可奈子  
那須企画管理室連絡調整チーム  
大里孝

本研究報告から転載、複製を行う場合は、独立行政法人農業・食品産業技術総合研究機構畜産草地研究所の許可を得て下さい。

平成 24 年 3 月 印刷

平成 24 年 3 月 発行

独立行政法人 農業・食品産業技術総合研究機構

## 畜産草地研究所

〒305-0901 茨城県つくば市池の台2

TEL 029-838-8600(代)

FAX 029-838-8606

印刷所 筑波印刷情報サービスセンター協同組合

## (目的)

第1条 畜産草地研究所研究報告及び畜産草地研究所研究資料への投稿については、独立行政法人農業・食品産業技術総合研究機構刊行物著作権取扱規程（14規程56号）に定めるもののほかこの要領の定めるところによる。

## (投稿者の資格)

第2条 投稿者は原則として、畜産草地研究所職員（以下「職員」という。）及び流動研究員、依頼研究員、日本学術振興会特別研究員、日本学術振興会外国人特別研究員等（以下「他の職員」という。）とする。

- 一 職員が投稿する内容は、主として畜産草地研究所（以下「研究所」という。）で行った研究とする。
- 二 他の職員が投稿する内容は、研究所で行った研究とする。

## (投稿原稿の内容)

第3条 投稿原稿の内容は次のとおりとする。

- 1 畜産草地研究所研究報告（Bulletin of NARO Institute of Livestock and Grassland Science / 略誌名：Bull NARO Inst Livest Grassl Sci）
  - 一 原著論文：研究所において行った試験研究及び研究所以外の者に委託して行った試験研究の成果に関わる論文とする。
  - 二 短報：一以外の研究の予報、速報などの短報とする。
  - 三 技術論文：新しい技術や技術の組立、実証などを主体とする報告。
  - 四 総説：畜産草地研究に関わるものとする。総説は投稿のほか、編集委員会が依頼したものを含む。
  - 五 学位取得論文：研究所において主として行った試験研究による学位取得論文とする。
- 2 畜産草地研究所研究資料（Memoirs of NARO Institute of Livestock and Grassland Science / 略誌名：Mem NARO Inst Livest Grassl Sci）  
調査資料・技術資料・研究資料：研究所において行った試験研究及び研究所が研究所以外のものに委託して行った試験研究のうち、学術的・産業的に有用な未発表の資料とする。

## (原稿の執筆)

第4条 原稿の執筆にあたっては、別に定める畜産草地研究所研究報告及び畜産草地研究所研究資料執筆要領（13畜草B第44号）に基づくものとする。使用する言語は日本語又は英語とする。

## (原稿の提出)

第5条 次の手続きにより原稿及び原稿提出票を事務局に提出する。

- 一 職員は原稿提出票に必要事項を記載し、所属研究領域長等の校閲を受ける。
- 二 他の職員は原稿提出票に必要事項を記載し、所属研究領域長等の校閲を受ける。

## (受付)

第6条 原稿及び原稿提出票を事務局が受け取った日を受付日とする。受理日は編集委員会の審査の結果、掲載が妥当と認められた日とする。

## (審査)

第7条 編集委員会は次の手続きにより論文を審査する。ただし、学位取得論文については審査を省略することができる。

- 一 編集委員会は論文の内容により審査員正副をそれぞれ1名決定し、論文審査を依頼する。審査員は研究所内及び研究所外の研究者等とし、その氏名は公表しない。
- 二 審査員は論文審査票により審査を行う。また必要に応じて指摘事項を書き出し提出する。
- 三 事務局は審査員と著者の間のやり取りの対応にあたる。
- 四 編集委員会は審査員の審査結果を参考にして掲載の可否を判断する。  
審査の内容によっては著者に原稿の訂正を求めることができる。
- 五 著者は審査結果を受領後、編集委員会が指定する期日までに修正原稿を事務局に提出する。

## (校正)

第8条 著者による校正は原則として初校のみとする。校正は誤植の訂正程度にとどめる。やむを得ず大きな変更等を行う場合には編集委員会の承認を得なければならない。

## (別刷り)

第9条 別刷りは次のとおりとする。

- 一 100部とし、筆頭著者が代表で受け取る。
- 二 別刷りの追加を希望する場合は研究費負担で印刷する。

## 附 則

この規定は、平成14年4月1日から施行する。

## 附 則

この規定は、平成15年10月1日から施行する。

## 附 則

この規定は、平成18年4月1日から施行する。

## 附 則

この要領は、平成20年4月1日から施行する。

## 附 則

この要領は、平成23年4月1日から施行する。

## 附 則

この要領は、平成23年8月8日から施行する。

